Report No. BDK84 977-14

Final Report

Hydroplaning on Multi Lane Facilities

M. Gunaratne, Ph.D., P.E.
Principal Investigator

Q. Lu, Ph.D., P.E.
Co-Principal Investigator

J. Yang, Ph.D. P.E
Consultant

and

J. Metz
W. Jayasooriya
M. Yassin
S. Amarasiri
Graduate Assistants

Submitted to

Florida Department of Transportation

By the

Department of Civil and Environmental Engineering
College of Engineering
University of South Florida
Tampa, FL 33620
Ph. (813)974-2275

November 2012

DISCLAIMER

The opinions, findings, and conclusions expressed in this publication are those of the authors and not necessarily those of the Florida Department of Transportation.

This document is disseminated under the sponsorship of the Department of Transportation in the interest of information exchange. The United States Government assumes no liability for the contents or use thereof.

CONVERSION FACTORS

To convert	British		SI	multiply by
Acceleration	ft/s^2	m/s^2	$3.048E-1$	
Area	ft^2		m^2	$9.290E-2$
Density	$slugs/ft^3$		kg/m^3	$5.154E+2$
Length	ft		m	$3.048E-1$
Pressure	lb/ft^2		N/m^2	$4.788E+1$
Velocity	ft/s		m/s	$3.048E-1$

1. Report No.	2. Government Accession No.	3. Recipient's Catalog No.
4. Title and Subtitle Hydroplaning on Multi Lane Facilities		5. Report Date November 8, 2012
		6. Performing Organization Code
7. Author(s) M. Gunaratne, Q. Lu, J. Yang, J. Metz, W. Jayasooriya, M. Yassin, and S. Amarasiri		8. Performing Organization Report No.
9. Performing Organization Name and Address Department of Civil and Environmental Engineering College of Engineering University of South Florida, Tampa, FL 33620		10. Work Unit No. (TRAIS)
		11. Contract or Grant No. BDK84 977-14
12. Sponsoring Agency Name and Address Florida Department of Transportation 605 Suwannee St. MS 30 Tallahassee, FL 32399		13. Type of Report and Period Covered Final report July 2010 – July 2012
		14. Sponsoring Agency Code
15. Supplementary Notes Prepared in cooperation with the Federal Highway Administration		

16. Abstract

The primary findings of this research can be highlighted as follows. Models that provide estimates ofwet weather speed reduction, as well as analytical and empirical methods for the prediction of hydroplaning speeds of trailers and heavy trucks, were gathered and verified in a field study. The investigators have been able to provide Florida Dept. of Transportation (FDOT) with a predictive tool that combines the best of the available prediction models. Pavement properties needed to estimate the water film thickness produced during sheet flow were obtained from the literature and field studies. The investigators have been able to formulate analytical equations for predicting the critical water film thickness with respect to hydroplaning under different road geometric conditions, such as straight runs, super-elevations, and transition sections. A wet weather crash analysis was performed using crash statistics, geometrical data, pavement condition data, and other relevant information available in numerous FDOT databases. The results of this effort indicate that (i) wider sections are more likely to produce hydroplaning crashes, (ii) dense-graded pavements are more likely to induce conditions conducive to hydroplaning than open-graded ones, (iii) NCHRP's PAVDRN software would have predicted, to a significant degree of accuracy, most of the documented hydroplaning incidents, and (iv) the PAVDRN program is relatively unreliable for predicting hydroplaning in the inner lanes.

17. Key Words Hydroplaning, water film thickness, pavement, PAVDRN		18. Distribution Statement No restrictions. This document is available to the public through the National Technical Information Service, Springfield, VA 22161		
19. Security Classif. (of this report)Unclassified	20. Security Classif. (of this page) Unclassified		21. No. of Pages 130	22. Price

Form DOT F 1700.7 (8-72) Reproduction of completed page authorized

ACKNOWLEDGMENTS

EXECUTIVE SUMMARY

Florida Department of Transportation's (FDOT) Plans Preparation Manual (PPM) specifies a maximum of three travel lanes with a cross slope in one direction to mitigate the potential for hydroplaning by limiting the thickness of the water film formed due to heavy rains. Therefore, when highways are widened exceeding the PPM criteria, the common practice is to slope the inside lane toward the median, thus increasing the construction costs. The need for additional construction costs can be precluded if FDOT is equipped with an analytical procedure for evaluating the actual potential for hydroplaning, particularly for relatively wide sections that exceed the PPM criteria. Therefore, a comprehensive study consisting of several specific tasks was conducted by USF researchers based on the guidelines provided by FDOT to achieve the project objectives.

The primary findings of this research can be highlighted as follows. Models that provide reliable estimates of wet weather speed reduction, as well as analytical and empirical methods for the prediction of hydroplaning speeds of locked-wheel trailers and heavy trucks, were gathered and further verified through field studies. The investigators' field test results are in general agreement with most of the above mentioned models, and hence, the investigators have been able to provide FDOT with a predictive tool that combines the best of all the available prediction models. Pavement properties needed to estimate the water film thickness formed during sheet flow in open-graded and dense-graded pavements were obtained from literature search. In addition, the investigators have been able to formulate analytical equations for predicting the critical water film thickness under different road geometric conditions, such as straight runs, super-elevations, and transition sections.

An extensive wet weather crash analysis was performed using crash statistics, geometrical data, pavement condition data, and other relevant information available in numerous FDOT databases. The results of this effort clearly indicated that (i) wider sections are more likely to produce hydroplaning crashes, (ii) dense-graded pavements are more likely to induce conditions conducive to hydroplaning than open-graded ones, (iii) NCHRP's PAVDRN software would have predicted, to a significant degree of accuracy, most of the documented hydroplaning incidents in Florida, and (iv) the PAVDRN program is relatively unreliable for predicting hydroplaning in the inner lanes. Finally, a numerical model based on the finite difference method was also formulated to predict the water film thicknesses needed to produce critical friction conditions for smooth tires sliding on wet and rough pavement surfaces.

TABLE OF CONTENTS

LIST OF FIGURES

xi

LIST OF TABLES

CHAPTER 1

INVESTIGATION OF THE EFFECT OF RAIN INTENSITY ON SPEED REDUCTION

1.1 Introduction of the research project

FDOT's Plans Preparation Manual (PPM) specifies a maximum of three travel lanes with a cross slope in one direction to mitigate the potential for hydroplaning by limiting the thickness of the water film formed due to heavy rains. Therefore, when highways are widened exceeding the PPM criteria, the common practice is to slope the inside lane toward the median, thus increasing the construction costs. The need for additional construction and costs can be precluded if FDOT is equipped with an analytical procedure for evaluating the actual potential for hydroplaning particularly for relatively wider sections that exceed the PPM criteria. The PAVDRN computer program formulated based on an NCHRP (1998) investigation on improved methods for drainage design for multilane pavements with hydroplaning provides promising tools for analyzing the hydroplaning potential of pavement sections based on pavement characteristics, highway geometrics, and rainfall data.

Even with the versatile analytical capabilities offered by PAVDRN, some of its conspicuous limitations warrant a more detailed investigation of the applicability of its predictions to rainfall conditions, properties of specific pavement surface types, and the drivers' behavior in the state of Florida in particular. Hence researchers of the University of South Florida (USF) initiated a systematic investigation to validate the currently established analytical procedures and develop FDOT specific procedures and guidelines on how hydroplaning risk analysis shall be conducted in advance of highway expansion projects. The USF team designed a multi-task procedure within the general guidelines provided by FDOT to achieve the project objectives in the most efficient manner.

The main tasks performed by the USF team can be summarized as: (1) comparison of the hydroplaning potentials predicted by available analytical techniques under similar conditions; (2) evaluation of the impact of each attribute on hydroplaning potential; (3) examination of the possibility of expressing the hydroplaning potential as a risk estimate; (4) evaluation of the increased hydroplaning risk on relatively wider sections; (5) comparison of the predictions of available analytical techniques with actual hydroplaning related crash data; (6) field verification of hydroplaning speed vs. water film thickness using USF's rainfall simulator; (7) recalibration of PAVDRN or alternative analytical tools for FDOT applications; and (8) possible extension of USF's recent finite element modeling of the tire and wet pavement friction interaction to formulate an analytical procedure for prediction of hydroplaning speeds.

1.1.1 Outline of the study of wet weather speed reduction

Based on a review of past research studies, the factors identified to influence drivers' speed during rain include the following features:

- Rainfall intensity
- Water depth on pavement
- Visibility
- Lighting conditions
- Traffic volume
- Travel lane
- Wind levels
- Facility types

Given the difficulties associated with data acquisition and the wide variation of drivers responding to these conditions, it is quite challenging to simultaneously account for all the factors. The models developed to predict the reduction of driver speeds with different levels of rain intensity are generally empirical. Some studies have summarized the effect as an overall reduction percentage regardless of other factors described above while others have been based on regression techniques considering one or more factors. Recent studies have centered on the weather adjustment factors (WAF), which were modeled as functions of rainfall intensity and visibility. In this study, the capabilities of these models have been further evaluated using the Monte Carlo simulation, where the inputs were treated as random variables and a sample of 1000 simulation runs was drawn for each level of rainfall intensity. Following the research by Hranac et al. (2006), three levels of rainfall intensity were considered: light rain (<0.01 in/h), medium rain (0.01-0.25 in/h), and heavy rain (>0.25 in/h). The statistics of the simulation runs were compared to understand the performance of different models under different rainfall conditions. This comparison aims to lay the groundwork for investigation and modeling of the specific effects of rainfall on the speed of the drivers in Florida.

1.2 1.2 Summary of significant and state-of-the-art studies on wet weather speed reduction methods

Highway Capacity Manual (HCM (TRB, 2010))

- Light rain reduces free flow speed of freeways by 6 mph
- Heavy rain reduces free flow speed of freeways by 12 mph

Federal Highway Administration (FHWA)
(http://www.ops.fhwa.dot.gov/weather/q1_roadimpact.htm),

- Freeways: light rain reduces speed by about 2-13% and heavy rain reduces speed by about 6-17%

Ibrahim and Hall (1994)
Ibrahim and Hall estimated the following drops in speed for different levels of rainfall:

- Light rain reduces speed by 2 km/h.
- Heavy rain reduces speed by 10 km/h.

Kyte et al. (2000)
Kyte et al. sought to determine the impact of traffic operations for four environmental variables, precipitation intensity, wind speed, visibility, and road surface condition (dry, wet, or icy/snowy), when compared to normal conditions. The following relationship was derived:

$$Speed = 100.2 - 16.4(snow) - 9.5(wet) + 77.3(vis) - 11.7(wind) \tag{1.1}$$

where,
Speed = passenger-car speed (km/h)
snow = variable indicating presence of snow on roadway
wet = variable indicating that pavement is wet
vis = visibility, equal to 0.28 km (919 ft) when visibility $\geq$ 0.28 km and actual value of visibility when visibility $<$ 0.28 km
wind = variable indicating that wind speed exceeds 24 km/h (15 mph)

Chin et al. (2004)
Chin et al. (2004) estimated speed reduction by level of rainfall, summarized in Table 1.1.

Table 1.1 Speed Reduction by Facility Type and Level of Rainfall

Weather	Urban		Rural	
Condition	Freeway	Arterial	Freeway	Arterial
Light Rain	10%	10%	10%	10%
Heavy Rain	16%	10%	25%	10%

Hranac et al. (2006)
Hranac et al. estimated the following model using data collected in three cities (Baltimore, Twin Cities, and Seattle). The parameter estimates are shown in Table 1.2

$$WAF = \beta_1 + \beta_2 I + \beta_3 I^2 + \beta_4 v + \beta_5 v^2 + \beta_6 Iv \tag{1.2}$$

where,
WAF = weather adjustment factor
I = precipitation intensity of rain (cm/h)
v = visibility level (km)
$\beta_1, \beta_2, \beta_3, \beta_4, \beta_5$ and β_6 are model parameters

Table 1.2 Regression Analysis Summary Results (Hranac et al., 2006)

Precip.	City	n	c_1	c_2	c_3	c_4	c_5	c_6	P-value	R^2_{Adj}	Normality Test A²	Normality Test P-value	Levene Variance Test
Rain	Baltimore	32	0.963 (0.000)	-0.033 (0.001)	–	–	–	–	0.001	0.304	0.485	0.211	0.684
	Twin Cities	45	0.980 (0.000)	-0.0274 (0.000)	–	–	–	–	0.000	0.540	0.553	0.146	0.424
	Seattle	43	0.973 (0.000)	-0.0650 (0.000)	0.0240 (0.004)	–	0.0010 (0.044)	–	0.000	0.607	0.336	0.493	0.067
	Aggregate	111	0.981 (0.000)	-0.050 (0.000)	0.014 (0.011)	–	–	–	0.000	0.734	0.646	0.089	0.168
Snow	Baltimore	8	0.955	–	–	–	–	–	–	–	–	–	–
	Twin Cities	32	0.842 (0.000)	-0.131 (0.002)	–	–	0.0055 (0.000)	–	0.000	0.866	0.456	0.251	0.704
	Aggregate	40	0.838 (0.000)	-0.0908 (0.025)	–	–	0.00597 (0.000)	–	0.000	0.824	0.340	0.482	0.624

Note: Minitab reports a P-value of less than 0.0005 as 0.000.
Values in columns c_1 through c_6 represent coefficient value (p-value).

<u>Hablas (2007)</u>
Hablas estimated a free-flow reduction factor using normalized data and his model takes form of:

$$WAF = a(I)^b \tag{1.3}$$

where,
    WAF = weather adjustment factor
I = rainfall intensity (cm/h)
    a,b = model coefficients
The calibrated models are summarized in Table 1.3.

Table 1.3 Calibrated Model Coefficients (Hablas, 2007)

Precept.	City	N	*a*	*b*	*Pseaudo-R^2*	*P*-value
Rain	Baltimore	*3*	*0.9122*	*-0.0125*	98.36	*0.0032*
	Twin Cities	3	0.9588	-0.0048	83.64	0.0043
	Seattle	3	0.9495	-0.0075	90.64	0.0046
Snow	Baltimore		0.5988	-0.0971	98.93	0.0132
	Twin Cities	3	0.6946	-0.0546	99.97	0.0012
	Seattle		0.7266	-0.0205	80.75	0.0134

Mahmassani et al. (2009)

Mahmassani et al. estimated a weather adjustment factor (WAF) for the speed intercept of the speed-density relationship model. WAF takes the following form:

$$WAF = \beta_0 + \beta_1 v + \beta_2 I + \beta_3 s + \beta_4 vI + \beta_5 vs \qquad (1.4)$$

Where,

WAF = weather adjustment factor for parameter
v = visibility (miles)
I = precipitation intensity of rain (in/h)
s = precipitation intensity of snow (in/h)

$\beta_1, \beta_2, \beta_3, \beta_4$ and β_5 are model parameters

In calibrating DYNASMART, a traffic estimation and prediction system, the following relationship was derived:

$$WAF = 0.91 + 0.009v - 0.404I - 1.455s \qquad (1.5)$$

Table 1.4 provides a comparison of the speed reduction values predicted by a number of alternative methods documented in the Phase I of this study under three selected rainfall conditions.

Table 1.4 Comparison of the wet weather speed reduction predicted by alternative methods

Scenario				Free-Flow Speed Reduction Predicted by Previous Studies (mph)							
Free-Flow Speed (mph)	Rain Intensity Inch/hour			Visibility (Feet)	HCM 2000	Ibrahim & Hall 1994	Kyte et al. 2001	Chin et al. 2004	Hranac et al. 2006	Hablas (Seattle Model) 2007	Mahmassani et al. 2009	Rakha et al. (Seattle Model) 2009
70	Light	<=0.01	0.01	1500	6	4.6	5.9	7.0	1.4	1.7	6.4	2.0
				800			4.1				6.5	2.0
	Medium	0.01 - 0.25	0.1	1500	6	4.6	5.9	7.0	2.2	2.8	8.9	2.9
				800			4.1				9.0	2.9
	Heavy	> 0.25	0.5	1500	12	6.5	5.9	11.2	4.2	3.7	20.3	4.9
				800			4.1				20.3	5.0

1.3 Evaluation of the speed reduction models using a simulation process

The wet weather speed reduction (WAF) models were further evaluated by the investigators using Monte Carlo simulation, where the driving speed and rainfall intensity were considered as random variables with the following assumptions:

Facility Free-Flow Speed = 70 mph
Driving Speed (mph) ~ Normally distributed in the range (60, 5)
Rainfall intensity (in/h, light) ~ Uniformly distributed in the range (0, 0.01)
Rainfall intensity (in/h, medium) ~ Uniformly distributed in the range (0.01, 0.25)
Rainfall intensity (in/h, heavy) ~ Uniformly distributed in the range (0.25, 2)

$$\text{Sight Distance (ft)} = \frac{2000}{I^{0.68}} \frac{40}{v} \tag{1.6}$$

(Based on the study by Ivey et al., 1975)

A sample of 1,000 was drawn from each level of rainfall intensity and the WAF models were applied to predict the speed reduction accordingly. The simulation statistics are summarized in Table 1.5.

Table 1.5 Speed Reduction (mph) Statistics: Monte Carlo Simulation Results

Model	Rainfall Intensity	Mean	Std Dev.	95% CI LB	95% CI UB
Hranac et al. (2006, Aggregate Model)	Light (<= 0.01 in/hr)	1.175	0.098	1.169	1.181
	Medium (0.01 - 0.25 in/hr)	2.003	0.460	1.974	2.032
	Heavy (>0.25 in/hr)	1.650	2.530	1.493	1.807
Hablas (2007, Seattle Model)	Light (<= 0.01 in/hr)	1.120	0.266	1.104	1.136
	Medium (0.01 - 0.25 in/hr)	2.462	0.378	2.439	2.485
	Heavy (>0.25 in/hr)	3.410	0.369	3.387	3.433
Mahmassani et al. (2009)	Light (<= 0.01 in/hr)	0.023	2.583	-0.137	0.183
	Medium (0.01 - 0.25 in/hr)	7.778	2.184	7.643	7.913
	Heavy (>0.25 in/hr)	31.699	12.494	30.925	32.473
Rakha et al. (2009, Seattle Model)	Light (<= 0.01 in/hr)	-17.653	20.388	-18.917	-16.389
	Medium (0.01 - 0.25 in/hr)	2.292	1.101	2.224	2.360
	Heavy (>0.25 in/hr)	-0.959	5.760	-1.316	-0.602

As shown in Table 1.5, the shaded rows indicate either a negative mean (speed increase) or a negative lower bound of the 95% confidence interval. These negative values imply that the empirical models may not be appropriate for these rainfall scenarios. The speed reduction predicted by the aggregate model (Hranac et al., 2006) under heavy rain condition is also suspicious as it is smaller than that of the medium rain scenario and the standard deviation is much bigger. In summary, the models developed by Hranac et al. (2006) appear to be suitable for light and medium rain conditions. The models developed by Mahmassani et al. (2009) seem to be more appropriate for medium and heavy rain conditions.

1.4 Wet weather speed reduction verification study

Methods proven to be reliable in Phase I such as Mahmassani's method (Mahmassani et al., 2009) can be used to predict the probable vehicle speeds at the time of crashes in Chapter 4. A preliminary field test was conducted to verify or calibrate Mahmassani's equation (Mahmassani et al., 2009) for predicting the wet weather speed reduction under Florida conditions.

1.4.1 Experimental Setup for Data Collection

The study site was chosen near the mid block of an arterial section where the speed would not be affected by the upstream and downstream traffic signals. Visibility reduction in rain was measured using a video camera. A group of evenly distributed (at a spacing of 150 feet) highly visible power transmission posts or light posts along a road section was used for this study. The above posts were used for two purposes: (1) to serve as references for measuring the visibility in terms of distance (i.e., how far can a person see clearly during rain), and (2) to estimate the speed of a vehicle knowing the time taken by that vehicle to travel between the two reference posts. Because of the difficulty in real time analysis during rain, the recorded videos can be replayed to retrieve visibility and speed data. Based on the weather forecast, the field experimental equipment was set up during clear weather prior to a rain event. The field

experimental setup utilized is illustrated in Figure 1.1 where the field of view of the camera is indicated by the shaded triangle.
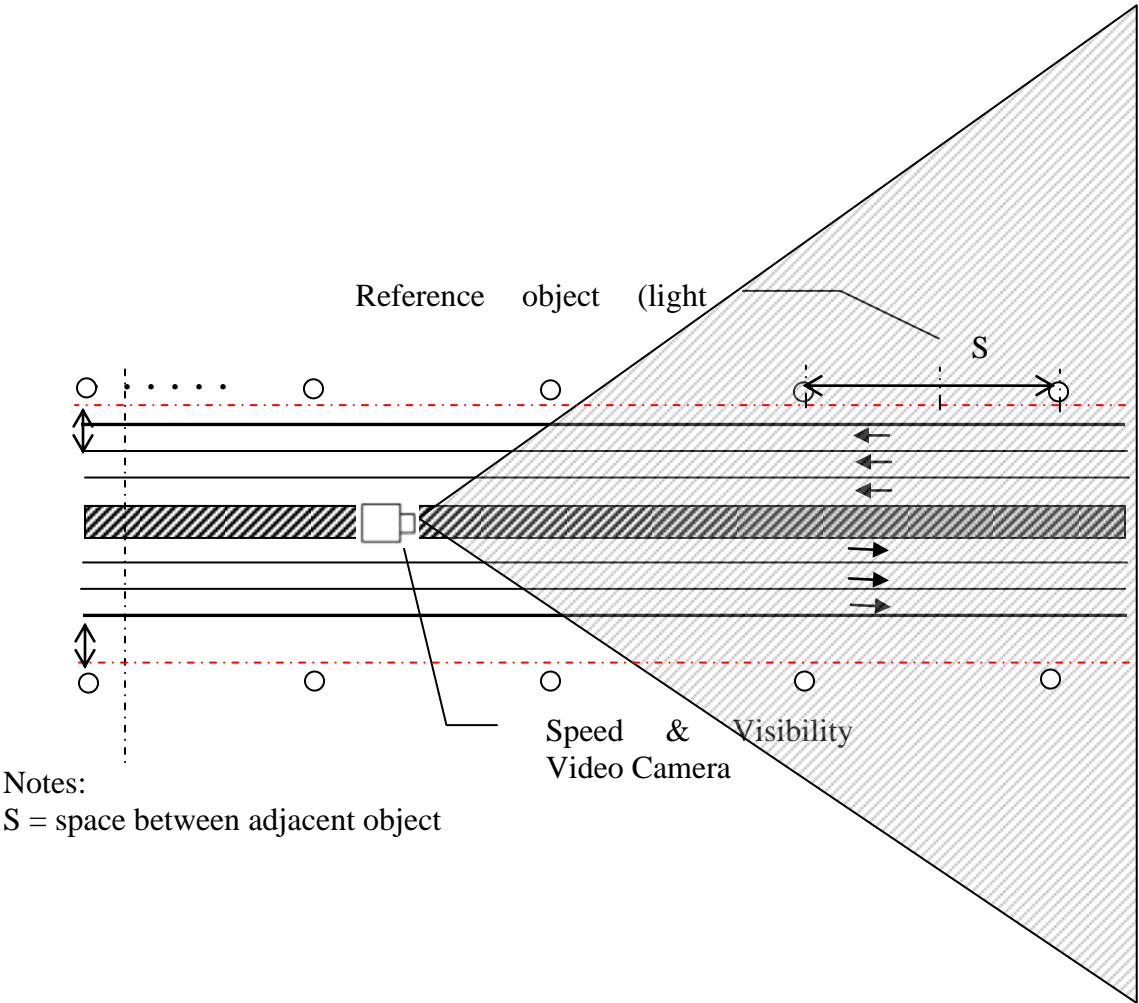
Figure 1.1 Experimental setup for measuring the wet weather visibility and speed reduction

The rainfall intensity and water film thickness on the outermost lane were measured concurrently using a rain gauge and water film gauge respectively. The visibility was measured as a distance

up to the farthest pole (or post) that can be seen with the naked eye. In addition, each vehicle was identified manually using video cameras focused on different lanes. This helped the retrieval of speed data by lane. The speed was measured based on the time (from video camera clock display) taken by a target vehicle to travel between the two selected posts.

(a) Dry weather condition

(b) Wet weather condition

Figure 1.2 Comparison of vehicle speeds under dry and wet weather conditions
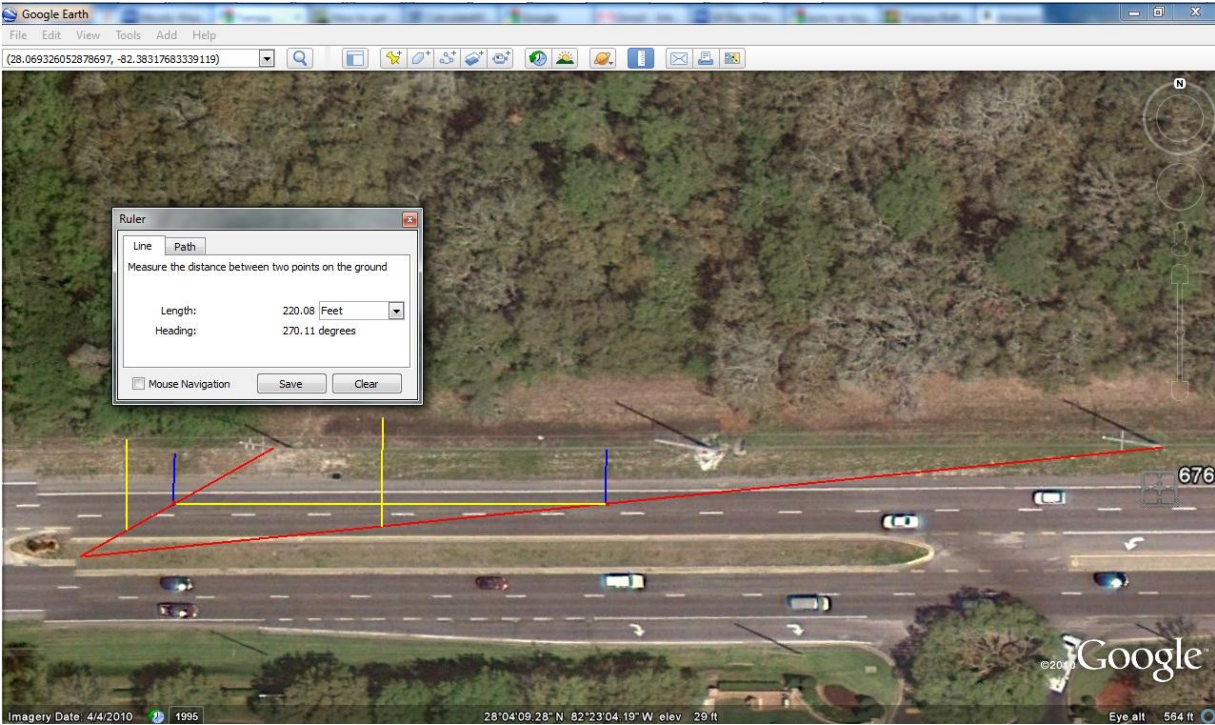
Figure 1.3 Site data evaluation using GIS maps

1.4.2 Summary of Experimental Results

As seen in Table 1.6, the USF experimental study confirmed that the reduction of vehicle speed has a significant dependence on the rainfall intensity and the vehicle density.

Table 1.6 Reduction of vehicle speed (mph) with density with rainfall intensity

		Rainfall intensity (in/h)		
		Slight rain	Medium rain	Heavy rain
density	6	1.72*	5.53	9.80
	7	2.70	5.54	10.19
	9	4.04	9.75	10.60
	11	5.67	11.76	11.80*
Vehicle (veh/mile)	14	5.80	12.67	13.22*
	16	4.13	10.88	14.24
	18	5.82*	9.14	15.12*

Video camera records were used to estimate the vehicle density by direct counting and evaluate the vehicle speeds using the video time records. During the observation period, it was not possible to obtain the traffic densities at certain rainfall intensities. Therefore the corresponding values, indicated by the asterisks, have been estimated based on the 3D surface distribution of speed reduction values.

10

CHAPTER 2

CHARACTERIZATION OF THE EFFECTS OF PERMEABILITY AND MACROTEXTURE OF PAVEMENTS

2.1 Summary of pavement permeability characteristics retrieved from literature review

Based on the current investigation, it was concluded that pavement permeability can be evaluated using the following different ways:

1. Average approximate values can be obtained from previous studies

Field permeability of FC5 was measured on US-27 in Highlands County from 2003 through 2009, showing results in the range of 0.15-0.6 cm/s (FDOT, 2009). In a recent laboratory experimental study of performance of various asphalt mixes, completed at the University of California Pavement Research Center (UCPRC), a mix (G125 or Georgia's OGFC – Open - graded Friction Course) following the same design as FC5 was tested. The permeability values were measured on slabs compacted in the laboratory using a small ride-on tandem roller compactor. Those slab specimens did not experience any traffic loading, and the permeability test was done immediately after the slabs were compacted. Therefore, the slabs were not aged. The permeability measured with a NCAT (National Center for Asphalt Technology) field permeameter had an average value of 0.31 cm/s with a standard deviation of 0.09 cm/s (Lu et al., 2010). This matched the results of the FDOT study cited above (FDOT, 2009). The UCPRC study also revealed that the above mix (G125, which is similar to FC5) had a permeability of the same magnitude as that of California 9.5-mm or 12.5-mm OGFC mixes, as shown in Figure 2.1 in which RW95 and RW125 represent California OGFC mixes with 9.5-mm nominal maximum aggregate size (NMAS) and 12.5-mm NMAS, respectively.
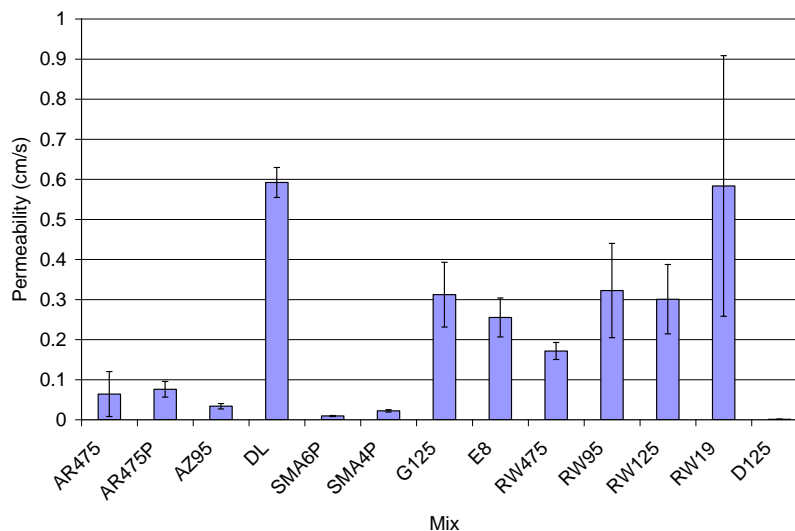
Figure 2.1 Permeability of various surface asphalt mixes (Lu et al., 2010)

The abbreviations used in Fig. 2.1 are described below:
 AR475: an open-graded mixture with a NMAS of 4.75 and an asphalt rubber binder.
 AR475P: the same as AR475 mixture except that AR475P contains a small amount (about 5%)
 of aggregates with sizes in between 4.75 mm and 9.5 mm.
 AZ95: a rubberized open-graded asphalt mixture typically used in Arizona, with a 9.5 NMAS.
 SMA6P: a stone mastic asphalt with a NMAS of 6 mm, recently experimented in Denmark.
 SMA4P: a stone mastic asphalt with a NMAS of 4 mm, recently experimented in Denmark.
 E8: an open-graded asphalt concrete mix with a 8-mm NMAS, typically used in Europe.
 RW475: same as AR475, except that it uses a PG 64-16 binder
 RW19: an open-graded asphalt concrete mixture with a NMAS of 19 mm.
 D125: a California dense-graded asphalt concrete with a 12.5 mm NMAS.

2. Specific values from the in-place air void ratios can be obtained from Figures 2.2 and 2.3.

Permeability of Superpave mixes was analyzed in a study by the Research Section and the Materials Division in Arkansas State Highway and Transportation Department (Westerman, 1998). The correlation of permeability versus lift thickness and permeability versus density was investigated and plotted as shown in Figure 2.2.
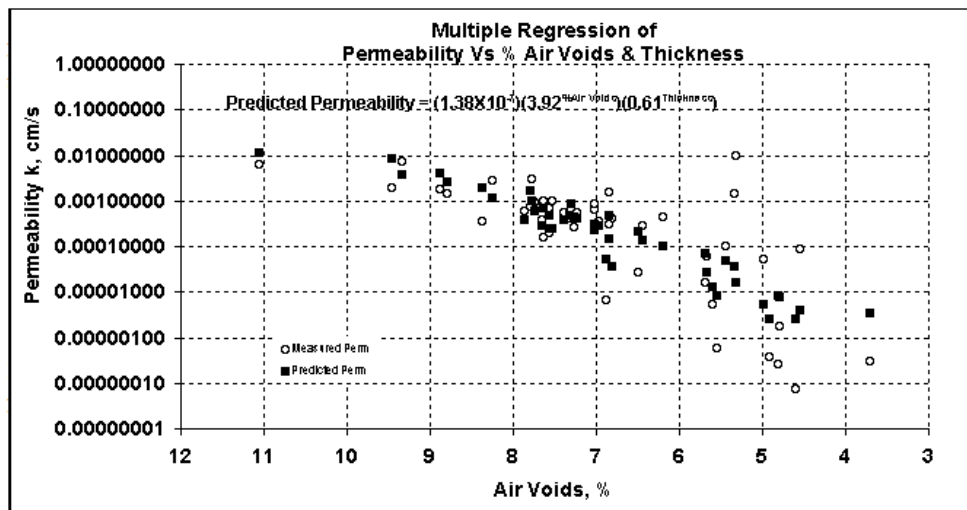
Figure 2.2 The relationship of permeability coefficient vs. in-place air voids and lift thickness (Westerman, 1998).

FDOT also investigated the permeability of coarse graded Superpave mixes (Choubane et al., 1998) and concluded that an average water permeability value not exceeding 100×10^{-5} cm/s may be low enough to prevent the infiltration of excessive water into the pavement structure. Current acceptable level of water permeability for a dense-graded mix is 125×10^{-5} cm/s.

3. A multiple-year survey of field permeability of OGFC mixes in California shows that the permeability reduces with pavement age, and roughly the reduction is one order of magnitude of every five years as shown in Figure 2.3 (in the figure, OGAC represents

OGFC with conventional or polymer modified binder; RAC-O represents OGFC with asphalt rubber binder).
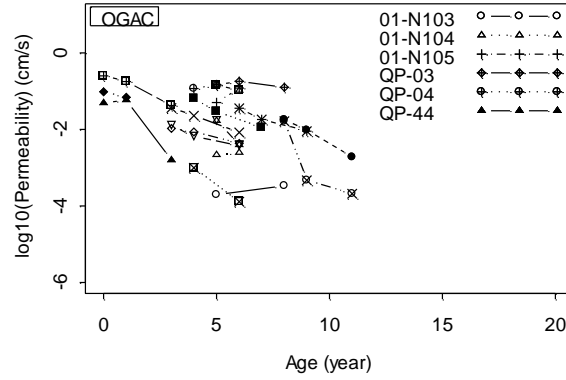
(a)
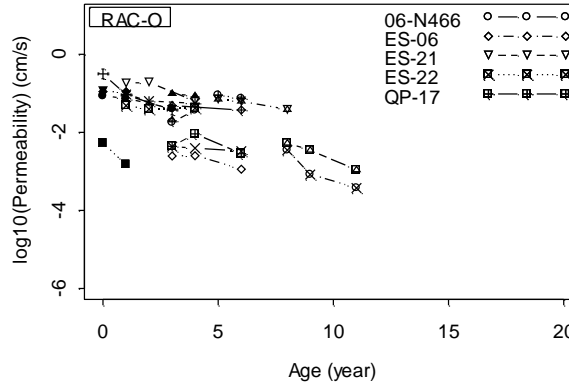
(b)

Figure 2.3 Trend of permeability of OGFC mixes (a) with and (b) without asphalt rubber binder (Lu et al., 2009).

4. Permeability of cracked and jointed pavements can be computed with Equation (2.1).

Permeability properties of pavements can be modified to account for the infiltration through cracks and joints using the following expression for infiltration rate per unit area q_i (Huang, 1993):

$$q_i = I_c \left(\frac{N_c}{W_p} + \frac{W_c}{W_p C_s} \right) + k_p \tag{2.1}$$

where I_c is the crack infiltration rate (0.22 m^3/day/m as suggested by Ridgeway [1976]), N_c is the number of longitudinal cracks, W_p is the width of pavement subjected to infiltration, W_c is the length of transverse cracks or joints, C_s is the spacing of transverse cracks or joints, and k_p is

the rate of infiltration through uncracked pavement surface, which is numerically equal to the coefficient of permeability of HMA (hot mix asphalt) or PCC (Portland cement concrete).

Based on the investigators' experience of testing at the University of California Pavement Research Center (UCPRC), the permeability of dense-graded hot mix asphalt concrete is nearly zero when the air-void content is below 5 percent, while the permeability of conventional Portland cement concrete (PCC) is also extremely small. Typically, permeability coefficients for moderate-strength concrete and low-strength concrete are of the order of 1×10^{-10} cm/sec and 30×10^{-10} cm/sec, respectively (Mehta and Monteiro, 1993). Therefore, water infiltration through uncracked dense-graded asphalt concrete pavement with an air-void content less than five percent or through PCC pavement slabs can be neglected.

2.2 Summary of pavement drainage characteristics retrieved from literature review

Due to the differences in permeability and macrotexture among various pavement surface types (i.e., open-graded friction course [OGFC], dense-graded asphalt concrete [DGAC], Portland cement concrete [PCC]), the thickness of the water film formed on a pavement surface during rain will also vary. The pavement surface texture parameters that govern the water film thickness are, Manning's coefficient, n, and the surface texture depth. From Manning equation for sheet flow, the Manning's n is calculated using the following expression (Charbeneau et al., 2008)

$$n = \frac{\sqrt{S_0}\, h^{5/3}}{q} \tag{2.2}$$

where

S_o = slope of the surface in the flow direction
H = flow depth
q = quantity of flow per unit width (m^3/s/m)

Manning's coefficient can be found by several methods: (1) based on the Reynolds number; (2) based on the drainage length and rainfall intensity; and (3) based on direct experimentation. These methods are detailed in the following pages.
:

1. Based on the Reynolds number

Anderson et al. (1998) synthesized previous research results and conducted additional laboratory experiments to develop equations of Manning's n for different pavement surfaces using regression analysis. The above equations were used in PAVDRN (NCHRP, 1998) and are reproduced below.

Portland cement concrete surfaces

$$n = \frac{0.319}{N_R^{0.48}} \qquad (N_R<1000) \qquad (2.3a)$$

$$n = \frac{0.345}{N_R^{0.502}} \qquad (N_R<500) \qquad (2.3b)$$

Dense-graded asphalt concrete

$$n = 0.0823 N_R^{-0.174} \qquad (2.3c)$$

Porous asphalt concrete

$$n = \frac{1.49 S^{0.306}}{N_R^{0.424}} \qquad (2.3d)$$

where

$$N_R = \frac{q}{v} \qquad (2.4)$$

N_R = Reynolds number
v = kinematic viscosity of water

Charbeneau et al. (2007) developed a model for a surface type similar to a PCC surface, as shown below

$$n = \frac{7.5}{N_R + 0.0122} \qquad (2.5)$$

Results from Anderson et al. (1998)'s model for PCC pavements and Charbeneau et al. (2007)'s model are illustrated in Figure 2.4.
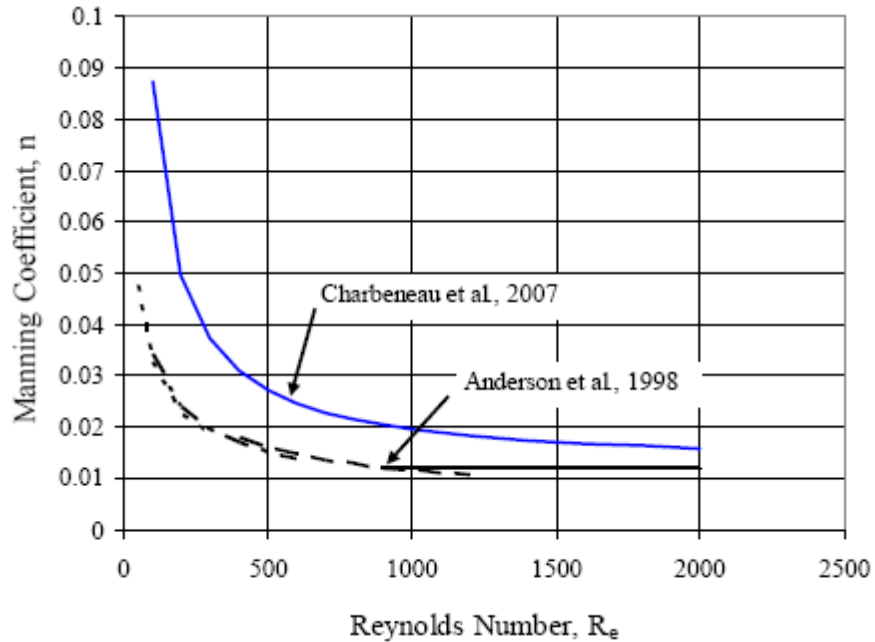
Figure 2.4 Manning's coefficient as a function of Reynolds number (Charbeneau et al., 2008)

Charbeneau et al. (2007) constructed a rainfall simulator and roadway model to investigate the sheet flow behavior on rough impervious surfaces during storm events, and suggested a model equation for Manning's n:

$$n = \frac{c_1}{N_R} + n_e \tag{2.6}$$

Where c_1 and n_e are parameters used to characterize the hydraulic properties.

Figure 2.5 shows the Manning's coefficient plotted as a function of Reynolds number for two surfaces included in their study (Charbeneau et al., 2007). Surface 1 has an effective Manning's coefficient identical to that of finished concrete (with $n_e = 0.012$). Surface 2 is much rougher than typical dense-graded asphalt concrete pavement. The parameters for Equation (2.6) are found in Table 2.1.

16
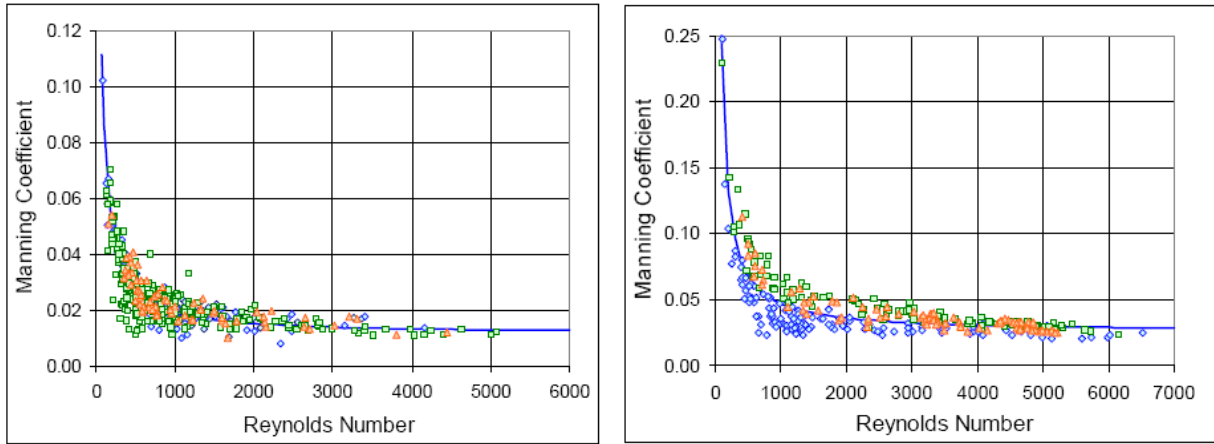
Figure 2.5 Comparison of Manning coefficient for surface 1 (left) and surface 2 (right) experiment data (Charbeneau et al., 2007).

Table 2.1 Model parameters for Manning's coefficient (Charbeneau et al., 2009)

Surface	c_1	n_e
1	7.5	0.0122
2	21.3	0.0253

Charbeneau et al. (2009) used the same system to study the sheet flow on a simulated pavement surface with intermediate roughness (a mean texture depth of 2.2 mm). They used the Manning's equation in the form of a linear regression model to analyze experiment data:

$$h = c_0 + c_1 \left(\frac{q}{\sqrt{S_0}} \right)^{0.6} + e \tag{2.7}$$

where c_0 and c_1 are regression parameters, and e is a random error term. From this equation, Manning's coefficient can be calculated as

$$n = \frac{(h - c_0)^{5/3} \sqrt{S_0}}{q} \tag{2.8}$$

The calculated Manning's coefficient versus Reynolds number for that surface is shown in Figure 2.6.
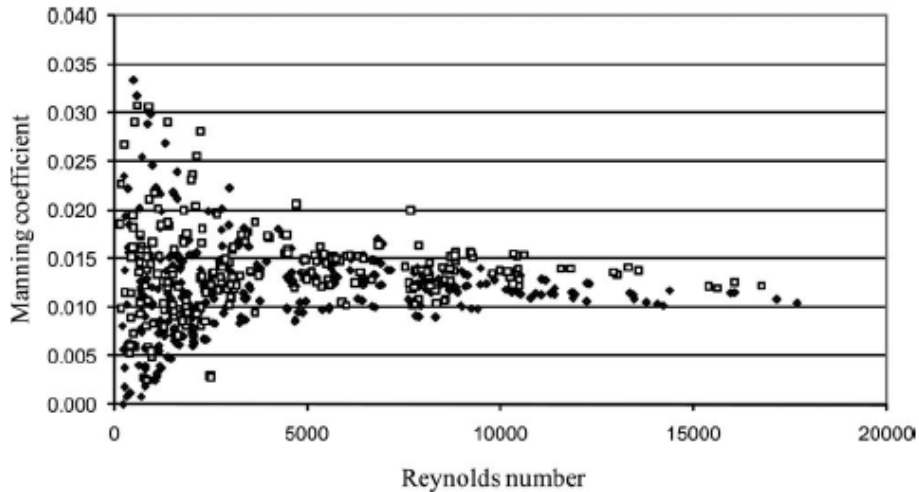
Figure 2.6 Manning's coefficient as a function of Reynolds number for Surface 3; (shaded diamond) no-rain conditions; (open square) rainfall conditions (Charbeneau et al., 2009)

2. Based on the drainage length and rainfall intensity

NCHRP (1998) also provides the relationships for Manning's n with respect to the rainfall intensity and the drainage length for different pavement types. Fig. 2.7 is one such relationship valid for porous asphalt concrete (OGFC). Similar plots are also given for DGFC and PCC pavements (NCHRP,1998). The rationale for these relationships can be understood based on the realization that the Reynolds number of sheet flow can be related to the rainfall intensity and drainage length.
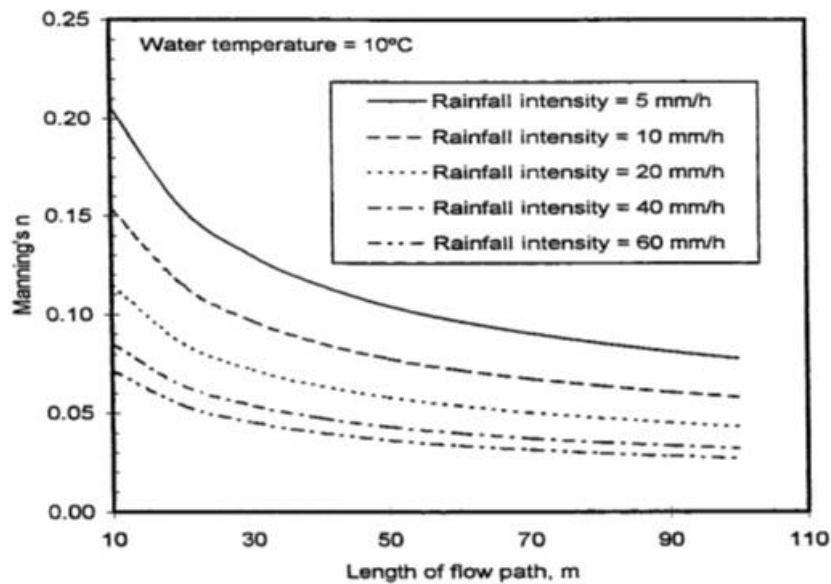
Figure 2.7 Manning's n vs. length of flow path for variousrainfall rates (NCHRP, 1998)

3. Based on direct experimentation

The following pavement surface properties were obtained from the field rainfall simulation described in Chapter 6 (Section 6.1).

Macrotexture depth = 0.0159 inches
Manning's coefficient = 0.075

2.2.3.1 Results of USF's Experimentation

Investigators used a NCAT permeameter to evaluate the field permeability of OGFC and Dense -graded asphalt. The results are illustrated in Tables 2.2 and 2.3.

Table 2.2 Permeability of Open-graded Friction Course (OGFC) (Fowler Avenue, Tampa, Florida)

Permeability of Open-graded Friction Course (OGFC) –in/s		
Site	Average	Std. Dev.
A	0.004044488	0.000352362
B	0.002956299	0.000536614
C	0.004363386	0.000831102
All	0.003788189	0.000573228

Table 2.3 Permeability of Dense-graded Asphalt (DGA) (Fletcher Avenue, Tampa, Florida)

Permeability of Dense-graded Asphalt (DGA) (in/s)		
Site	Average	Std. Dev.
A	6.10236E-05	2.91339E-05
B	0.000316929	0.000125591
C	0.000417323	6.29921E-05
All	0.000264961	7.24409E-05

It must be noted that the test values represent the average of many trials performed with running water and under regular falling head conditions. As seen in Figure 2.8, there was no significant difference between the two types of test results. Figure 2.8 also shows that the coefficient of permeability decreases with test repetitions until it stabilizes after a large number of trials. This trend can be explained by the gradual saturation process that is achieved by the initial tests, during which water is used to saturate the pavement pores. Hence, the steady-state coefficient of permeability can be obtained from the stabilized flow rate that occurs after the saturation process is complete.
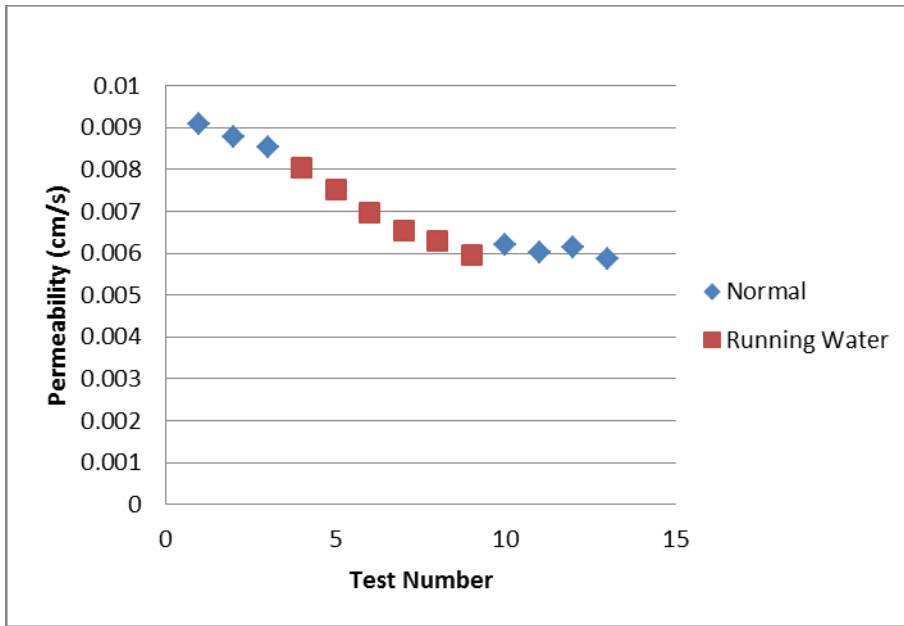
Figure 2.8 Comparison of permeability values (on Fowler Avenue) obtained from two testingconditions (normal conditions and under running water)

CHAPTER 3

COMPARISON OF THE HYDROPLANING SPEED VS WATER FILM THICKNESS RELATIONSHIPS

3.1 Summary of hydroplaning speed prediction methods

Based on the current investigation, several distinct but reliable hydroplaning speed prediction methods were seen to be available:

1. National Aeronautics and Space Administration (NASA) original and modified equations

2. PAVDRN equations

3. TXDOT equations

4. USF's equations based on Ong and Fwa's (2007b) comprehensive numerical predictions

Of the above, the first three predictive methods are *empirical in nature* and developed *under specific experimental conditions* (e.g., locked-wheel skid tester tires under one wheel load, tire pressure, and water film thickness). Hence their applicability is restricted for investigations that involve a wide variety of vehicle types. On the other hand, Ong and Fwa's (2007b) numerical predictions are based on a model that considers the mechanics of the entire hydroplaning scenario and hence accounts for all the relevant variables. In USF's current investigation, this has also been verified against the first three methods under conditions where the former methods are applicable. Availability of alternative and reliable tools for the prediction of hydroplaning threshold is encouraging. USF possesses the equipment to *further verify* the applicability of the above predictive methods before the final recommendations are delivered thus addressing the risks involved in lane expansion over the recommended limits.

3.1.1 NASA original equation (Horne and Dreher, 1963)

Based on tests conducted on *ribbed* and *smooth* aircraft and automobile tires on an average water depth of 7.62 mm, the following equation was first developed at NASA:

$$v_p = 6.36\sqrt{p_t} \tag{3.1a}$$

where v_p = Hydroplaning speed (km/h) and t = Water film thickness (mm)

3.1.2 NASA modified equation (Horne et al, 1986)

Based on tests conducted on ASTM E 501 *ribbed* and ASTM E 524 *smooth* tires and *worn truck* tires traveling on flooded pavements, the above equation was modified to include the tire aspect ratio as follows:

$$v_p = 83.35 - 27.59(FAR) + 0.168p_t \tag{3.1b}$$

where, v_p = hydroplaning speed (km/h), t = water film thickness (mm) and *FAR*= footprint aspect ratio = width/length ratio of footprint

3.1 3 PAVDRN equations (NCHRP, 1998)

The hydroplaning model used in PAVDRN is based on the work of Gallaway et al. (1979) and his colleagues and further developed by others (Henry and Meyer, 1980) and Huebner et al., 1986)). On the basis of the work reported by the authors of PAVDRN,

For water film thicknesses (WFT) less than 2.4 mm,

$$v_p = 96.3t^{-0.259} \tag{3.2a}$$

Where, v_p = Hydroplaning speed (km/h), t = Water film thickness (mm)

For water film thicknesses greater than or equal to 2.4 mm,

$$v_p = 4.94A \tag{3.2b}$$

where *A* is the greater of the values calculated using Equations (3.3a) and (3.3b):

$$\left[\frac{12.64}{t^{0.06}} + 3.507 \right] \tag{3.3a}$$

or

$$\left[\frac{35.15}{t^{0.06}} - 7.817 \right](0.0393MTD)^{0.14} \tag{3.3b}$$

where
v_p = Hydroplaning speed (km/h), t = Water film thickness (mm), *MTD* = macrotexture depth (mm). It is noted that equations (3.2)-(3.3) do not consider the effect of the tire inflation pressure probably because the tests were performed under an inflation pressure of 165.5 kPa which is thetypical inflation pressure of the locked-wheel tester tires (ASTM E 501 *ribbed* and ASTM E 524 *smooth* tires).

3.1.4 TxDOT equations (Gallaway et al., 1979)

English

$$v = SD^{0.04} p_t^{0.3} (TD+1)^{0.06} A \tag{3.4a}$$

Metric

$$v = 0.9143 SD^{0.04} p_t^{0.3} (TD+0.794)^{0.06} A \tag{3.4b}$$

where TD= tire tread depth (0.5 mm recommended),

$$SD = \left(\frac{\omega_d - \omega_w}{\omega_d} \right) 100$$

= Spin down ratio (approximately 10% at initiation of hydroplaning)

ω_d and ω_w are rotational velocity of wheel on dry and wet surfaces respectively, and
A is the greater of,

English

$$(10.409 / t^{0.06}) + 3.507 \text{ or } \{(28.952 / t^{0.06}) - 7.817\} * TXD^{0.14} \tag{3.5a}$$

Metric

$$(12.639 / t^{0.06}) + 3.50 \text{ or } (22.351 / t^{0.06} - 4.97) * TXD^{0.14} \tag{3.5b}$$

TXD = Pavement texture depth (0.5 mm recommended)

Inspection of equations (3.4)-(3.5) show that they do not include the wheel load as a parameter, which is an important attribute of hydroplaning.
Figure 3.1 shows that the PAVDRN and TXDOT equations match reasonably well for water film thickness values above 2.4 mm whereas PAVDRN over-predicts hydroplaning speed for water film thicknesses less than 2.4 mm.
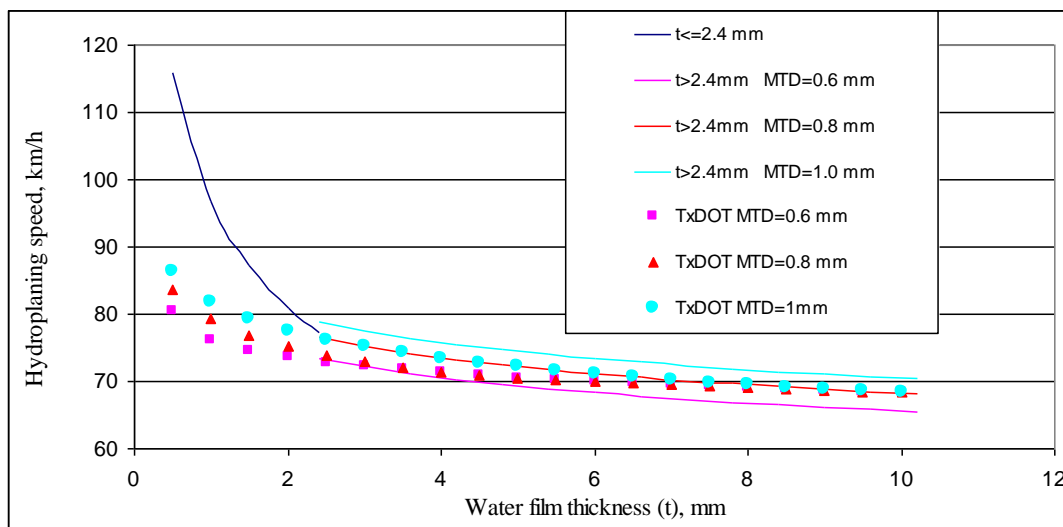
Figure 3.1 Comparison of TXDOT and PAVDRN equations for hydroplaning speed

3.1.5 Investigators' extension of Ong and Fwa (2007b) relationships for the Locked Wheel Tester tire (ASTM E524-88 standard smooth tire)

Ong and Fwa (2007a) presented the results of a comprehensive finite element model that was formulated for accurate prediction of the hydroplaning conditions. As discussed in Section 3.1.3 the analysis of hydroplaning and skid resistance presented by Ong and Fwa (2007b) considered the ASTM E524-88 standard *smooth* tire. Figure 3.2(a) and 3.2(b) show the variation of hydroplaning speed with wheel load, tire inflation pressure and water film thickness.
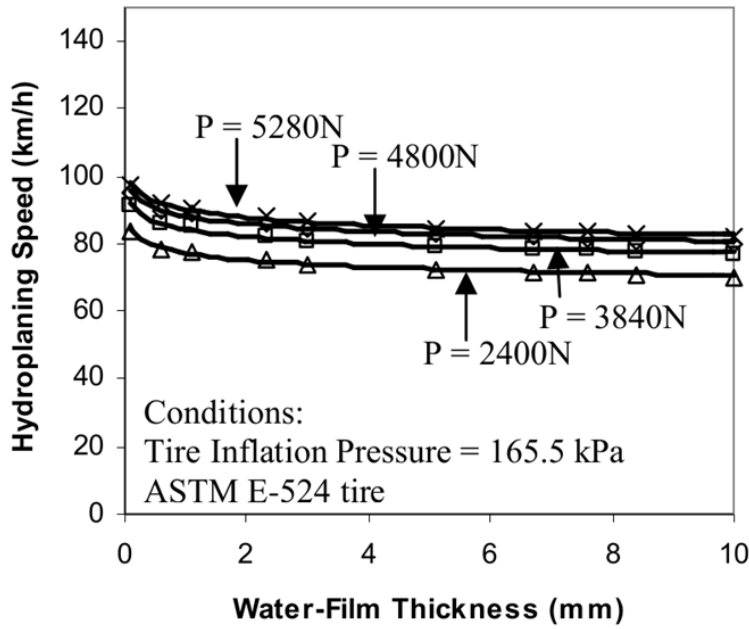
(a)
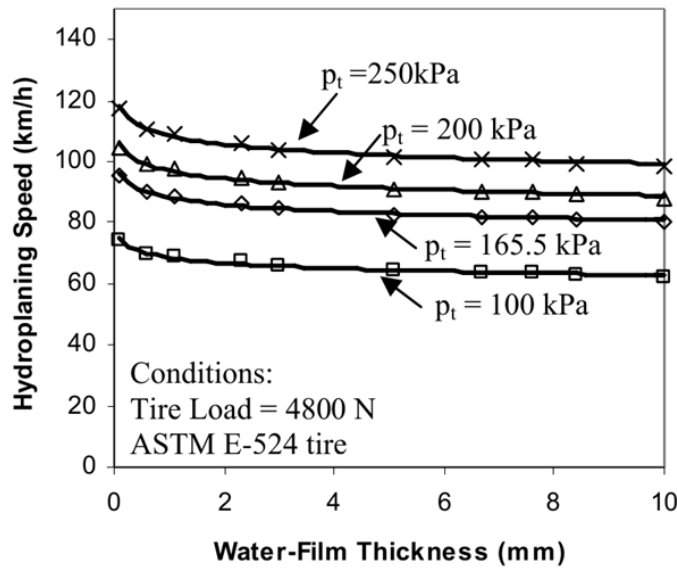
(b)

Figure 3.2 Sample plots of Ong and Fwa (2007b) showing the dependency of the hydroplaning speed on the water film thickness, inflation pressure, and the tire load

The following relationships were established by the investigators based on the plots in Figure 3.2.

Hydroplaning speed vs. tire load

$$v_p = \frac{10.49(WL)^{0.1957}}{t_w^{0.06}} + 6.28(WL)^{0.1961} \tag{3.6a}$$

Hydroplaning speed vs. inflation pressure

$$v_p = \frac{4.27(P_t)^{0.5001}}{t_w^{0.06}} + 2.58(P_t)^{0.4989} \tag{3.6b}$$

By combining equations (3.6a) and (3.6b) the following equation was developed:

$$V_P = (WL)^{0.2}(P_t)^{0.5}\left[\frac{0.82}{t^{0.06}} + 0.49\right] \tag{3.6c}$$

The investigators believe that equation (3.6c) can be used to predict the hydroplaning speeds for many different light vehicles that employ tires that are compatible with the locked-wheel tester tires. Passenger cars also fall into this category.
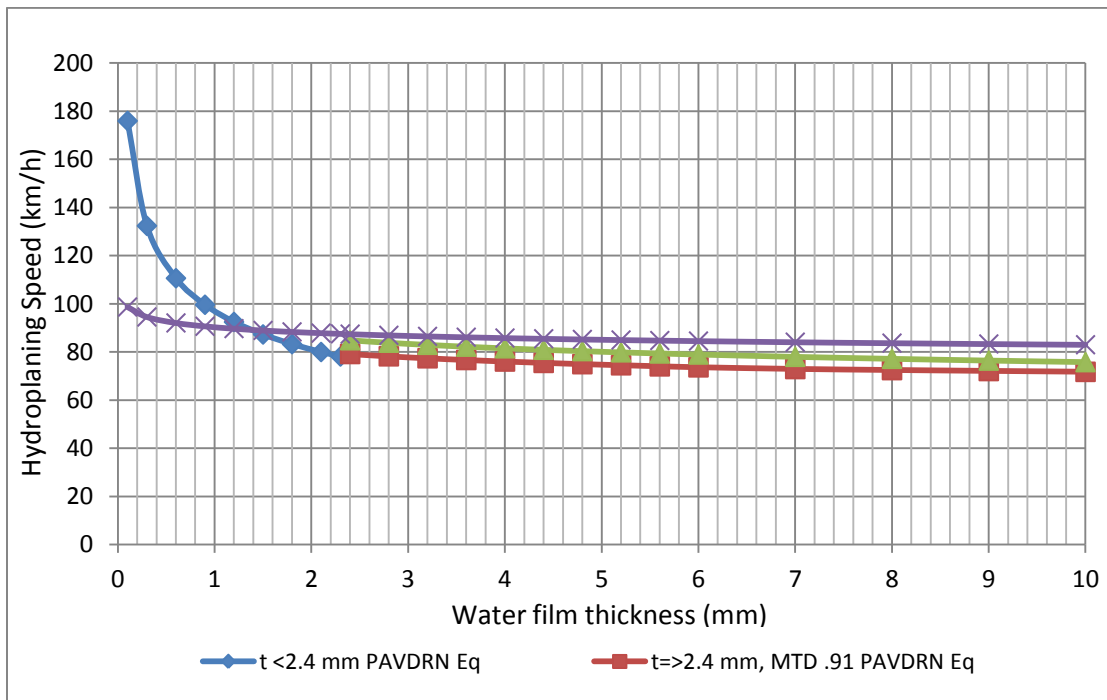
Figure 3.3 Comparison of Ong and Fwa (2007b) and PAVDRN equations for hydroplaning speed (equations (3.6c) and equations (3.1)-(3.3))

The applicability of equation (3.6c) was investigated by comparing its predictions with those of PAVDRN. To achieve this objective the predictions of equation (3.6c) for the specific case of the locked-wheel tire were plotted against those of PAVDRN as seen in Figure 3.3. While it is seen that both methods are more or less in agreement for water film thicknesses in excess of 2.4 mm, once again PAVDRN equations over-predicts the hydroplaning speed for thicknesses lower than 2.4 mm.

Moreover, it has been shown that the Ong and Fwa (2007a) predictions are also in agreement with the corresponding predictions based on the NASA hydroplaning equation (Figure 3.4).
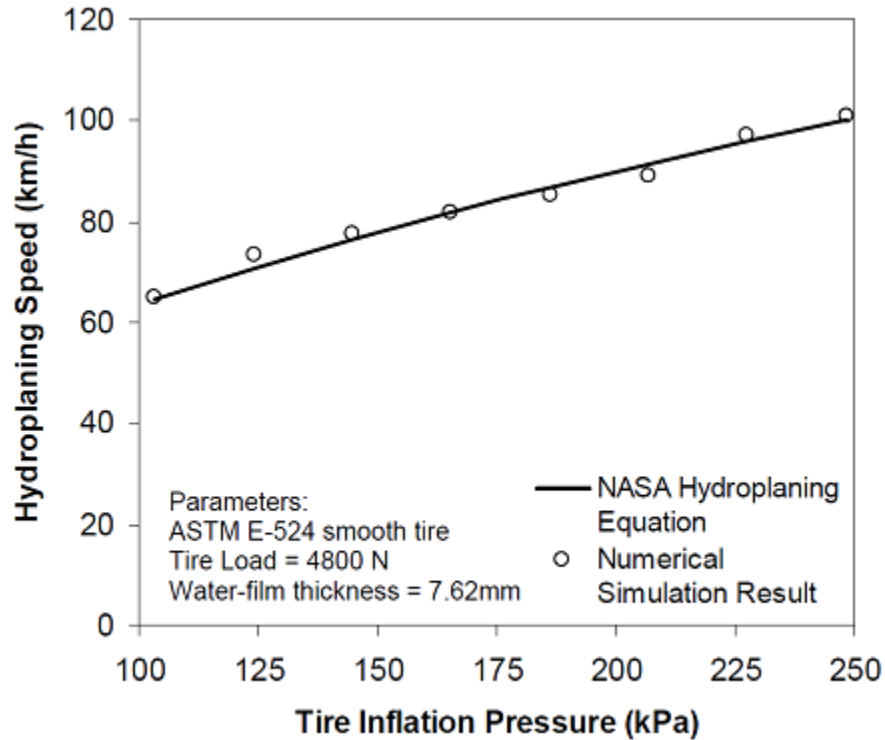
Figure 3.4 Comparison of the Ong and Fwa (2007b) hydroplaning model prediction with NASA hydroplaning equation

3.1.4 Investigators' extension of Ong and Fwa (2008) relationships for truck tires

Ong and Fwa (2008) have compared their numerical hydroplaning predictions for worn truck tires with the following Horne and Dreher's (1963) equation developed based on the research performed at NASA.

$$v_p = 25(p_t)^{0.21}\left(\frac{1.4}{FAR}\right)^{0.5} \tag{3.7a}$$

where FAR is the tire footprint aspect ratio

26

The investigators modified Horne's equation to include the water film thickness in the following format based on the numerical results published in Figure 3.5.

$$v_p = a(p_t)^{0.21}\left(\frac{1.4}{FAR}\right)^{0.5}\left(\frac{b}{t_w{}^n}+1\right)$$ (3.7b)
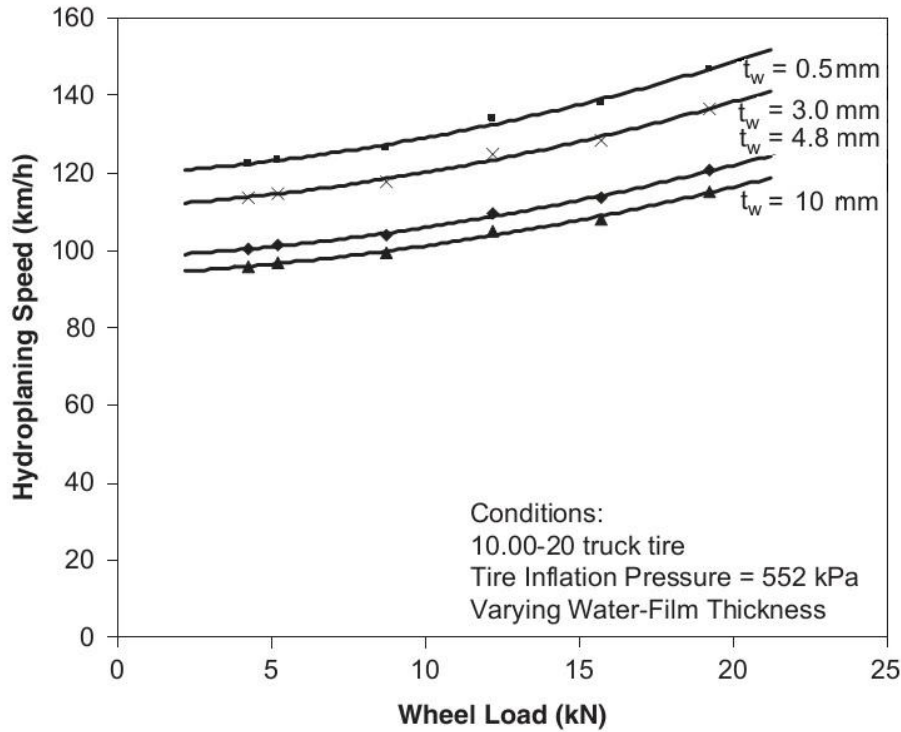
Figure 3.5 Sample plots of Ong and Fwa (2008) showing the dependency of the hydroplaning speed on the water film thickness, inflation pressure and the tire load

Then the investigators plotted the data from the above relationship on a hydroplaning speed Vs water film thickness plot as seen in Figure 3.6. The curves in Figure 3.6 are extended up to water film thickness of 20 mm to evaluate the constant *a* in equation (3.7b). In fitting the equation (3.7b), the FAR value corresponding to a given wheel load was determined from Figure 3.6. Finally, the relationship developed by the authors can be expressed as:

$$v_p = 23.1(p_t)^{0.21}\left(\frac{1.4}{FAR}\right)^{0.5}\left(\frac{0.268}{t_w{}^{0.651}}+1\right)$$ (3.7c)

Equation (3.7c) can be used conveniently to evaluate the hydroplaning speed of truck tires for any inflation pressure, tire load and water film thickness combination.

27
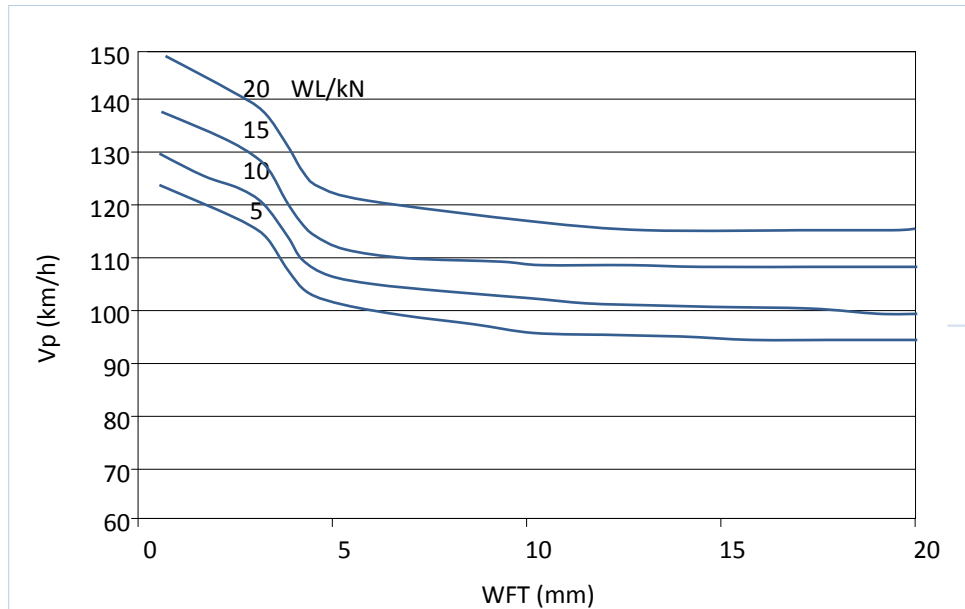
Figure 3.6 Data in Figure 3.2 replotted on Vp vs. water film thickness (t) plot
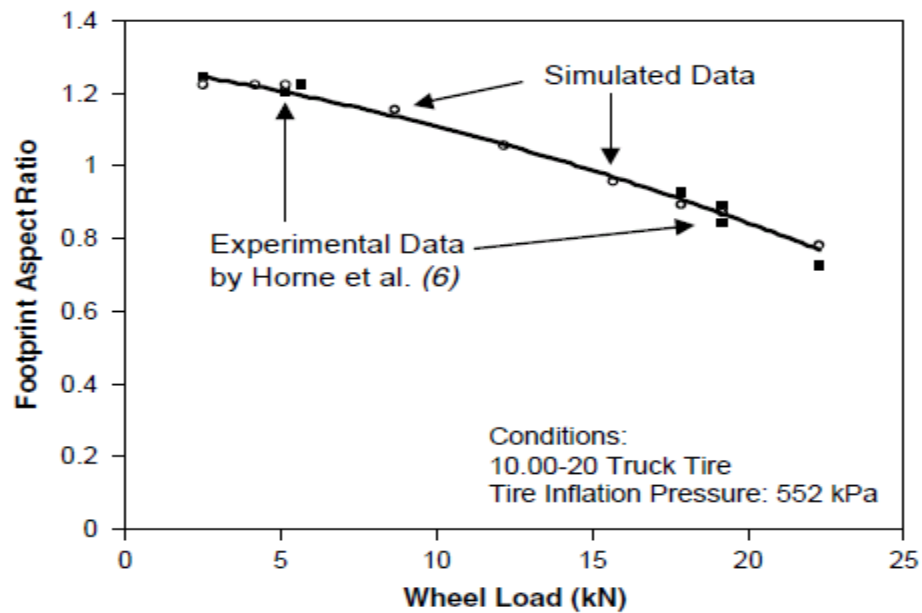
Figure 3.7 Sample plots of Ong and Fwa (2008) showing the variation of *FAR* with tire load

Figure 3.8 shows the comparison of the developed relationship (equation 3.7(c)) and the data in Figure 3.7.
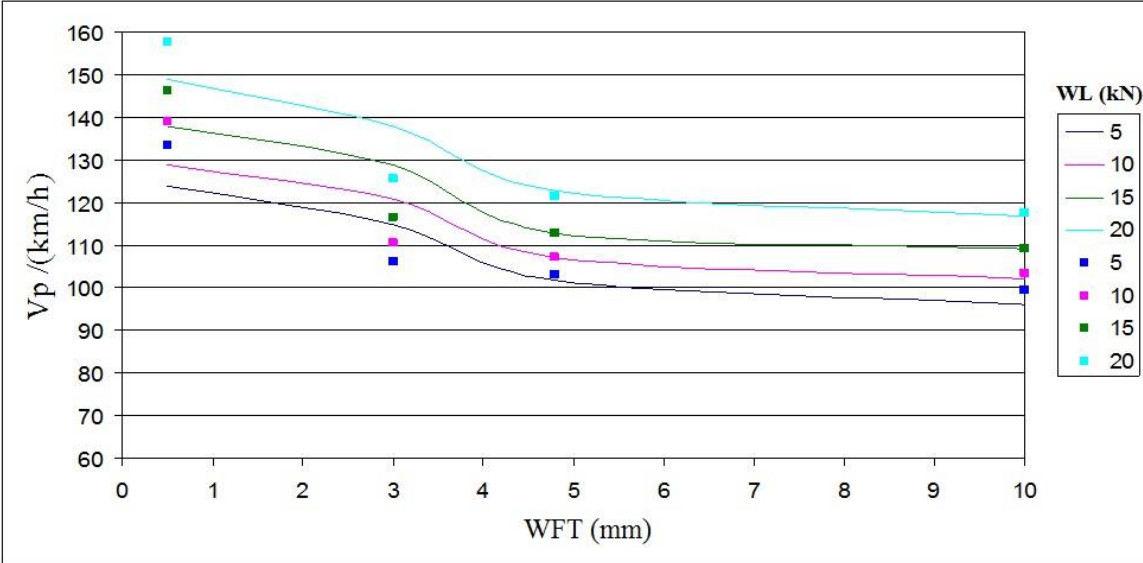
Figure 3.8 Verification of the expression for hydroplaning speed (WFT=water film thickness)

Figure 3.9 shows the effect of microtexture of the pavement surface on the hydroplaning speed.
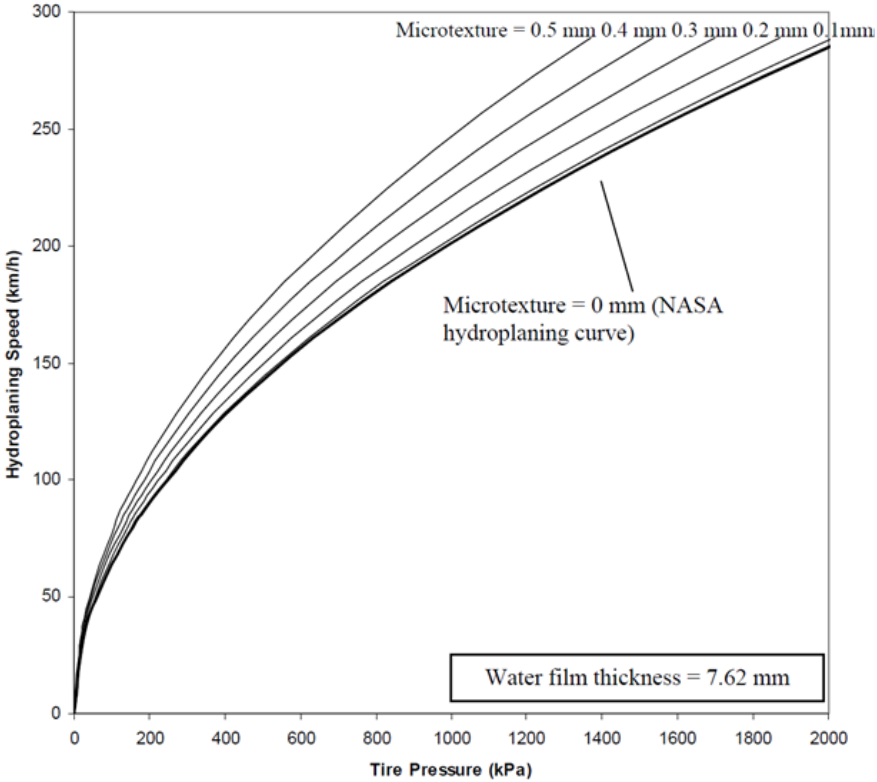
Figure 3.9 Effect of pavement microtexture on the hydroplaning speed (Ong, 2006)

3.1.5 Analysis of the impact of contributing factors on the hydroplaning potential

Prior to designing any experimental procedure to evaluate the tributary parameters of a given model, it is an appropriate and essential practice to determine the impact of each parameter on the final outcome, i.e., the risk of hydroplaning. This process is known as the sensitivity analysis in the analytical modeling arena. The USF team conducted a simple statistical procedure to achieve this objective.

3.1.5.1 Sensitivity of hydroplaning speed attributes of a locked-wheel tire

The versatility of equation (3.7c) for prediction of the hydroplaning speed of a locked-wheel tire enabled the USF investigators to determine the impact of each attribute on the hydroplaning speed and its sensitivity. A sensitivity study was conducted for this purpose using the ranges of values shown in Table 3.1 for each significant attribute. Figure 3.10 demonstrates the results of the sensitivity study where it is seen that the tire inflation pressure had the most significant impact on the hydroplaning speed.

Table 3.1 Data range matrix used for sensitivity analysis

Wheel load (N)	Water film thickness (mm)	Tire inflation pressure (kPa)
2500	1	100
3500	4	150
4500	7	200
5500	10	250

3.2 Summary of water film thickness prediction methods

Based on Phase I of the investigation, the following were concluded for the prediction of water film thickness on pavements during rainfall events:

1. NCHRP (1998) theoretical equation based on the Manning's n under-predicts the water film thickness, compared to the empirical method provided in NCHRP (1998).
2. PAVDRN program results are based on the empirical method.
3. Charbenaeu et al.'s (2008) numerical predictions of the water depths at normal crown sections agree reasonably well with those of NCHRP.
4. USF investigators also have developed an empirical tool for prediction of water depths at one of the most critical sections for this project, i.e., superelevation transition sections.

Once again, the availability of alternative and reliable tools for the prediction of the water film depth during rainfall events is encouraging. USF possesses the equipment to further verify the

applicability of the above predictive methods before the final recommendations are delivered thus addressing the risks involved in lane expansion over the recommended limits.
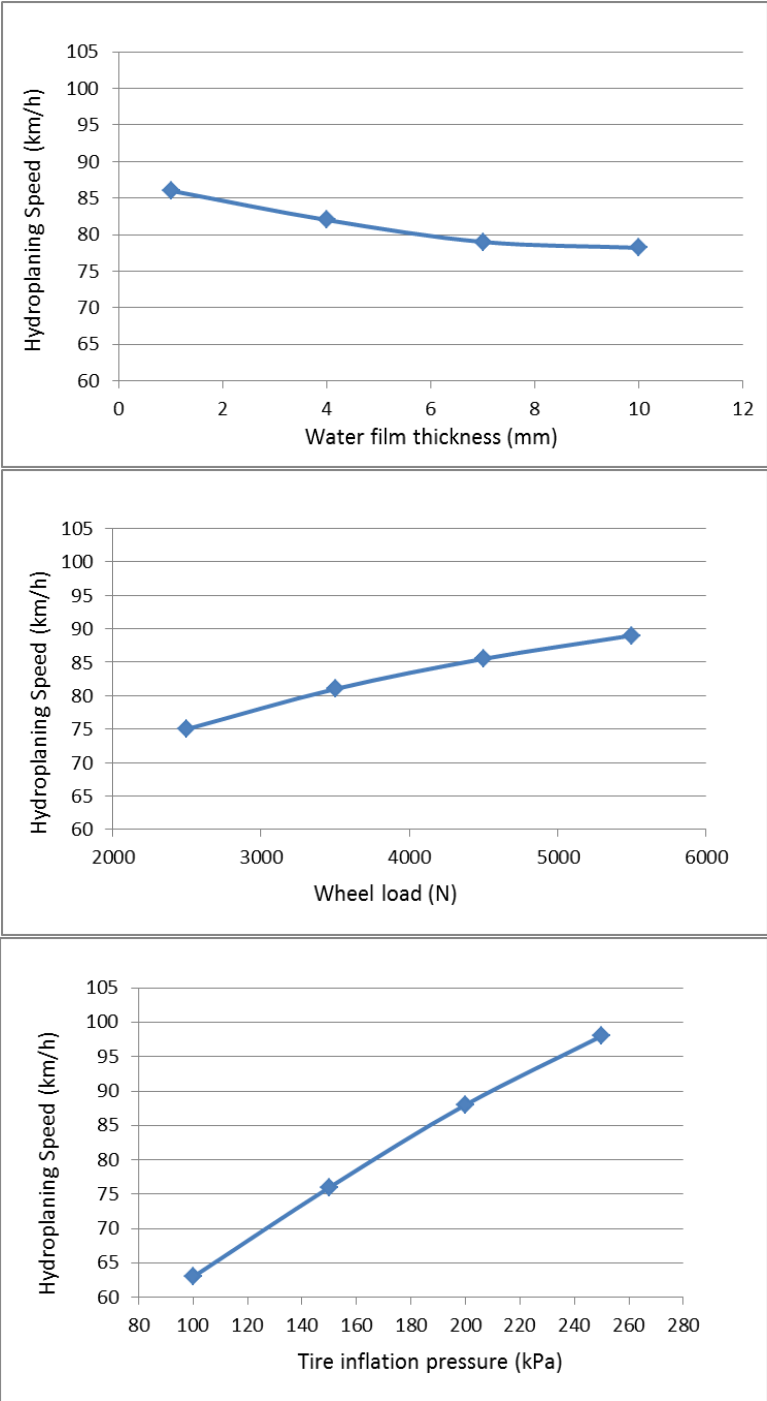
Figure 3.10 Sensitivity analysis of the hydroplaning speed

3.2.1 Comparison of the alternative water film thickness predictions on non-superelevations

Based on Phase I of the current investigation, the following equations were found to be available for the prediction of water film thickness due to a rainfall event:

Empirical equation from NCHRP (1998) (PAVDRN software)

$$t = \frac{0.003726 L^{0.519} I^{0.562} MTD^{0.125}}{S^{0.364}} - MTD \qquad (3.8a)$$

t = Water depth from top of asperities (in)
I = Rainfall intensity (in/h)
S = Slope of pavement
MTD = Texture depth (sand patch) (in)
L = Drainage length (ft)

Figure 3.11 shows the variation of the water film thickness with the drainage length as predicted by the empirical equation (3.8a) for different rainfall intensities (I).
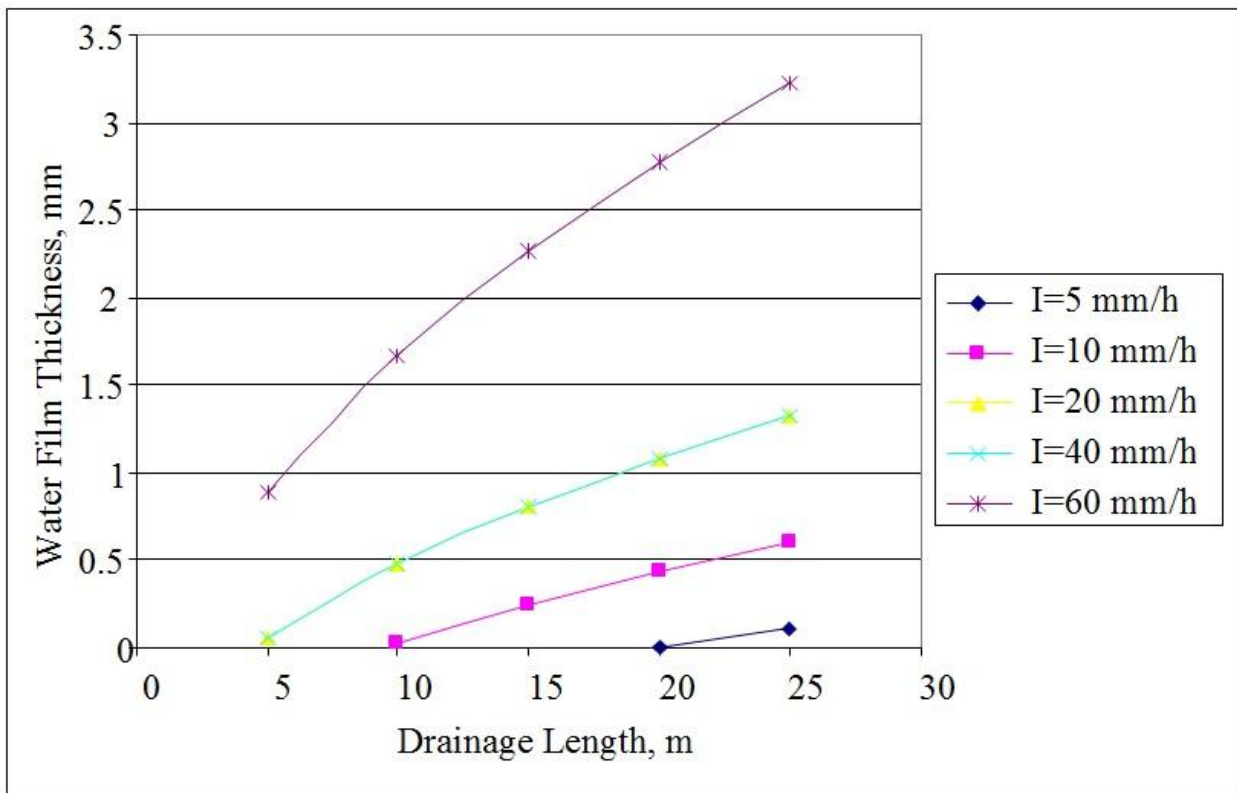
Figure 3.11 Water film thickness Vs drainage length plot based on equation (3.8a)

Empirical equation due to Gallaway et al. (1979)
(For concrete surfaces)

$$t = [0.203](MTD)^{1.325}(L)^{0.443}(I)^{0.598}(1/S)^{0.355} - MTD \qquad (3,8b)$$

Empirical equation due to Gallaway et al. (1979)

$$t = [0.003338](MTD)^{0.11}(L)^{0.43}(I)^{0.59}(1/S)^{0.42} - MTD \qquad (3.8c)$$

New Zealand Road Research Laboratory Equation (Chesterton et al., 2006)

$$t = [0.046](L)^{0.5}(I)^{0.5}(1/S)^{0.2} - MTD \qquad (3.8d)$$

t = Water depth from top of asperities (mm)
I = Rainfall intensity (mm/h)
S = Slope of pavement
L = Drainage length (m)

Water film thickness computation from Manning's equation (NCHRP, 1998)

English

$$t = \left[\frac{nLI}{36.1S^{0.5}}\right]^{0.6} - MTD \qquad (3.9a)$$

n = Manning's roughness coefficient,
L = Drainage path length (in)
I = Rainfall rate (in/h)
S = Slope of drainage path (in/in)
MTD = Mean texture depth (in)

Metric

$$t = \left[\frac{nLI}{105.42S^{0.5}}\right]^{0.6} - MTD \qquad (3.9b)$$

n = Manning's roughness coefficient,
L = Drainage path length (m)
I = Rainfall rate (mm/h)
S = Slope of drainage path (mm/mm)
MTD = Mean texture depth (mm)

Roughness parameters shown in Table 3.2 have been used to obtain the water film thickness evaluation in (3.9a) and (3.9b).

Table 3.2 Typical roughness parameters used in PAVDRN (NCHRP, 1998)

Pavement type	MTD (mm)	Manning's n
PCC	0.91	0.031
DGAC	0.91	0.0327
OGAC	1.5	0.0355

Figures 3.12(a) and 3.12(b) show the NCHRP (1998) plot and the corresponding plot developed by the investigators for prediction of the variation of water film thickness for different drainage lengths at a rainfall intensity of 40 mm/h for PCC, DGAC and OGAC pavements, based on equation (3.9a). Although the plots in Figures 3.12(a) and 3.12(b) are in agreement, it can be seen that a significant disparity is observed when one compares either of the Figures (3.12a or 3.12b) with the plot for I = 40 mm/h in Figure 3.11. The investigators discovered that the source of this discrepancy is the inaccurate constant term 36.1 of equation (3.9a). It was also discovered that the corresponding metric version (equation 3.9b) provides more reasonable predictions.

Figures 3.13(a)-(d) illustrate the comparison between the predictions of the theoretically derived equation (3.9b) and those of the empirical equation 3.8(a) for different pavement types. It must be noted that in Figures 3.13(a)-(d), the plots corresponding to the Research equation refers to equation 3.9(b) with Manning's n evaluated from Figure 2.7 whereas the empirical equation refers to equation 3.8(a).
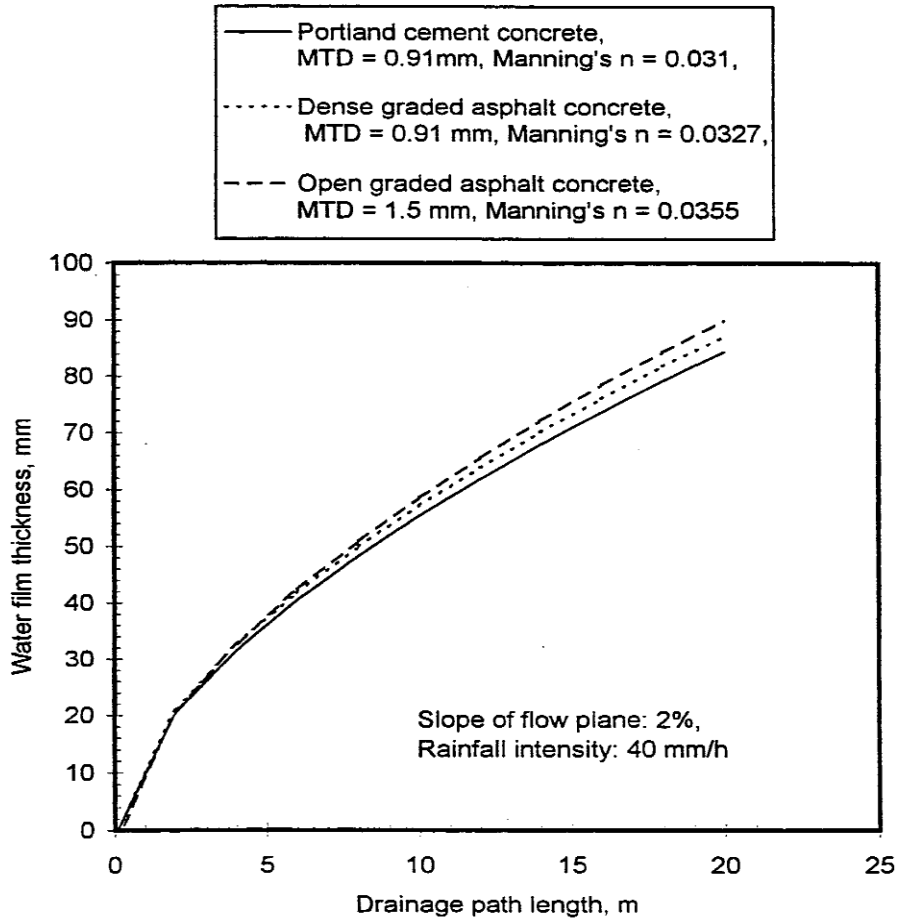
Figure 3.12(a) Water film thickness vs. drainage length plot based on equation (3.9a) (NCHRP, 1998)

Observation of Figures 3.13(a)-(d) clearly shows that NCHRP (1998) theoretical equation based on the Manning's n under-predicts the water film thickness significantly compared to the empirical equation 3.8(a). Therefore, the USF investigators sought a more mechanistic model based predictions of the water film thickness.
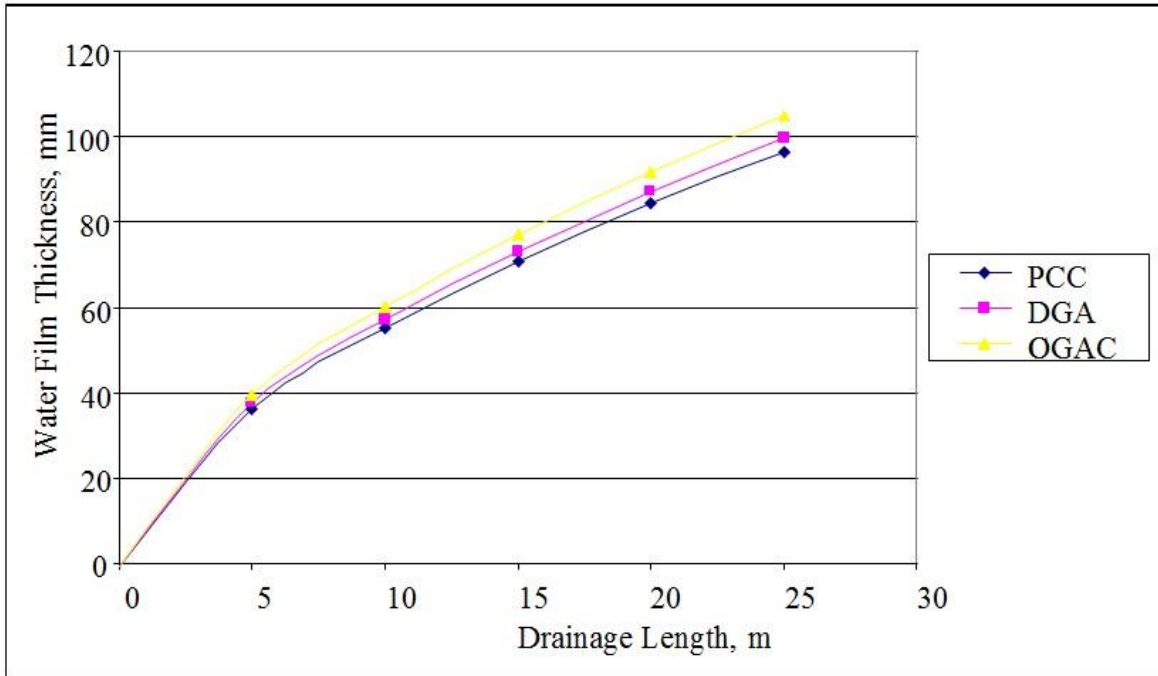
Figure 3.12(b) Water film thickness vs. drainage length plot based on equation (3.9a) based on investigators' calculations
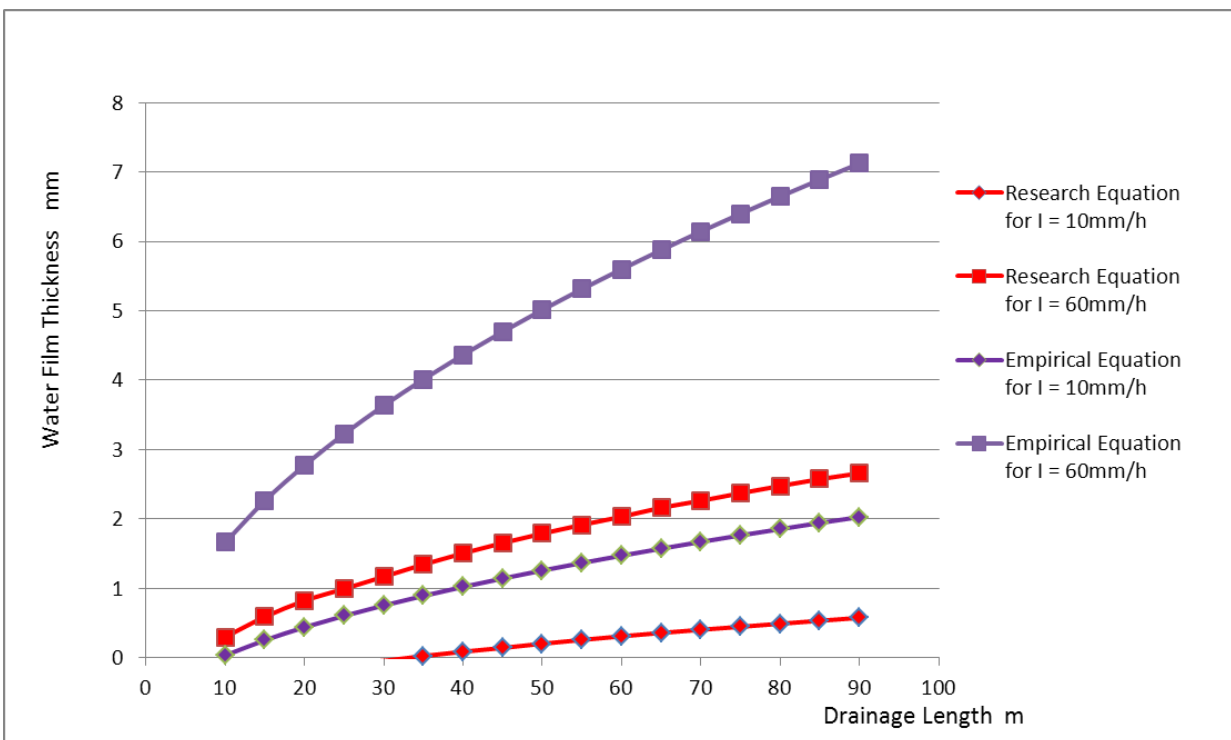
Figure 3.13(a)Water film thickness vs. drainage length for DGAC
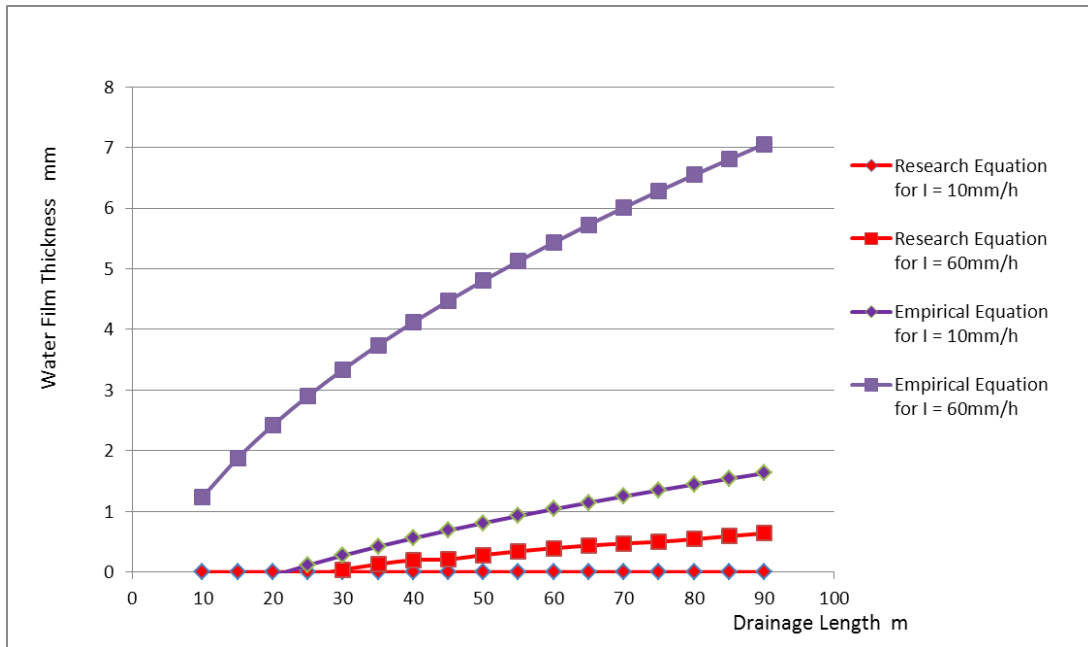
Figure 3.13(b) Water film thickness vs. drainage length for OGFC
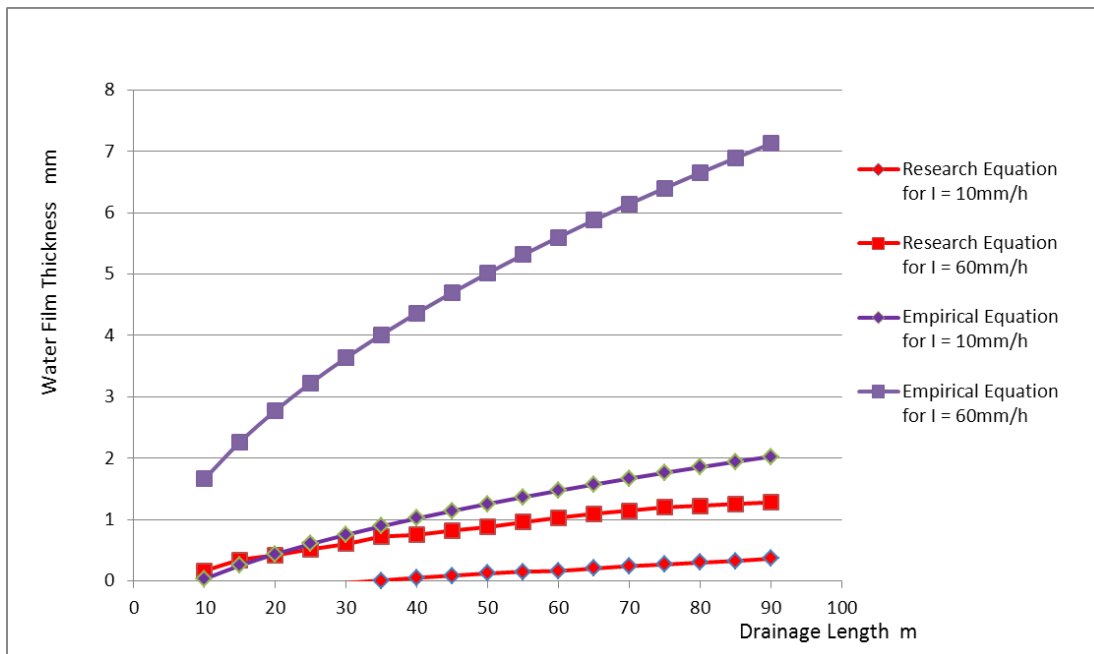
Figure 3.13(c) Water film thickness vs. drainage length for PCC ($N_R < 500$)

37
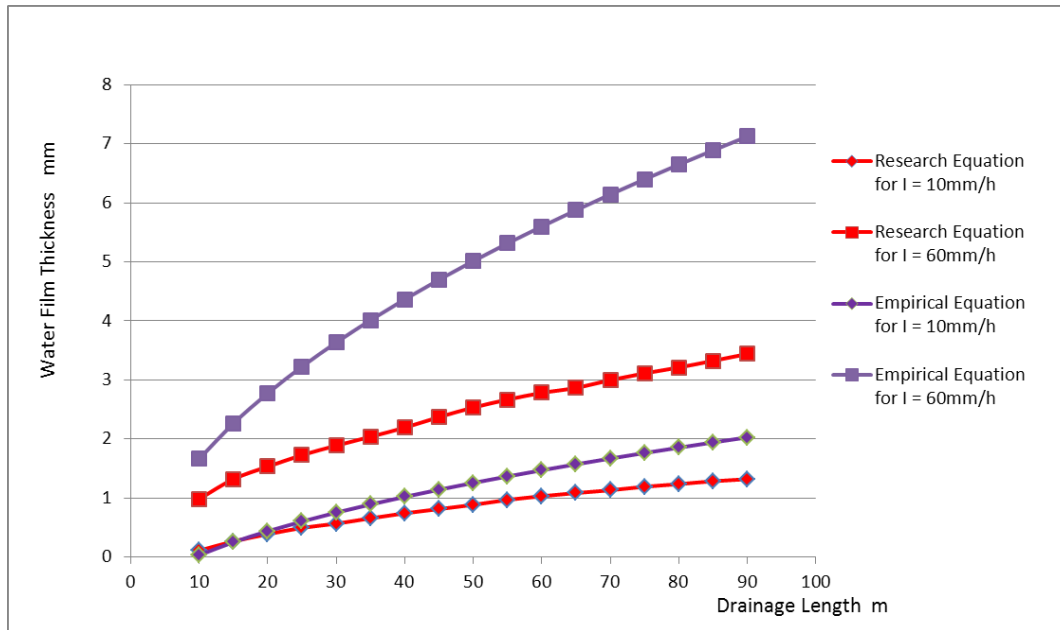
Figure 3.13(d) Water film thickness vs. drainage length for (500<N_R<1000)

3.2.2 Water film thickness predictions at normal crown-superelevation transitions

Charbeneau et al. (2008) have published the numerical results of a hydro-dynamic model that is capable of predicting the water film thickness of sheet flow produced by rainfall at both normal crown and superelevation sections.
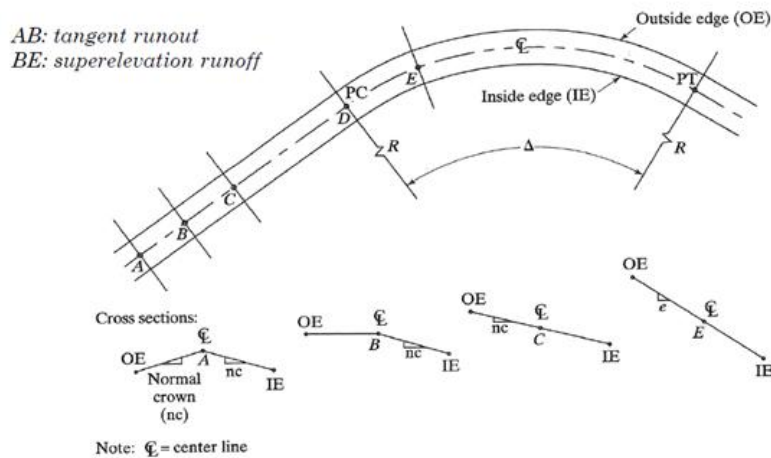
Figure 3.14 Layout of the cross slopes in superelevation design

Typically the cross slopes on either side are symmetric about the center line, and they are denoted as normal crown (Location A in Figure 3.14). But at a curve (superelevation), the cross slopes about the center line change as shown in Figure 3.14. From A to C, the cross slopes of the lanes between the center line and the inside edge remain constant and are equal to the normal crown. However, the cross slopes between the center line of the road and the outside edge change between A and C. At point A, it is the normal crown, at B it becomes horizontal,

38

and at C its magnitude becomes equal but higher than the cross slope on the other side. From C to E, the cross slope rotates about the center line.

Figures 3.15 and 3.16 respectively show the variation of cross-slopes and the 3-D view of the cross-slope variation in the layout illustrated in Figure 3.14.
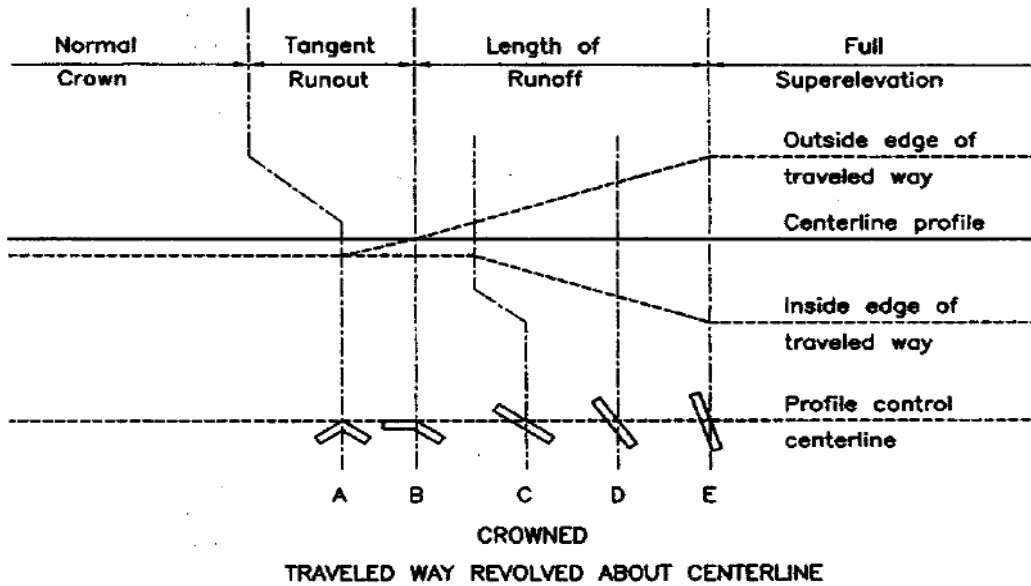
Figure 3.15 Continuous variation of cross slopes with the centerline remaining at the same level

Elements of a Superelevation Transition (Right Curve)
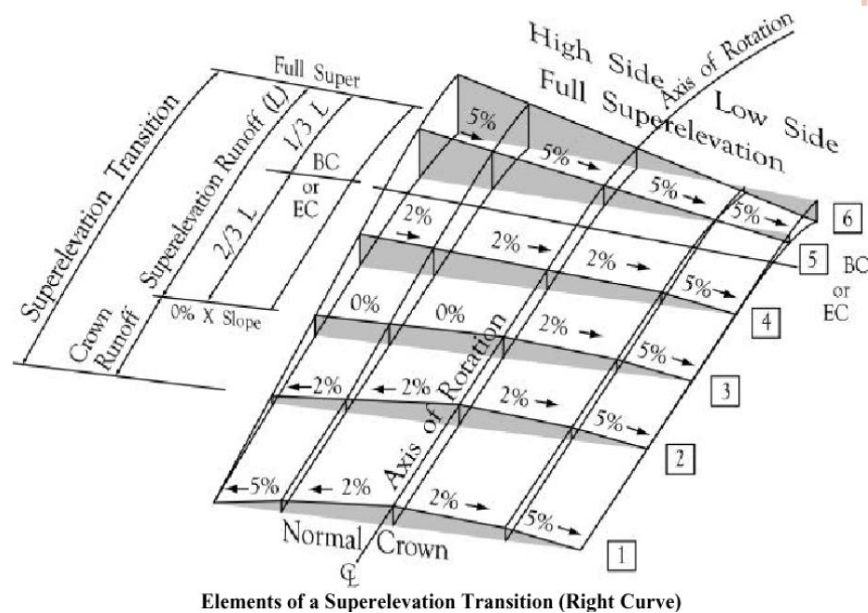
Figure 3.16 Three-dimensional variation in the profiles

39
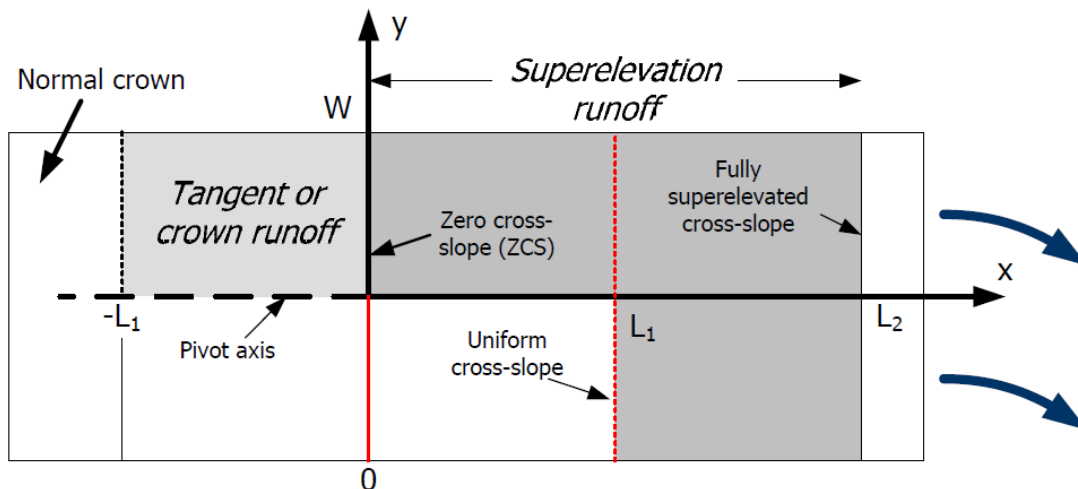
Figure 3.17 Plan view of different sections.

Figure 3.17 shows the plan view of the above section with the x axis at the center line of the road. It is noted that the most critical location with respect to sheet flow lies around the area of the zero-cross slope (B of Figure 3.14).
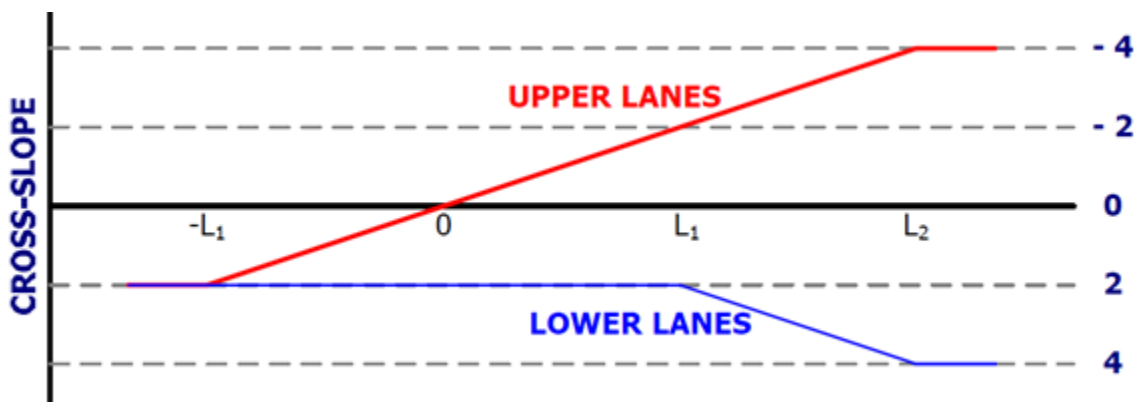
Figure 3.18 Lateral alignment of superelevation transition with cross slope = 4% (Charbeneau et al., 2008)

From Figure 3.18 it is noted that the slopes of the normal crown is 2% and the slope of the full superelevation is 4%.

Charbeneau et al. (2008) model uses the kinematic wave theory to numerically evaluate the water film depth along a continuous road section such as the one that is illustrated in Figures 3.14-3.18.

3.2.2.1 Modeling of water film depth at crowned sections (Charbeneau et al., 2008)

A sample of Charbeneau et al. (2008) results are shown in Tables 3.3 and 3.4.

Concrete pavements

Table 3.3 Water film thickness (in mm) at different lateral stations (Manning's n =0.012, normal crown cross slope = 2%, rainfall intensity = 100 mm/h (4 in/h).

	Longitudinal Slope, S_o							
	0	0.005	0.01	0.02	0.03	0.04	0.05	0.06
Lane 1 Center	0.61	0.61	0.63	0.68	0.73	0.78	0.82	0.86
Lane 1 Edge	0.92	0.93	0.96	1.02	1.10	1.18	1.24	1.30
Lane 2 Center	1.18	1.19	1.22	1.31	1.41	1.50	1.59	1.66
Lane 2 Edge	1.40	1.41	1.45	1.55	1.67	1.78	1.88	1.98
Lane 3 Center	1.60	1.62	1.66	1.78	1.91	2.04	2.15	2.26
Lane 3 Edge	1.79	1.80	1.85	1.98	2.13	2.27	2.40	2.52

Asphalt pavements

Table 3.4 Water film thickness (in mm) at different lateral stations (Manning's n =0.015, normal crown cross slope = 2%, rainfall intensity = 100 mm/h (4 in/h).

	Longitudinal Slope, S_o							
	0	0.005	0.01	0.02	0.03	0.04	0.05	0.06
Lane 1 Center	0.70	0.70	0.72	0.77	0.83	0.89	0.94	0.98
Lane 1 Edge	1.06	1.07	1.09	1.17	1.26	1.34	1.42	1.49
Lane 2 Center	1.35	1.36	1.39	1.49	1.61	1.71	1.81	1.90
Lane 2 Edge	1.60	1.62	1.66	1.78	1.91	2.04	2.15	2.26
Lane 3 Center	1.83	1.85	1.89	2.03	2.18	2.33	2.46	2.58
Lane 3 Edge	2.04	2.06	2.11	2.27	2.44	2.60	2.75	2.88

3.2.2.1.1 Comparison of Charbeneau et al. (2008) data with empirical predictions

For crowned sections, the data shown in Tables 3.3 and 3.4 were compared with the corresponding predictions from equation (3.8a). The following assumptions were made in this comparison:

$$TXD = 1 \text{ mm}, \quad S = \text{Resultant slope} = \sqrt{long.slope^2 + cross.slope^2}$$

L = perpendicular distance from center line * resultant slope/cross slope

Figures (3.19a) and (3.19b) illustrate the comparisons. Figures 3.19(a) and 3.19(b) show that Charbeneau et al. (2008) predictions agree reasonable well with those of the empirical equation (3.8a).
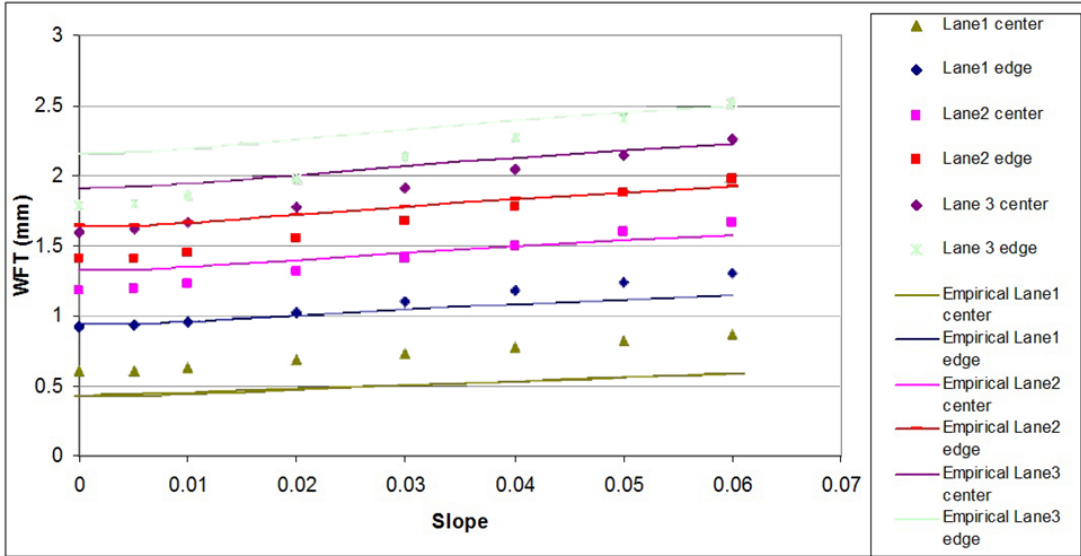
Figure 3.19(a) Comparison of Charbeneau et al. (2008) data with predictions ofequation (3.8a) (WFT = water film thickness)
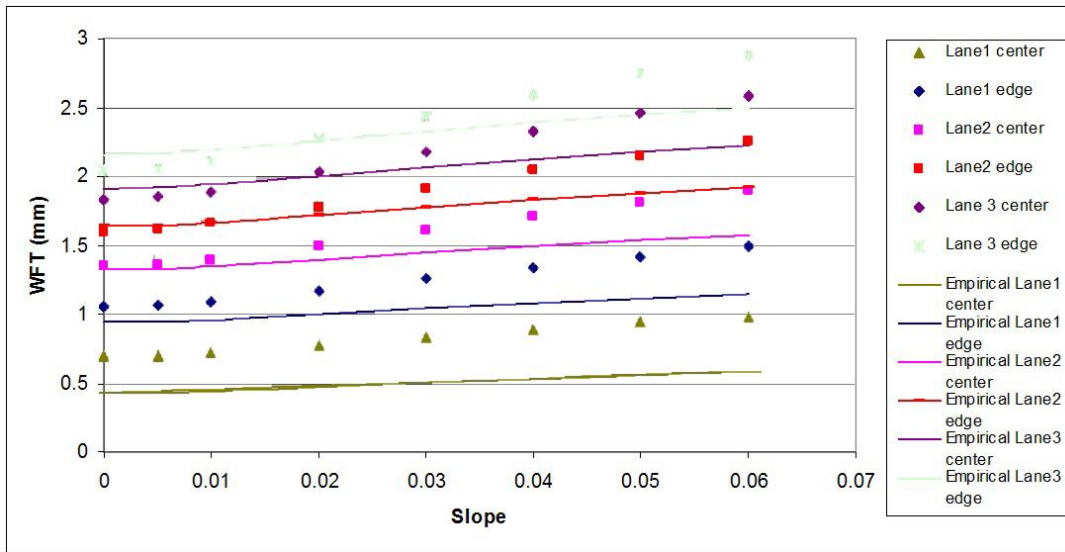
Figure 3.19(b) Comparison of Charbeneau et al. (2008) data with predictionsof equation (3.8a) (asphalt pavements) (WFT = water film thickness)

3.2.2.2 Modeling of water film depth at superelevation transitions (Charbeneau, 2008)

Figures 3.20(a) and 3.20(b) show a sample of the water film depths predicted by (Charbeneau, 2008) at the superelevations as a function of the distance to the considered section from the section with a zero cross slope. It is obvious from Figures 3.20(a) and 3.20(b) that the most critical sections where the water film depths are maximized are zero-cross-sloped sections such as B in Figure (3.14) where the tangent-superelevation transition occurs.

42
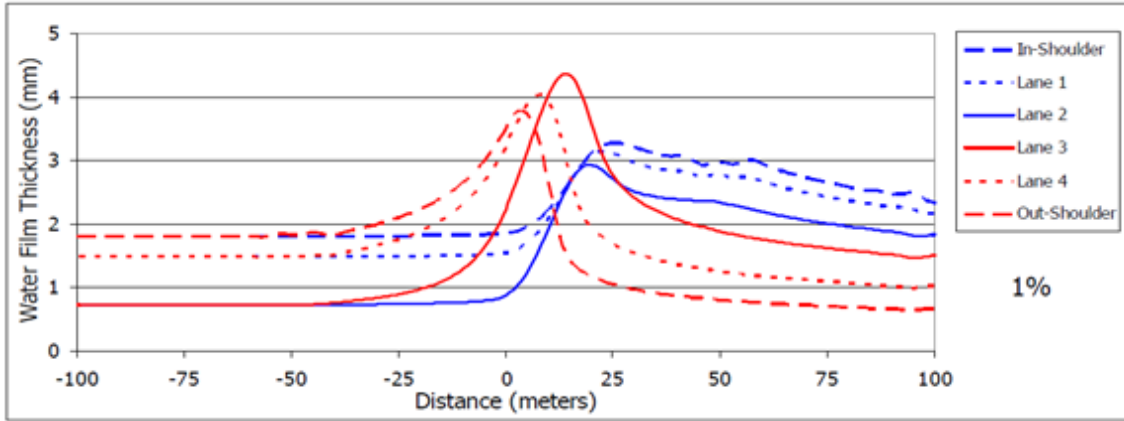
(a) Longitudinal slope = 1%
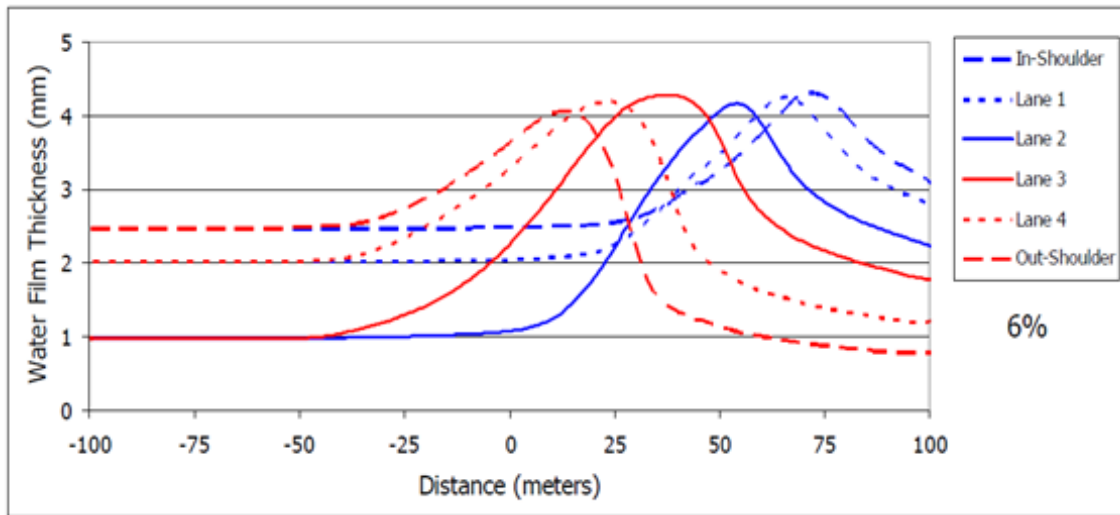
(b) Longitudinal slope = 6%

Figure 3.20(a) Variation in the water film thickness for roadway with four travel lanes and downward longitudinal slope (Manning's n =0.015, normal crown cross slope = 2%, rainfall intensity = 100 mm/h (4 in/h))
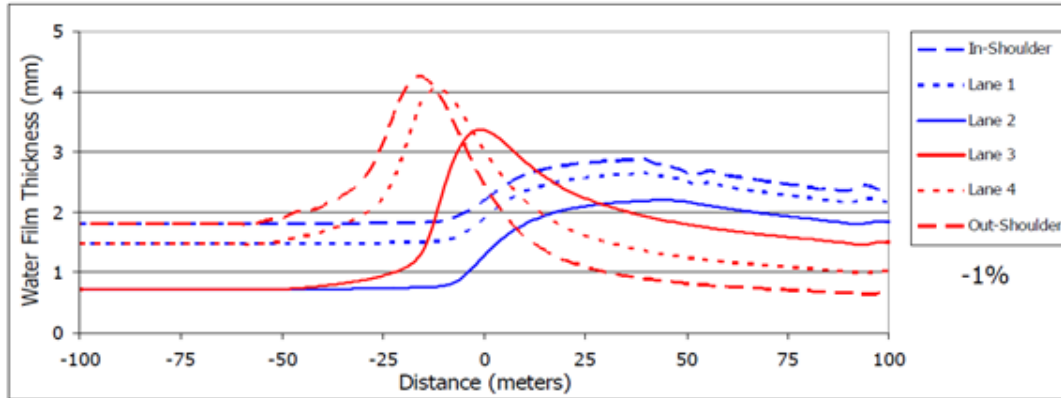
(a) Longitudinal slope = -1%
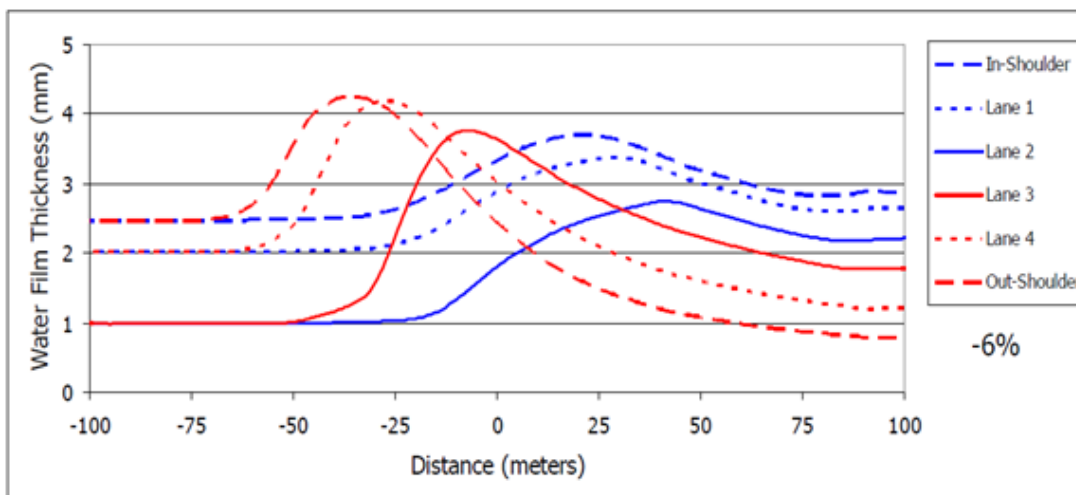
(b) Longitudinal slope = -6%

Figure 3.20(b) Variation in the water film thickness for roadway with four travel lanes and upward longitudinal slope (Manning's n =0.015, normal crown cross slope = 2%, rainfall intensity = 100 mm/h (4 in/h))

3.2.2.1 Fitting of an empirical equation for Charbeneau (2008) water film depth predictions at superelevations

It must be noted that the empirically derived equation 3.8(a) cannot be applied directly to predict the water film depths at superelevations. Moreover, since any other method is not currently available in the literature to predict the water film depth at the superelevation transitions, the investigators used Charbeneau et al.'s (2008) numerical data presented in figures such as 3.20(a) and (b) to develop a new equation for prediction of water depths at superelevation transitions.

For zero cross slope locations L cannot be calculated as,

44

L = perpendicular distance from center line along the normal slope or resultant slope
Since the normal slope = 0

Hence the following new variables L and S are defined:
L = longitudinal distance from the zero-cross line (m)
S = longitudinal slope (%)

Therefore the following equation is derived through regression (R^2 = 0.887) for a rainfall intensity of 100 mm/h with the data shown in Table 3.5.

$$t = 1.1537(L)^{0.3712}(S)^{0.0055}$$ (3.10a)

Figures 3.21(a) and (b) demonstrate the comparison of the predictions of equation 3.10(a) with the data that were used for its development.

Equation (3.10a) can be modified to

$$t = K(I)(L)^{0.3712}(S)^{0.0055}$$ (3.10b)
for any rainfall intensity (I) where K(I) can be evaluated from Charbeneau's (2008) sample plots such as Figure 3.20 for other rainfall intensities, I.

Table 3.5 Data extracted from Figures 3.20(a) and 3.20(b)

Long. Slope	Water film thickness (mm)					
	Lane 1	Lane 2	Lane 3	Lane 4	Inside should.	Outside should.
0.002	1.45	0.9	1.75	3.5	1.75	4
0.005	1.6	1	2.5	3.3	1.85	3.3
0.01	1.55	0.9	2.3	3.2	1.9	3.7
0.02	1.6	0.9	2.2	3.3	2	3.6
0.06	2	1.05	2.25	3.25	2.55	3.65
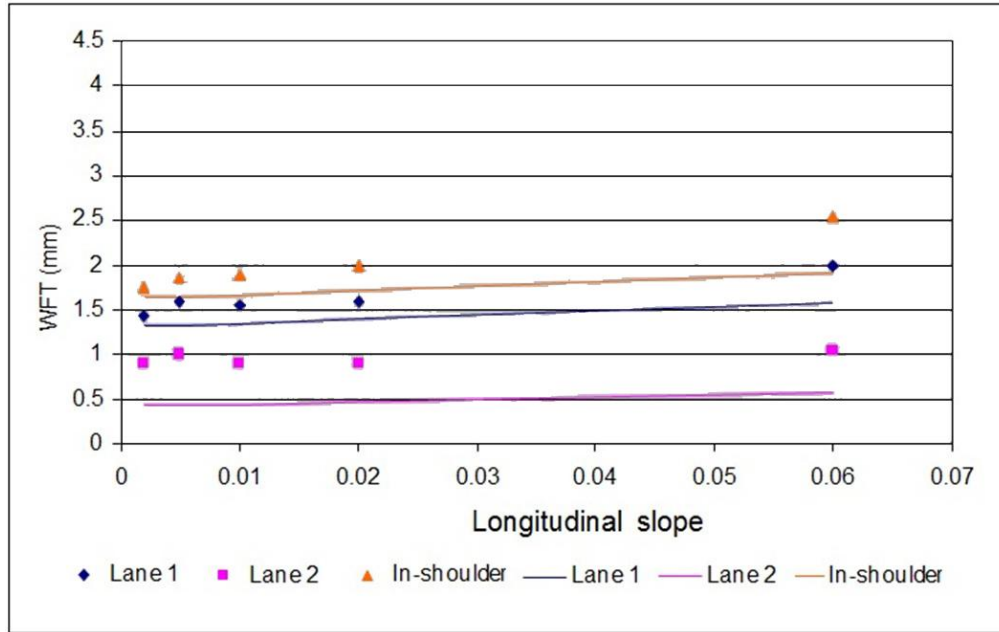
(a) Inner lanes and inner shoulder
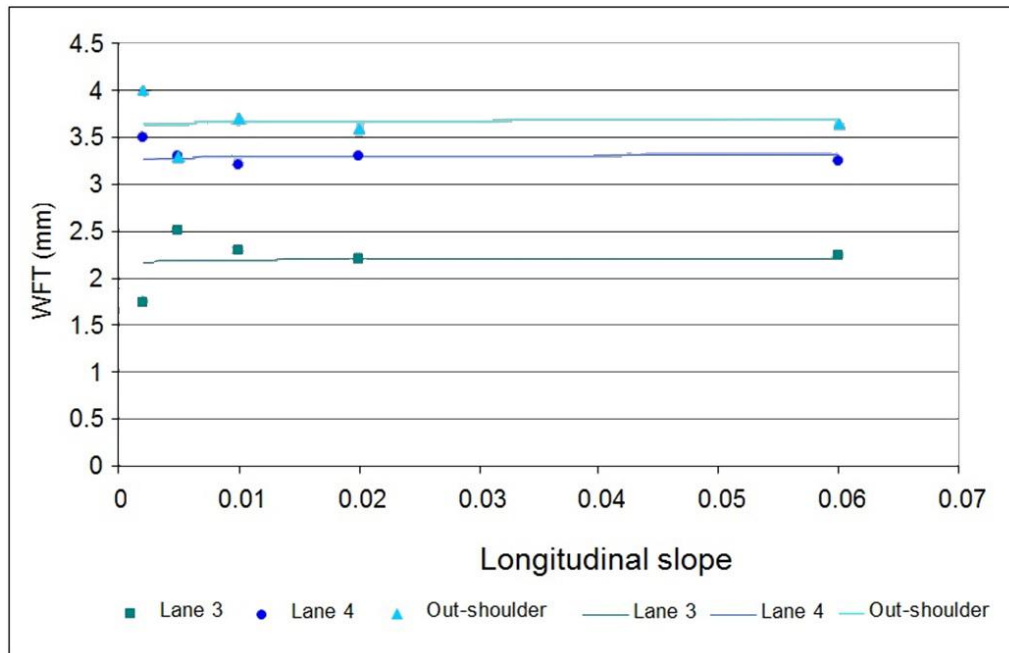
(b) Outer lanes and outside shoulder

Figure 3.21 Verification of the fitting equation (3.10a) (WFT = water film thickness)

46

CHAPTER 4

HYDROPLANING CRASH ANALYSIS BASED ON FDOT CRASH STATISTICS

4.1 Comprehensive Project–Level Crash Analysis

4.1.1Identification of study sections and data collection for analysis

During the initial part of this task the investigators used the FDOT Crash database which is setup in two formats:
1. Crash Analysis Reporting System(CARS) formatted in Excel.
2. *Sharepoint* data provided in a GIS format.

A sample from the database (CARS) is shown in Table 4.1. It must be noted that Table 4.1 includes only the data that are relevant to the sections that will be used in this study. On the other hand, Fig. 4.1 shows the algorithm used to screen the database with the relevant parameters.

Table 4.1 A sample extract of the FDOT crash database

CARNUM	CRASHDATE	TIME	DAYOFWEEK	DISTRICT	DOTCOUNTY	SECTION	SUBSECT	LOCMP	LOCNODE	LOCDIST	UNITS	DIRECTION	ROUTEID
Crash Report Number	Crash Date	Time of Crash	Day of Crash: possible values 1-7 1= Mon. etc.	Managing District	DOT County Number (combines with Section number and Subsection number to form 8-character Roadway Id)	Section Number (combines with DOT County number and Subsection number to form 8-character Roadway Id)	Subsection Number (combines with DOT County and Section number to form 8-character Roadway Id)	Located Mile-point (indicates mile-point location along located roadway id)	Nearest Node Number (indicates nearest reference point to point of crash)	Distance from Nearest Node	Feet or Miles	Direction from Nearest Node	Located Route Id (lowest-numbered "SR" route at point of crash location)
753854600	3/18/2009	7:15	3	1	1	10	0	2.339	165	0			SR 45
753854640	8/19/2009	6:30	3	1	1	10	0	2.339	165	0			SR 45
753854670	8/10/2009	9:10	1	1	1	10	0	2.339	165	0			SR 45
900857990	2/6/2009	19:55	5	1	1	10	0	2.434	165	0.095	MI	N	SR 45
767606160	9/15/2009	6:52	2	1	1	10	0	2.841	166	0.379	MI	S	SR 45
772275390	2/18/2009	16:10	3	1	1	10	0	3.22	166	0			SR 45
753899820	1/11/2009	21:35	7	1	1	10	0	3.995	167	0.136	MI	S	SR 45
772385500	10/6/2009	17:43	2	1	1	10	0	6.677	173	0			SR 45
753522860	3/4/2009	13:15	3	1	1	10	0	6.995	174	0			SR 45
753854620	5/8/2009	13:36	5	1	1	10	0	8.177	179	0.009	MI	S	SR 45
772350220	7/2/2009	21:00	4	1	1	10	0	8.188	179	0.002	MI	N	SR 45
767600190	1/24/2009	7:12	6	1	1	10	0	8.484	180	0			SR 45
767606050	12/5/2009	11:45	6	1	1	10	0	8.583	181	0			SR 45
753522710	1/4/2009	12:49	7	1	1	10	0	8.698	673	0.038	MI	N	SR 45
753513440	6/7/2009	15:33	7	1	1	10	0	9.033	878	0.246	MI	S	SR 45
772350610	8/17/2009	17:45	1	1	1	10	0	9.324	878	0.045	MI	N	SR 45
753862460	1/12/2009	15:40	1	1	1	10	0	9.533	182	0			SR 45
753899870	4/18/2009	14:30	6	1	1	10	0	9.533	182	0			SR 45

Figure 4.1 Algorithm developed for filtering the database

In order to facilitate this task, several other databases provided by FDOT as listed below were also used:

1. Detailed crash data in the Unified Basemap Repository (UBR), https://www3.dot.state.fl.us/unifiedbasemaprepository/ where crash data shape-files from 2003 - 2010 are available.

2. Detailed hourly traffic data in http://www.dot.state.fl.us/planning/statistics/trafficdata/

3. As-built roadway plans in http://webapp01.dot.state.fl.us/EnterpriseInformationAssets/FDOTEnterpriseSearch/eDocument/EDocSearch.aspx

4. Detailed inter-lane traffic distribution from the Highway Capacity Manual (HCM (TRB, 2010)).

5. Roadway geometric design data from the Straight Line Diagrams (SLD).

6. Rainfall intensity data in Florida from weather stations listed in the following link. http://www.wunderground.com/weatherstation/WXDailyHistory.asp?ID=KFLWESLE4

The additional databases are more "project-oriented" than the "network-based" CARS database (Table 4.1). Therefore, the additional data had to be retrieved painstakingly. Furthermore, the additional information provided the investigators with an opportunity to "review" the hydroplaning crash analysis more closely.

4.1.2 Classification of hydroplaning-related crashes

The preliminary wet weather crash database set up using the CARS database was filtered further using the parameter of "standing water" provided in the crash report to identify the likely hydroplaning related crashes even more accurately. Due to this added filtering, the number of crashes were reduced further, and it was necessary to start at an earlier date in the database to obtain an adequate number of crashes for the ensuing statistical analysis. Thus, the crash database has been back-dated to 2003 for the renewed analysis. Furthermore, only crashes that occurred during the off-peak period were considered because, at low speeds that presumably occur during peak hours, hydroplaning crashes are unlikely. Traffic data given in the FDOT website (http://www.dot.state.fl.us/planning/statistics/trafficdata/) were used for this exercise.

Moreover, wet weather crashes on curves were excluded because the higher probability of skidding at curves is due to inadequate centripetal forces rather than hydroplaning, because banking on curves assures adequate runoff. The super-elevated segments and curves (Figure 4.2) with large radii have been identified from the as-built plans in the following link and excluded from further study.

However, the "zero cross slope locations" on the transitions cannot be ruled out similarly because of the poor drainage at such locations.

The investigators employed the parameter of "intersections" in the CARS database to screen out hydroplaning related crashes since wet weather crashes at these low speed locations could be attributed to other causes such as the low friction.
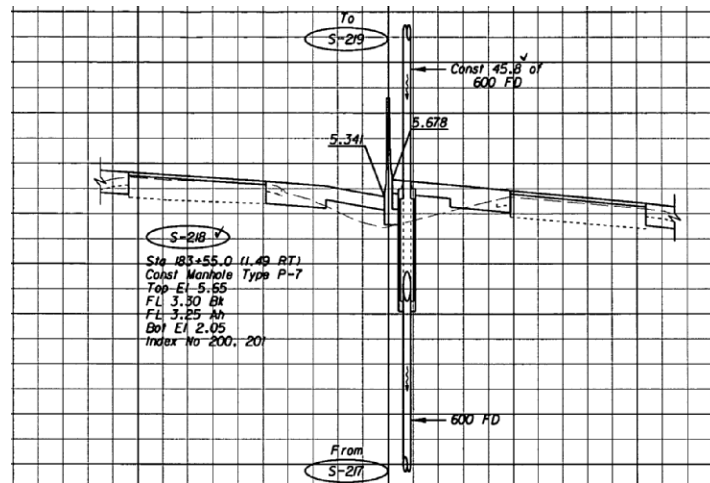
Figure 4.2 Super-elevated segments (As-built plan of roadway 93220000 Page no.329 of ADD.tiff)

4.1.3 Extraction of pavement condition data for hydroplaning crash locations

The CARS database contains vital information on every reported crash in the state of Florida. In conducting the research for this project the investigators were specifically interested in the number of lanes, the weather at the time of crash, the surface type, the speed, and the surface width. On the other hand, the Pavement Condition System (PCS) database maintained by FDOT contains pavement condition properties, such as the rut depth and the International Roughness Index (IRI) of the pavement surface. In order to determine the condition of the roadway at the exact location and time of the crash, the relevant information must be transferred from the PCS database to the CARS database. To achieve this task, a unique match number was assigned to every crash composed of the 8 digit roadway id, the crash mile post and the year in which it occurred. An example of this unique match number is given below:

If the Roadway ID is **13030102**, the crash mile post is **00.265**, and the year is **2009**, then the Match ID would be **30301020.26509**

The same method was used to create a match number for the PCS database with the crash mile post being replaced with the ending mile post of the tested segment. With the PCS database sorted with the Match IDs in the ascending order, the INDEX and MATCH functions in MSExcel were used to compare the Match ID from the CARS database to locate the corresponding PCS database entry. Then the information on rut, ride and crack ratings, IRI, and the lane tested were extracted.

Once the information is transferred, the lane tested and the lane in which the crash occurred needed to be compared. If the lane tested was different from the lane in which the crash occurred the databases needed to be compared manually to determine if the lane tested was an appropriate match to the lane in which the crash occurred. If the crash lane was left blank or was indicated as the shoulder, it is assumed to be an appropriate match and no other action was needed. If there was a discrepancy, the history of the considered condition test on the roadway section was compared to see if the lane in which the crash occurred was ever tested and, if so, how it compared to the most recent test. From this information the pavement conditions at the crash site can be compared with the database of pavements to see if the pavement conditions might have influenced the crash.

4.1.4 Modification of the crash database to account for inward sloping roadway segments

Inward sloping sections were identified from the as-built roadway plans, and the number of lanes in such abnormal sections were re-evaluated based on the cross slope variation, and the crashes that occurred on inward sloping sections were discarded. These plans (Figure 4.3) are available at:
http://webapp01.dot.state.fl.us/EnterpriseInformationAssets/FDOTEnterpriseSearch/eDocument/EDocSearch.aspx

After accounting for inwardly sloped segments, those sections with inward slope were re-classified into two separate segments. All the remaining roadway segments were assumed to have been constructed based on standard pavement cross-slopes stipulated in Plan Preparation Manual (PPM) available at the following Web link:
http://www.dot.state.fl.us/rddesign/PPMManual/2011/Volume1/2011Volume1.pdf (page 60).
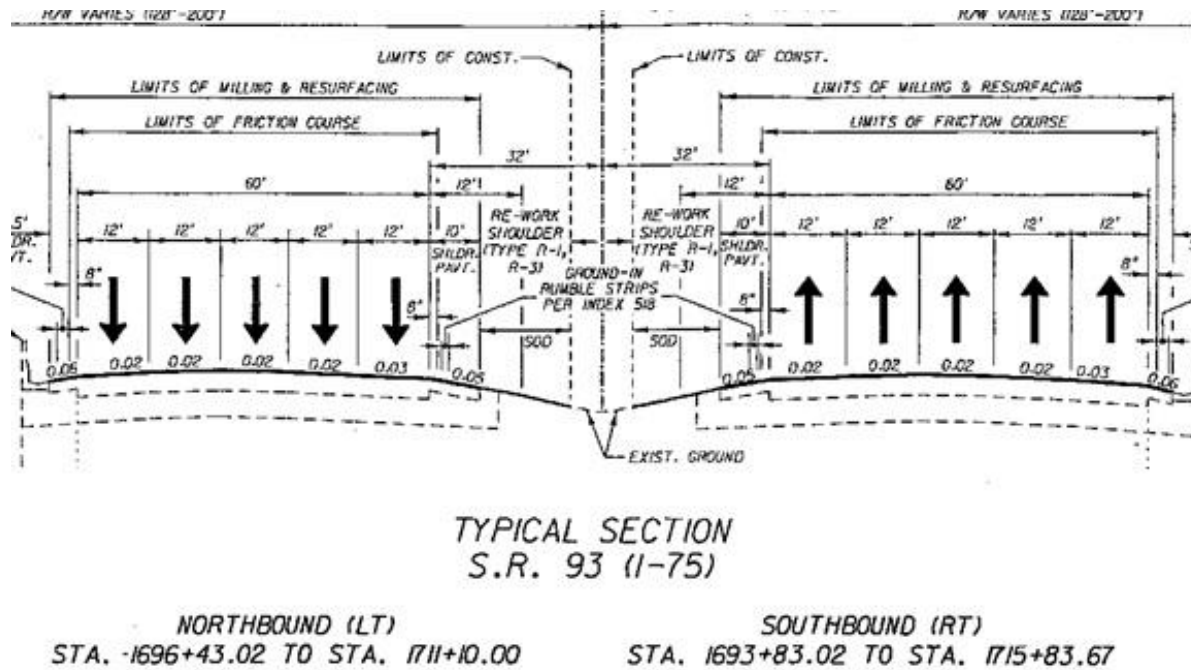
Figure 4.3 Sample inwardly sloped segment (As-built plan of roadway 86075000, Page 10 of Resurfacing from N. of Sheridan St, to SawgrassExpwy.tif)

4.1.5 Hydroplaning crash re-classification based on the detailed Police Report (Long-Form)

Around forty percent (40%) of hydroplaning related crashes have been reported as shoulder crashes in the CARS database. Since this percentage is abnormally high, all the reported crashes (including the shoulder crashes) were reclassified in this work based on the lane where the incident originated, using the information on the detailed Police Report (Long Form) (Figure 4.4)
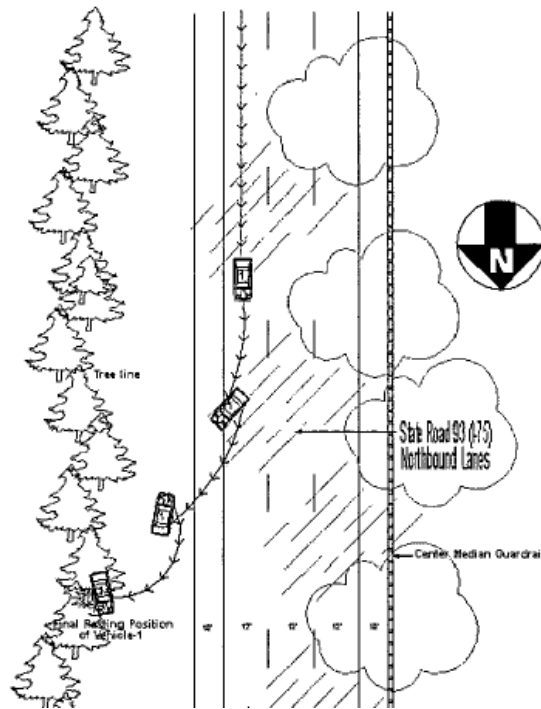
Figure 4.4 Sample identification of the incident originating lane (HSMV crash report number 71091910)

In addition, information such as the speed at which the vehicle was travelling prior to the crash and number of through lanes (other than the emergency lanes) were also identified for each crash based on the same Long Form.

In order to identify hydroplaning crashes, it is necessary to identify the lane on which the incident had started and the traveling speed. However the CARS database provides only the lane where the crash had occurred and not where the incident had started. Therefore the Long Forms were also used to obtain this vital information.
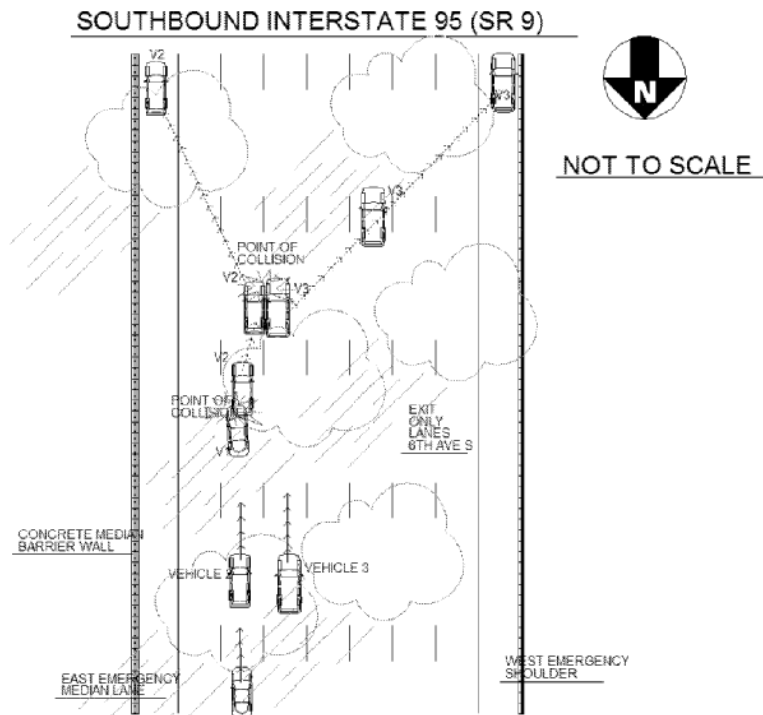
Figure 4.5 Sample identification of crashes due to viscous hydroplaning (HSMV crash report number 770557920)

Furthermore, during the data re-classification process information on the Long Form was also used to identify and remove crashes related to skidding or viscous hydroplaning (Figure 4.5). This is because these crashes are due to the reduction of safe stopping or braking distance in wet pavements and cannot be attributed to dynamic hydroplaning.

4.1.6 Determination of hourly traffic variation

Hourly traffic data has been obtained from the following FDOT site by considering forty seven (47) traffic counting locations as shown in Figure 4.6.
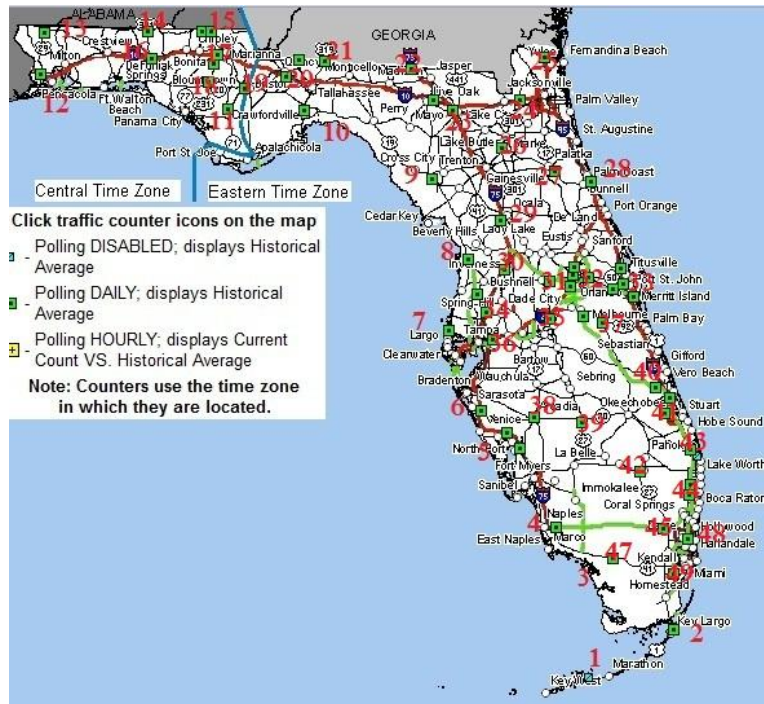
**Figure 4.6 Traffic counting locations in Florida
(http://www.dot.state.fl.us/planning/statistics/trafficdata/)**

The crash data has been re-categorized in to twenty one (21) major routes which consist mostly of interstates (i.e., I-4, I-10, I-75, I-95) and some other major state routes.

4.1.7 Determination of traffic distribution across lanes

Different distribution of traffic across lanes were also considered to be significant, since during the off-peak period, traffic variation is not uniform across lanes compared to that during the peak period. In order to determine the traffic distribution across lanes, the Highway Capacity Manual (HCM (TRB, 2010)) was used. The information in HCM 2010 was limited to three lane road sections. Therefore the information provided in the HCM 2010 had to be extended to road sections with more than three lanes, particularly the ones exceeding the PPM criteria, based on field observations conducted in Tampa.

The traffic monitoring experiment was conducted on a four lanes facility (I-275) in Tampa, during off-peak hours between the Tampa International Airport and the Howard Franklandbridge. Based on the HCM (TRB, 2010) data and the experimental data, appropriate lane distributions of traffic have been developed for three-five lane facilities as shown in Figure 4.7.
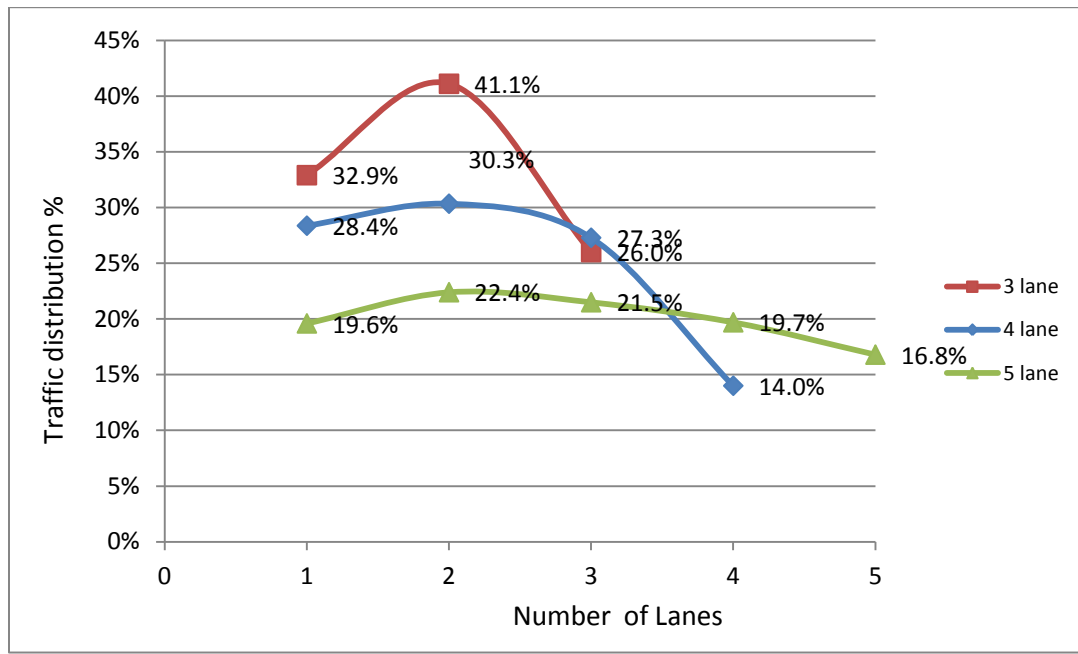
Figure 4.7 Traffic distribution across lanes

4.1.8 Identification of the paved material

The pavement surface type can be used to portray the effect of the surface material on hydroplaning potential of a pavement. Paved material on a given pavement section in the hydroplaning related crash database has been identified based on the Straight Line Diagrams (SLD) and the description included in the as-built plans.

In Straight Line Diagrams (Figure 4.8),roadway sections are classified into a number of friction course categories (such as FC2, FC3,..) . However in this research, the surface type has been broadly classified into three main categories: (1) DGAC, (2) OGFC and (3) PCC by following the FDOT flexible pavement design manual available at the following web link.
http://www.dot.state.fl.us/pavementmanagement/pcs/FlexiblePavementManualMarch152008.pdf
Even on one given roadway (or roadway ID), the surface material can vary from section to section. First, the beginning and ending mile posts of the crash section as well as the pavement type were recorded in a separate spreadsheet and once again the INDEX and MATCH functions in Excel were utilized to determine the pavement type at the location of the crash.
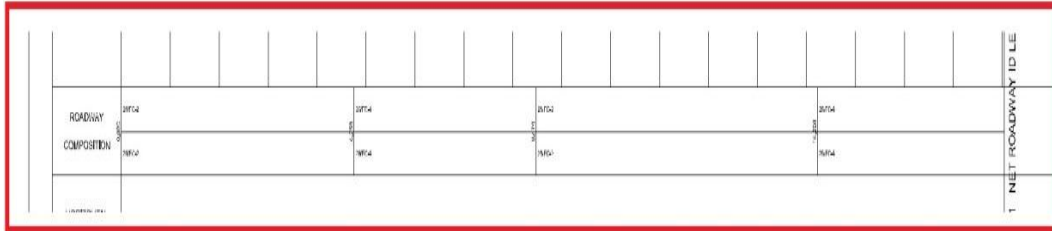
Figure 4.8 Segmented roadway from SLD (Roadway ID 09030000)

4.2 Results and Conclusions of the Extended Crash Analysis

4.2.1 Correlation of wet weather crashes to pavement condition

A number of plots were generated to illustrate the impact of common pavement distress parameters on wet weather crashes, based on a network level analysis. Figures 4.9, 4.10 and 4.12 respectively show that there are no significant impacts of pavement crack, ride, and rut indices on wet weather crashes. However, it is noticed from Figure 4.11 that IRI captures some significant effect of smoothness on increased wet weather crashes,
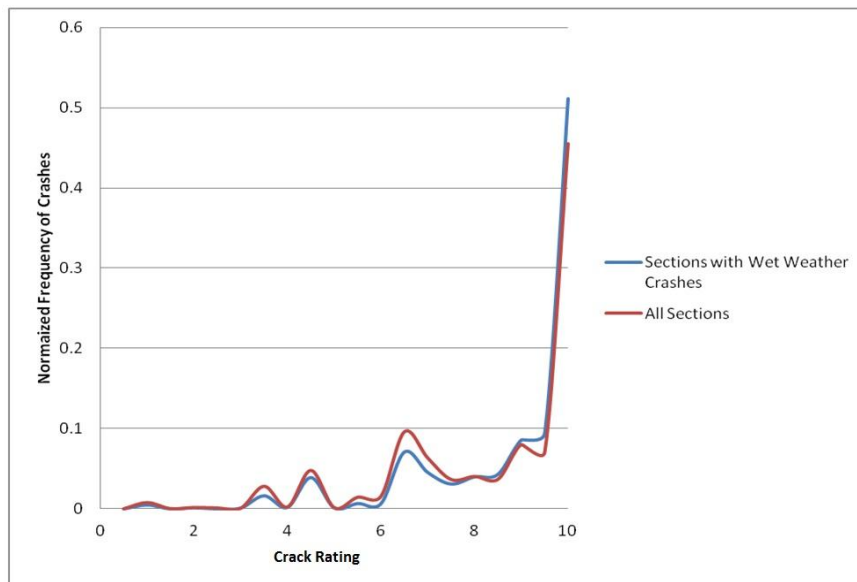
Figure 4.9 Impact of cracking on wet weather crashes
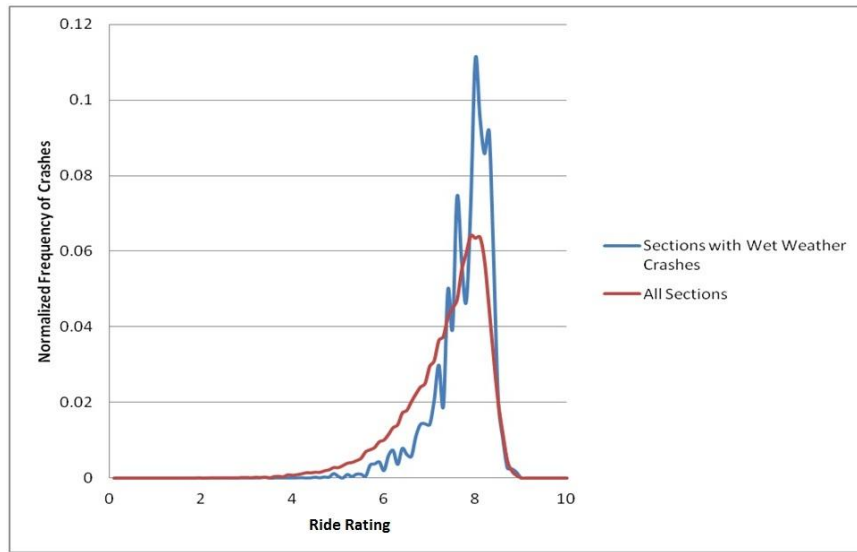
Figure 4.10 Impact of ride rating on wet weather crashes
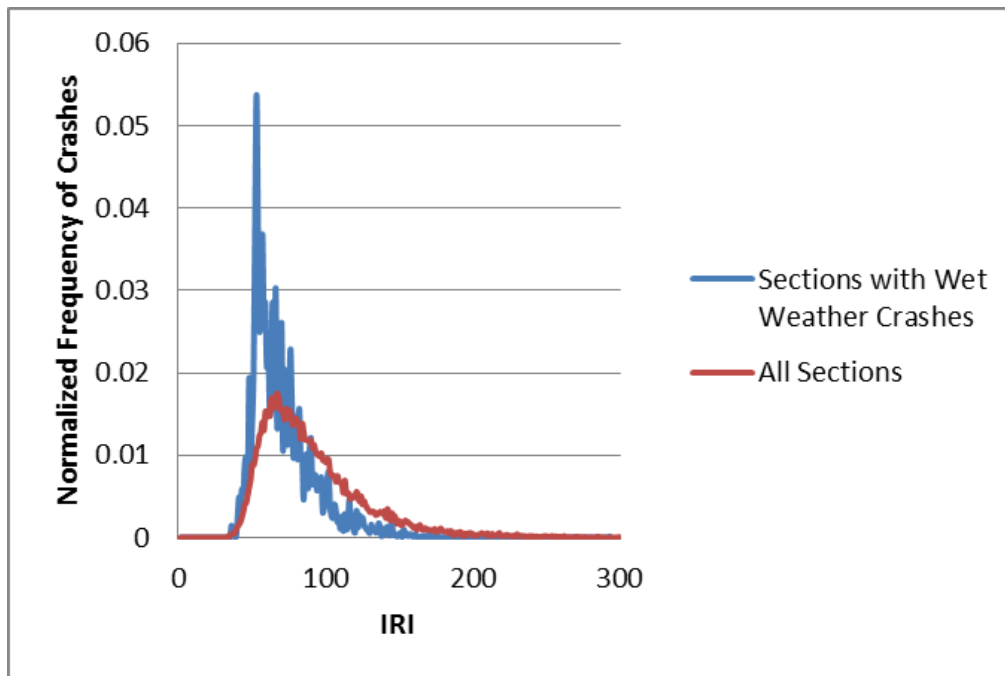
Figure 4.11 Impact of roughness (IRI) on wet weather crashes
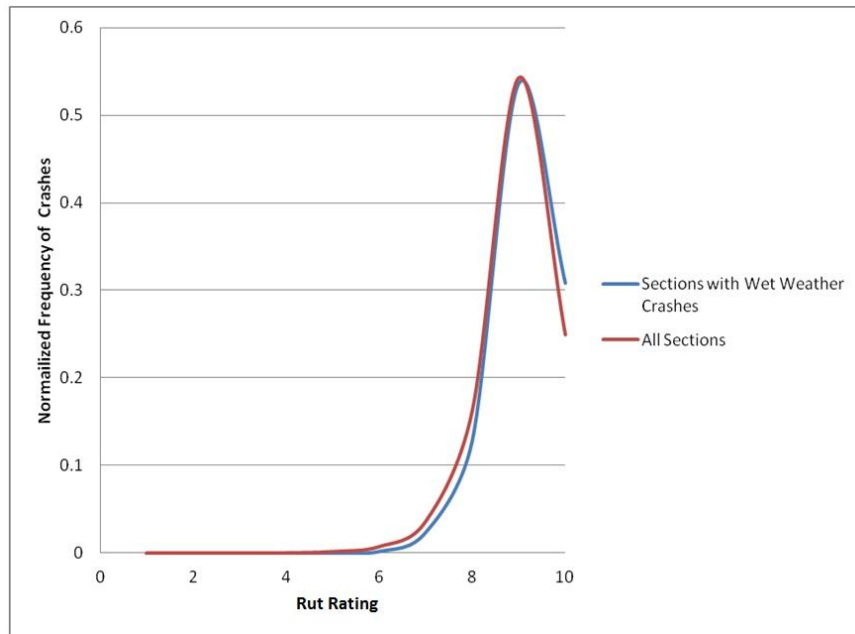
Figure 4.12 Impact of rutting on wet weather crashes

4.2.2 Comparison of the inter-lane hydroplaning potential of multilane facilities

Table 4.2 and Figures 4.13-4.15 illustrate the differences in hydroplaning-related crash rates of multilane facilities with 2-4 lanes in one direction. It must be noted that in the modified hydroplaning-related crash database, the number of facilities with more than four lanes were insignificant and hence not included in this analysis.
Crash rates can be computed in the following two ways:

1. Based on the spatial exposure of vehicles within the considered section,
Crash rate = crashes per unit section length*ADT
(ADT = Average daily traffic)

2. Based on the instant exposure of vehicles to traffic
Crash rate = averaged crashes per lane ADT

In the project-level analysis, the database was arranged by the hydroplaning crash incidents. Hence the crash rates were computed using the latter method.

Table 4.2 Comparison of inter-lane hydroplaning crash rates of facilities at different speeds

Travel Lane	Speed	Crash Frequency				Average Crash Rate			
		Inside lane	Mid-inside lane	Mid-outside lane	Outside lane	Inside lane	Mid-inside lane	Mid-outside lane	Outside lane
2 Lanes	40-50	68	90			0.0038	0.0073		
2 Lanes	55-65	100	204			0.0063	0.0103		
2 Lanes	70+	101	75			0.003	0.0042		
3 Lanes	40-50	32	27	39		0.0047	0.0018	0.0038	
3 Lanes	55-65	53	63	74		0.0025	0.0019	0.0031	
3 Lanes	70+	62	72	48		0.0025	0.0025	0.0031	
4 Lanes	40-50	9	6	6	8	0.0016	0.0012	0.0027	0.0028
4 Lanes	55-65	13	8	12	6	0.0016	0.0014	0.0023	0.0029
4 Lanes	70+	3	3	4	1	0.0017	0.0026	0.0054	0.0062
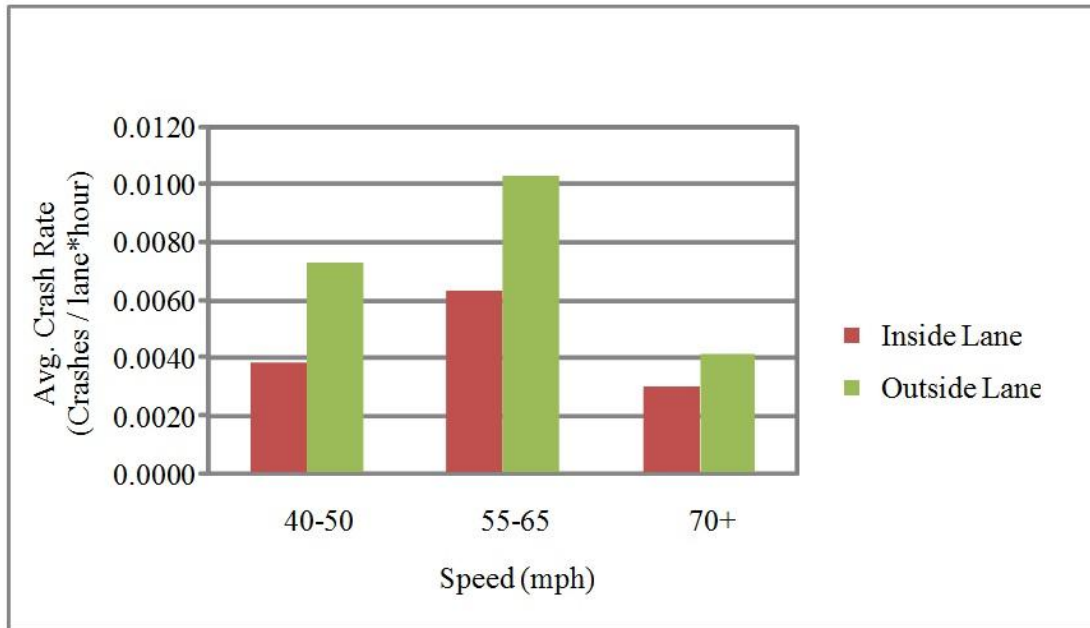
Figure 4.13 Inter-lane hydroplaning crash rate comparison on two-lane highways
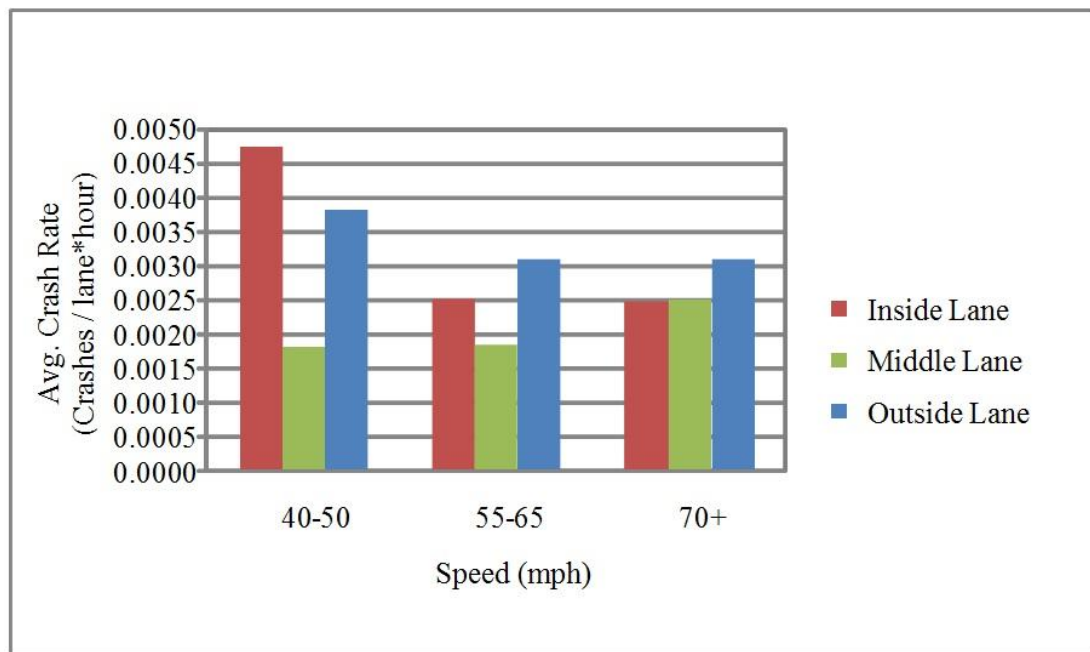
Figure 4.14 Inter-lane hydroplaning crash rate comparison on three-lane highways
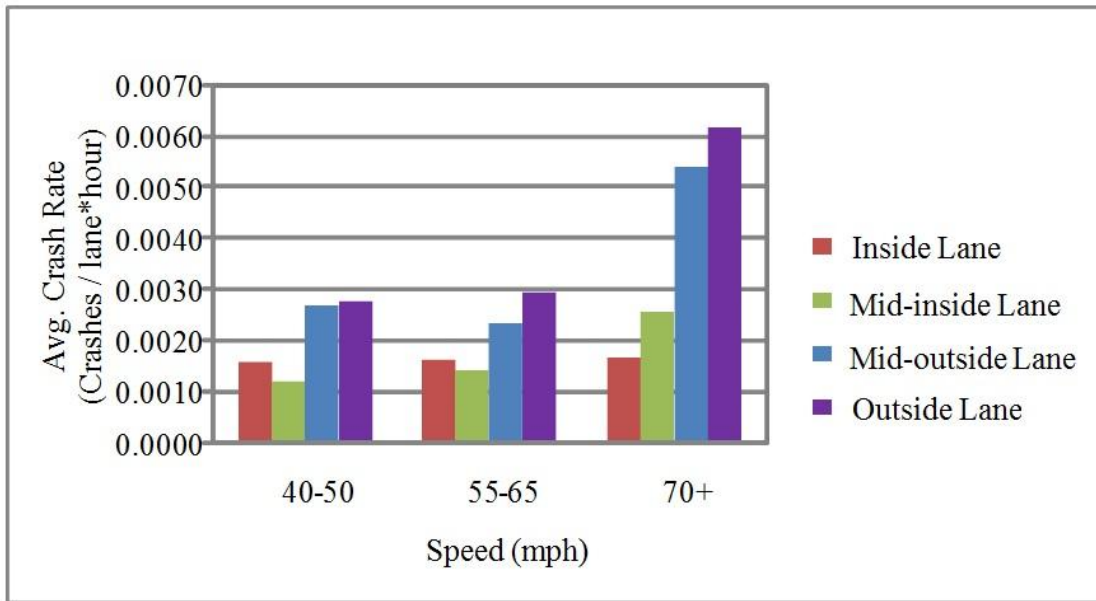
Figure 4.15 Inter-lane hydroplaning crash rate comparison on four-lane highways

Two conclusions can be drawn from the above results of the detailed analysis of hydroplaning related crashes on Florida's major highways.

1. Travel speed increases the hydroplaning potential on any lane.
2. In most cases, the outside lanes show a higher hydroplaning potential certainly due to the higher water film thickness.

4.2.3 Comparison of hydroplaning related crashes on different pavement surface types

Figure 4.16 illustrates the distribution of wet weather crashes among different pavement surface types. Figure 4.16 shows that more hydroplaning crashes occur on OGFC surfaces when compared to dense-graded asphalt surfaces. It must also be noted that according to the flexible pavement design manual cited above, if the road is multilane and the design speed is above 50 mph, then the pavement needs to be constructed with OGFC (FC5). Therefore the trend seen in Figure 4.16 can be attributed to the employment of the "multilane" and "high speed" criteria in screening the hydroplaning related crashes.
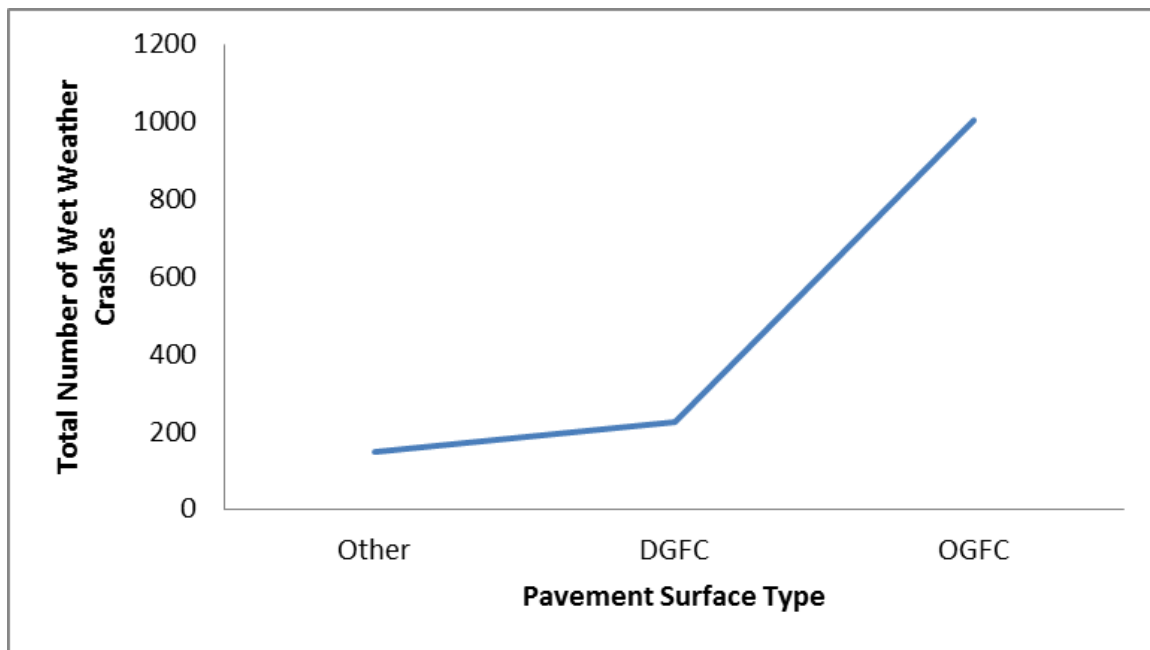
Figure 4.16 Variation of wet weather crashes on different pavement surface types

Table 4.3 and Figures 4.17-4.19 illustrate the differences in hydroplaning related crash rates of multilane facilities with 2-4 lanes in one direction. From the trends depicted in the above plots, it is interesting to note that, although more hydroplaning related crashes seem to occur in Florida's OGFC pavements, the hydroplaning potential, as indicated by the crash rate, is significantly higher on dense-graded pavement surfaces.

Table 4.3 Comparison of wet weather crash rates of facilities with different surface

Pavement Surfacing Material	Facility Type	Lane 1	Lane 2	Lane 3	Lane 4	Lane 5	Lane 6
DGAC	2 Lanes	0.0125 (6)	0.0148(25)				
	3 Lanes	0.0022(4)	0.0062 (4)	0.0036 (3)			
OGFC	2 Lanes	0.0023 (677)	0.0036 (562)				
	3 Lane	0.0025 (592)	0.0021 (588)	0.0029 (422)			
	4 Lane	0.0020 (228)	0.0021 (238)	0.0019 (179)	0.0035 (147)		
	5 Lane	0.0028 (135)	0.0024 (132)	0.0027 (141)	0.0029 (82)	0.0025 (70)	
	6 Lane	0.0021 (37)	0.0026 (26)	0.0025 (11)	0.0028 (21)	0.0025 (18)	0.0025 (14)
PCC	2 Lane	0.0025 (46)	0.0043 (53)				
	3 Lane	0.0014 (62)	0.0019 (57)	0.0023 (51)			
	4 Lane	0.0025 (58)	0.0025 (54)	0.0032 (26)	0.0052 (35)		
	5 Lane	0.0020 (16)	0.0018 (17)	0.0030 (23)	0.0028 (4)	0.0045 (15)	
	6 Lane	0.0011 (39)	0.0008 (38)	0.0022 (16)	0.0025 (19)	0.0035 (10)	0.0027 (8)

Note – The number of crashed used to determine the crash frequencies are indicated within parentheses
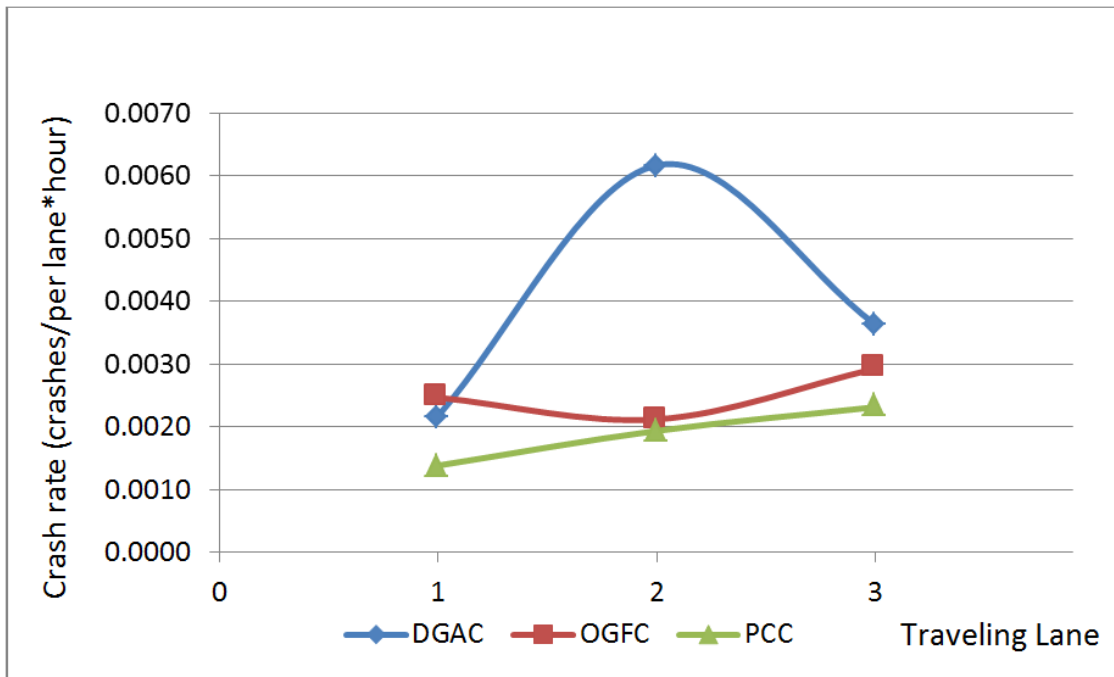
Figure 4.17 Hydroplaning crash rate comparison based on surface types (three-lane highways)
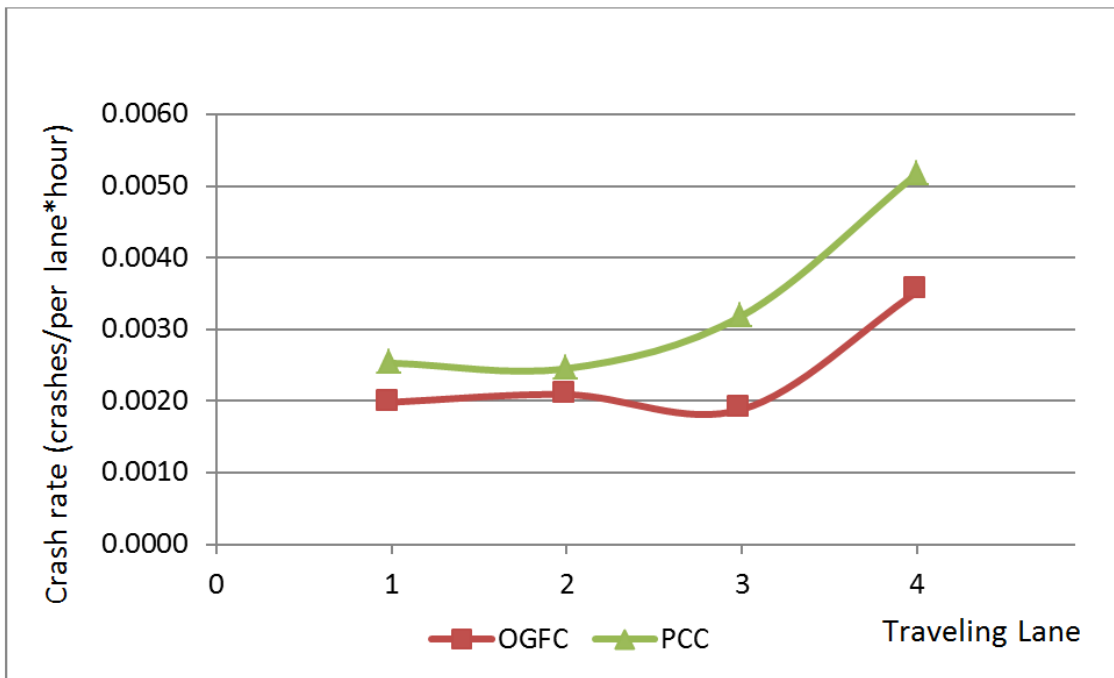
Figure 4.18 Hydroplaning crash rate comparison based on surface types (four-lane highways)
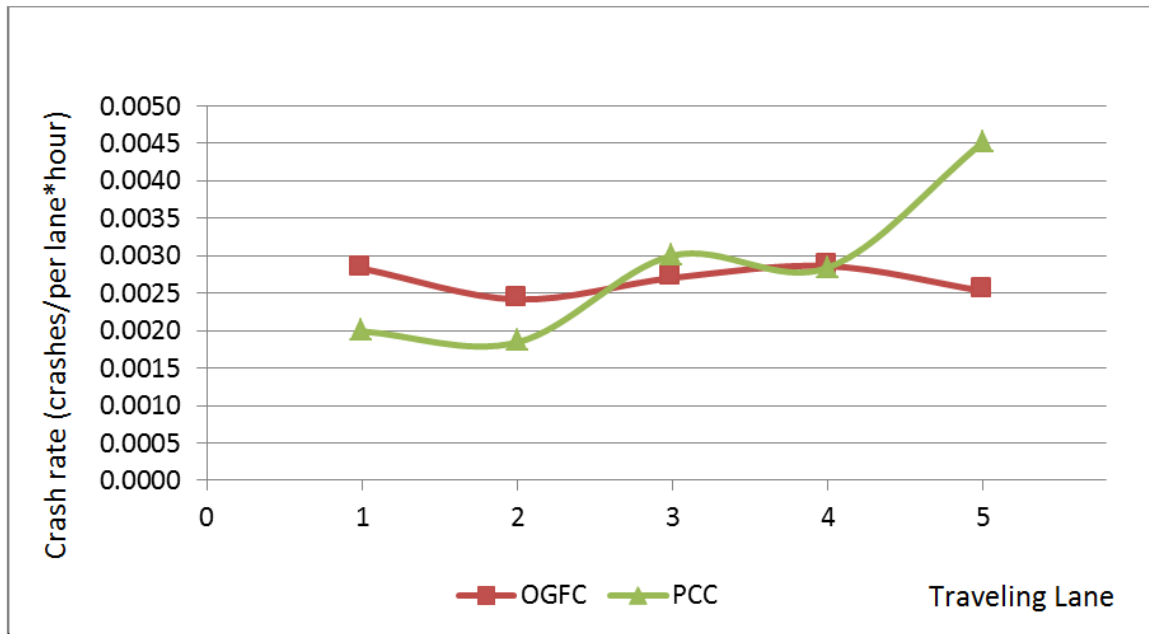
Figure 4.19 Hydroplaning crash rate comparison based on surface types (five-lane highways)

4.2.4 Comparison of the hydroplaning potential prediction of PAVDRN and the crash database

The following procedure was developed to estimate the reliability of PAVDRN in accurate prediction of hydroplaning crashes. The rainfall rate data availability from Weather underground website (http://www.underground.com/) limited the crash data that can be analyzed. The crash locations chosen needed a sufficient number of weather stations in close proximity to those roadway sections. An adequate number of weather station data was available for the years 2009 and 2010. The data was analyzed on four roadway sections, with locations having an adequate number of weather stations in close proximity and a large enough number of crashes. The locations chosen are one roadway section on I-75 and three sections on I-95.

The following sites/roadway IDs were analyzed:
- 10075000 (located on I-75) [181, and 178 total crashes in 2009 and 2010 respectively]
- 89095000 (located on I-95) [56, and 53 total crashes in 2009 and 2010 respectively]
- 93220000 (located on I-95) [82, and 314 total crashes in 2009 and 2010 respectively]
- 94001000 (located on I-95) [97, and 52 total crashes in 2009 and 2010 respectively]

Weather stations along the above roadway IDs were recorded using their unique IDs consisting of letters and numbers along with their GPS coordinates (sample weather stations are seen in Figure 4.20).

67

For I-95 roadway IDs, nine weather stations with data were found for 2009 and eleven weather stations with data were found for 2010. For I-75 roadway IDs, nine weather stations with data were found for 2009 and eleven were found for 2010.
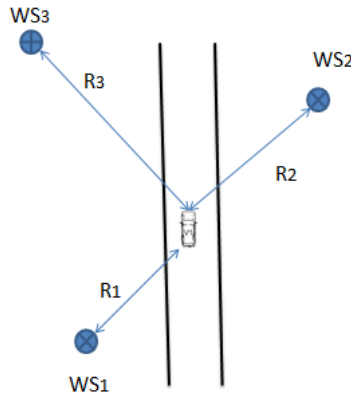
Figure 4.20 Sample crash site and three closest weather stations

To screen out hydroplaning crashes from other wet weather crashes more accurately, Florida Traffic Crash Reports (police long forms) were reviewed for each crash in the above roadway IDs. The crashes were chosen based on the sketch and description of events. Police long forms that included one of the following were chosen as possible hydroplaning crashes:

- description of a hydroplaning crash,
- description that included "skid", "lost control", or "hydroplane",
- apparent low traffic situations (removing rear end crashes caused by stop and go traffic from low pavement friction), and finally
- loss of control of the vehicle represented in long forms such as that shown in Fig. 4.21.
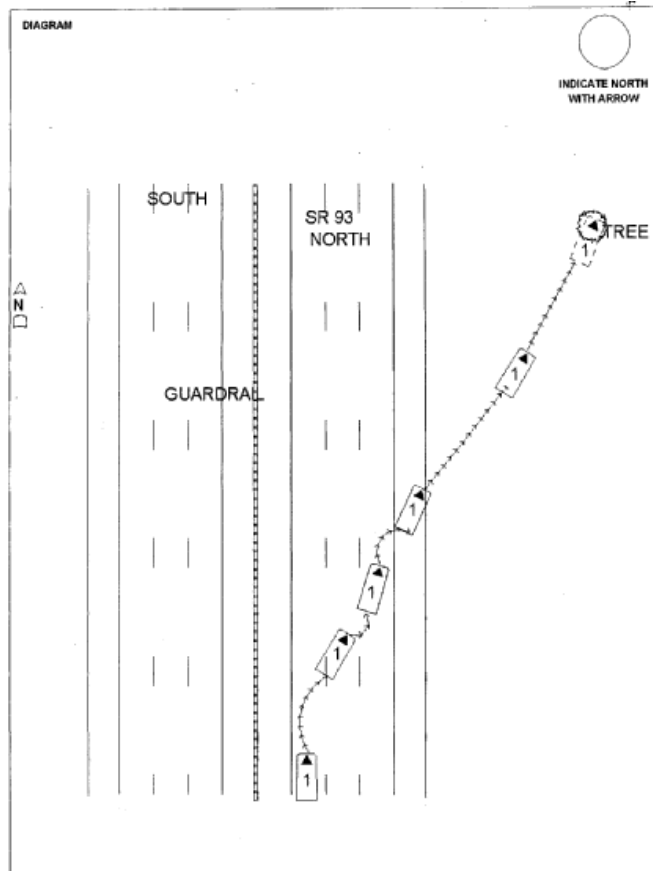
Figure 4.21 Details of the long form for a crash

For the selected possible hydroplaning crashes the distances between each crash site and all the weather stations relevant to that interstate were calculated using the GPS based X and Y coordinates. Then the closest three weather stations to each crash were recorded along with the distance between the weather stations and the crash site. Since the investigators dealt with large storms and heavy rainfall it was assumed that these types of storms can be maintained within a 30 km (18.6 miles) radius from the crash site (Figure 4.22). For this reason data provided by any weather stations found outside the 30 km radius was disregarded on account of being an unreliable reading.

Finally, all the crashes that had three closest weather stations within 30 km (18.6 miles) to each crash were recorded. Weather Wunderground website was used to obtain the rainfall intensity of each crash. Each weather station's history was accessed on Weather Wunderground website; the date and time for each crash was found on the corresponding three weather stations and recorded in mm/h.
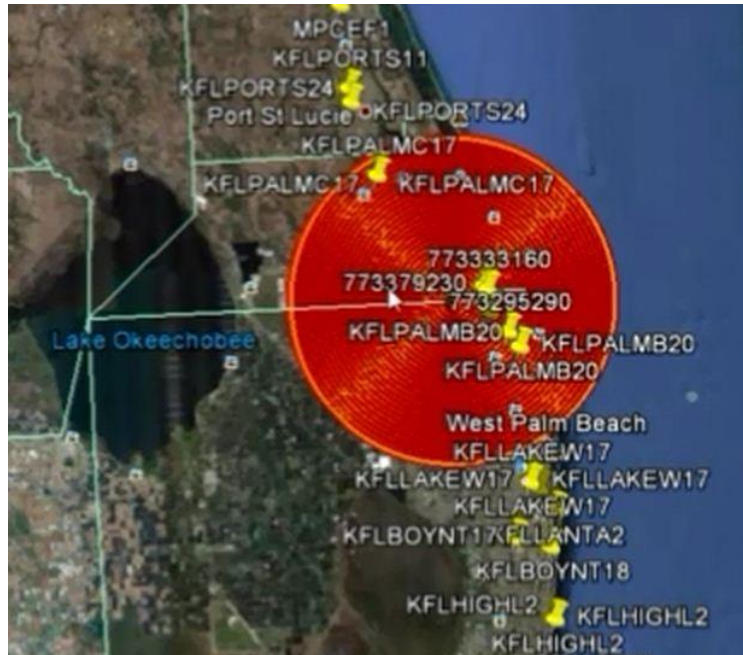
Figure 4.22 I-95 crash site with 30km (18.6 mile) radius (Google Earth)

When determining the effective rainfall intensity relevant to each crash it was assumed that the rainfall intensity attenuates with the distance and hence Equation (4.1) was used for the computation:

$$I_{avg} = \frac{I_1\left(\dfrac{1}{R_1}\right) + I_2\left(\dfrac{1}{R_2}\right) + I_3\left(\dfrac{1}{R_3}\right)}{\left(\dfrac{1}{R_1}\right) + \left(\dfrac{1}{R_2}\right) + \left(\dfrac{1}{R_3}\right)} \tag{4.1}$$

I_i = rainfall rate recorded at weather station i (mm/h or in/h)
R_i = distance from crash location to weather station i

Rainfall data that seemed to be unreliable or missing was disregarded. If the closest weather station was within 10 km (6 miles) from the crash site and the remaining two weather stations

70

were unreliable or further than 20 km from the crash then the rainfall rate from the closest weather station was used as the effective rainfall intensity.

Finally an additional screening criterion of a minimum of 30 mm/h (1.2 in/h) rainfall intensity was used to further screen the remaining crashes for those deemed to be hydroplaning crashes. The minimum rainfall intensity of 30 mm/h (1.2 in/h) corresponds to a minimum water film thickness on the pavement where hydroplaning is possible at a reasonable speed. The final crash count was 37 crashes in 2009 and 46 crashes in 2010, yielding a total of 83 hydroplaning crashes for this analysis.

To find the threshold hydroplaning speed from PAVDRN, the incident lane where hydroplaning began was needed. The police long forms (Fig. 4.22) were referenced to find the incident lane where the hydroplaning action was first observed based on the sketch and the description of events. Then, PAVDRN was run for each crash's characteristics to find the threshold hydroplaning speed on the middle of the incident lane.

Sample PAVDRN run:

The following example was worked out by the investigators to illustrate how the prediction of the hydroplaning potential of a given roadway based on PAVDRN software can be compared with actual hydroplaning incidents identified above.

Crash located on roadway ID 93220000
Rainfall intensity (Weather database)   = 48 mm/h (1.89 in/h)
Incident lane (Police long form)   = 2
Posted speed (Police long form)   = 65 mph
Traveling speed (Police long form)   = 65 mph

In PAVDRN's screen 1, the rainfall intensity is entered in in/h. All crashes in the dataset are on tangent sections. The kinematic viscosity and water temperature are kept at PAVDRN default values.

Figure 4.23 Sample PAVDRN screen 1

The user must then click on "Go to Screen 2". In the next screen (Fig. 4.24) the user must choose the number of planes on the roadway and in this example 2 planes are demonstrated. In the "Plane Properties" section the user must select the plane. Since the first plane has 2 lanes of 12 ft each, the "Plane Width" is set at 24 ft. The "Cross-slope" of the first two lanes is 2%. The "Pavement Type" at this crash site is OGAC". The "Mean Texture Depth" of OGAC pavement is entered in inches. The OGAC permeability is recommended at 0.02 inches in PAVDRN *Help*.

Figure 4.24 Sample PAVDRN Screen 2 Plane 1

The next step is to change plane 2 characteristics and Select Plane 2 (Fig. 4.25) in the drop down under "Plane Properties". The second plane has one lane with "Plane Width" = 12 ft. The "Cross-slope" of the third lane is 3% based on the Plans Preparation Manual, Volume 1 Design Geometrics and Criteria. The pavement type of plane 2 is the same as plane 1. All other values are kept at PAVDRN default values.

Figure 4.25 Sample PAVDRN Screen 2 Plane 2

To execute PAVDRN "Analysis" must be clicked. Then a window will open to notify the user that the program has finished the calculation. Finally on clicking "View PAVDRN Results", a new window will open with the results seen in Figure 4.26 and Figure 4.27.

```
            Results for Plane No.  1

   X       Y    Distance     WFT     Flow/width  Manning n   Reynolds No. Hydr. Speed
 (t,m)  (ft,m) (ft,m)    (in,mm)(cfs/ft,cms/m)                            (mph,km/hr)

    .0      .0      .00   -.59E-01    .00E+00      .000        0.         999999
   1.5     3.0     3.35   -.78E-02    .15E-03      .173       10.         999999
   3.0     6.0     6.71    .61E-02    .29E-03      .129       21.             98
   4.5     9.0    10.06    .16E-01    .44E-03      .108       31.             76
   6.0    12.0    13.42    .24E-01    .58E-03      .096       41.             69
   7.5    15.0    16.77    .30E-01    .73E-03      .087       52.             64
   9.0    18.0    20.12    .36E-01    .87E-03      .081       62.             62
  10.5    21.0    23.48    .41E-01    .10E-02      .076       72.             59
  12.0    24.0    26.83    .46E-01    .12E-02      .071       83.             58

Notes: 1) + denotes Reynolds numbers greater than  400.
           (Mannings n may be in error)
       2) * denotes hydroplaning speeds less than the facility design
           speed of   55. (mph, km/hr)
       3) Hydroplaning speed is equal to 999999. for water
```

Figure 4.26 Sample PAVDRN Plane 1 results

74

```
                    Results for Plane No.  2

   X     Y    Distance     WFT     Flow/width  Manning n  Reynolds No. Hydr. Speed
:t,m) (ft,m) (ft,m)     (in,mm)(cfs/ft,cms/m)                          (mph,km/hr)

 12.0   24.0   26.83     .42E-01    .12E-02      .079         83.          59
 13.0   27.0   30.00     .46E-01    .13E-02      .076         92.          58
 14.0   30.0   33.16     .50E-01    .14E-02      .073        102.          57
 15.0   33.0   36.32     .53E-01    .16E-02      .070        112.          56
 16.0   36.0   39.48     .56E-01    .17E-02      .067        122.          55

Notes: 1) + denotes Reynolds numbers greater than  400.
              (Mannings n may be in error)
       2) * denotes hydroplaning speeds less than the facility design
              speed of   55. (mph, km/hr)
       3) Hydroplaning speed is equal to 999999. for water
              film thickness less than or equal to 0.0
```

Figure 4.27 Sample PAVDRN Plane 2 results

To select the threshold hydroplaning speed for this crash the incident lane is taken into account. The threshold speed used is the speed in the middle of the incident lane, which in this example is the second lane. Therefore at 18 ft from the median the threshold speed is 62 mph (Figure 4.26). To verify PAVDRN's prediction the traveling speed must be compared to the threshold hydroplaning speed obtained above. The traveling speed is obtained from the police long form; these speeds are either estimated by the driver or by the police officer depending on the circumstances.

The reported traveling speeds cannot be relied on because the driver may not be truthful when reporting their speed to a police officer after a crash. Therefore, the investigators used three different ways to estimate the error of prediction (by PAVDRN).

Scenario 1: Travel Speed vs. PAVDRN Threshold Speed

In this analysis, the threshold speed of PAVDRN was compared to the traveling speed report by the police officer in the crash police long form. Table 4.4 is a sample of the data set which compares PAVDRN hydroplaning speed with the travel speed. If the hydroplaning speed reported by PAVDRN is less than or equal to the traveling speed, it is reported as a correct response by PAVDRN (denoted by 1 in PAVDRN VS TRAVELSPEED column). If the hydroplaning speed is greater than the traveling speed, it is reported as an incorrect response by PAVDRN (denoted by 0 in PAVDRN VS TRAVELSPEED column). Since the traveling speed is reported as a multiple of 5, an error buffer of ± 2 mph was created when comparing the hydroplaning speed with the traveling speed. If the hydroplaning speed is within 2 mph from the traveling speed, it is reported as a correct response by PAVDRN (1 in PAVDRN VS TRAVELSPEED column).

To find the probability of PAVDRN getting an incorrect measurement, a Bernoulli distribution was used, which denotes a value of 1 as a success probability p and the value of 0 as a failure probability $q=1-p$. Column y in Table 4.4 was created by comparing the Hydroplane column and the PAVDRN VS TRAVELSPEED column. If both column values are equal, then PAVDRN is correct and y=0; if both column values are not equal, then PAVDRN is incorrect and y=1. In this analysis, y is the probability of PAVDRN making an error:

$$y = \begin{cases} 0 \; if \; Hydroplanning = PAVDRNVSTRAVELSPEED \\ 1 \; if \; Hydroplanning \neq PAVDRNVSTRAVELSPEED \end{cases}$$

Since y can be assumed to follow a Bernoulli distribution:
$E(y) = p$

To find the probability of the error in the sample:

$$\hat{p} = \frac{\sum y_i}{N} \qquad E(\hat{p}) = p$$

N is the number of measurements.

Table 4.4 Sample dataset of PAVDRN predictions based travel speed (mph)

CARNUM	CRASHDATE	TIME	RDWYID	I (mm/hr)	I (in/hr)	Incident Lane	Traveling Speed	Hydroplane speed	Hydroplane	PAVDRN VS TRAVELSPEED	Type	YEAR	y (probability) (TRAVEL SPEED)
773379370	8/6/2010	5:19	93220000	48	1.8897638	2	65	62	1	1	Open	2010	0
773365070	8/5/2010	5:10	93220000	63	2.480315	3	65	54	1	1	Open	2010	0
773375160	8/8/2010	14:53	93220000	95.5	3.7598425	4	65	48	1	1	Open	2010	0
773295700	4/26/2010	8:50	93220000	51	2.007874	4	65	53	1	1	Open	2010	0
773362220	6/4/2010	21:04	93220000	89	3.503937	1	60	59	1	1	Open	2010	0
773372380	7/23/2010	11:46	93220000	108	4.2519685	5	50	52	1	1	Open	2010	0
773398970	8/29/2010	9:00	93220000	76	2.992126	4	65	50	1	1	Open	2010	0
773407520	8/8/2010	15:53	93220000	77.611075	3.0555541	2	45	56	1	0	Open	2010	1
773398560	6/4/2010	20:40	93220000	60.532725	2.3831781	1	60	65	1	0	Open	2010	1
773400250	8/29/2010	19:43	93220000	43.988808	1.7318429	1	65	71	1	0	Open	2010	1

Using traveling speed as the measure, the probability of PAVDRN obtaining a correct response is 63.86% (Table 4.5)

Table 4.5 Reliability of PAVDRN based on travel speed

Probability of PAVDRN being correct (q)	63.86%
Probability of PAVDRN being incorrect (p)	36.14%

Since the dataset is comprised of independent random variables (each crash is independent from another crash) the central limit theorem states that the dataset will approximately follow a normal distribution when N is large (N>30). To find the margin of error (MOE) (the difference between $\hat{p}$ and true p) of the dataset at a 95% confidence can be calculated as follows:

$$p = (|\hat{p} - p| \leq MOE) = 0.95$$

$$p\left(\frac{-MOE}{\sqrt{\frac{p(1-p)}{N}}} < \frac{\hat{p} - p}{\sqrt{\frac{p(1-p)}{N}}} < \frac{MOE}{\sqrt{\frac{p(1-p)}{N}}} \right) = 0.95$$

$$\phi\left(\frac{-MOE}{\sqrt{\frac{p(1-p)}{N}}} \right) = \frac{0.05}{2} = 0.025$$

$$\frac{dy}{dp} = p(1-p) = 0 \qquad 1 - 2p = 0; \quad p = \frac{1}{2}$$

Using the Standard normal variate (z) table at 95% confidence (N>30):

$$-1.965 = \frac{-MOE}{\sqrt{\frac{p(1-p)}{N}}} = \frac{-MOE}{\sqrt{\frac{0.5(1-0.5)}{83}}}$$

$$MOE = 0.10784; \quad 10.78\%$$

$\hat{p}$ is within 0.108 of the true p value which is acceptable.

Scenario 2: Posted Speed vs. PAVDRN Threshold Speed

It is expected that the traveling speed reported to the police officer is typically underestimated by the driver; therefore another type of verification was done which compares the PAVDRN threshold speed with the posted speed. In this scenario it is assumed that the vehicles are traveling at the posted speed limit, based on which the probability of correct hydroplaning prediction of PAVDRN can be calculated. The steps followed to obtain the probability of PAVDRN getting the correct measurement was the same as in Scenario 1. Below in Table 4.6 is a sample of the dataset when PAVDRN's threshold hydroplaning speed is compared with the posted speed.

Table 4.6 Sample dataset of PAVDRN predictions based on posted speed (mph)

CARNUM	CRASHDATE	TIME	RDWYID	I (mm/hr)	I (in/hr)	Incident Lane	Posted Speed	Hydroplane speed	Hydroplane	PAVDRN VS Posted speed	Type	YEAR	y (probability POSTED SPEED)
773379370	8/6/2010	5:19	93220000	48	1.8897638	2	65	62	1	1	Open	2010	0
773365070	8/5/2010	5:10	93220000	63	2.480315	3	65	54	1	1	Open	2010	0
773375160	8/8/2010	14:53	93220000	95.5	3.7598425	4	65	48	1	1	Open	2010	0
773295700	4/26/2010	8:50	93220000	51	2.007874	4	65	53	1	1	Open	2010	0
773362220	6/4/2010	21:04	93220000	89	3.503937	1	65	59	1	1	Open	2010	0
773372380	7/23/2010	11:46	93220000	108	4.2519685	5	65	52	1	1	Open	2010	0
773398970	8/29/2010	9:00	93220000	76	2.992126	4	65	50	1	1	Open	2010	0
773407520	8/8/2010	15:53	93220000	77.611075	3.0555541	2	65	56	1	1	Open	2010	0
773398560	6/4/2010	20:40	93220000	60.532725	2.3831781	1	65	65	1	1	Open	2010	0

Using posted speed as the measure, the probability of PAVDRN obtaining a correct response is 77.11% (Table 4.7). The probability of getting a correct response by PAVDRN is higher using the posted speed because it is generally higher than the estimated traveling speed reported to the police officer.

Table 4.7 Reliability of PAVDRN based on posted speed

Probability of PAVDRN being correct (q)	77.11%
Probability of PAVDRN being incorrect (p)	22.89%

4.2.4.1 PAVDRN reliability on lane by lane basis

The same procedure was repeated by classifying each crash on a lane by lane basis when both speeds were used in the comparison of results based on the incident lane design criterion, the results shown in Table 4.8 are as follows. It is apparent that most of the incorrect PAVDRN responses occur in the first lane with 53.3% and 78.9% of incorrect responses using travel speed and posted speed respectively.

Table 4.8 (a) Comparison of the reliability of PAVDRN predictions on a lane by lane based on travel speed

Incident Lane	Predictions using Travel Speed	
	Correct	Incorrect
1	24.50%	53.30%
2	43.40%	26.70%
3	20.80%	13.30%
4	9.40%	6.70%
5	1.90%	0.00%
Total	100.00%	100.00%

Table 4.8(b) Comparison of the reliability of PAVDRN predictions on a lane by lane based on posted speed

Incident Lane	Predictions using Posted Speed	
	Correct	Incorrect
1	21.90%	78.90%
2	43.80%	15.80%
3	21.90%	5.30%
4	10.90%	0.00%
5	1.60%	0.00%
Total	100.00%	100.00%

Scenario 3: Using an average hydroplaning speed range

Since using the crash speeds may be unreliable because the vehicle speed is unknown, another technique was preformed to find the average hydroplaning zones based on PAVDRN. In this method, the speed of vehicles is assumed to be a normal distribution. A study was done by Edwards (1999) at the University of Wales College, United Kingdom, to measure the speed reduction in different weather conditions. The study was done on a highway with a speed limit of 70 mph. Speed of vehicles was measured on clear days and on days of Steady/Heavy Rain in the course of 6 months (October to March). The results are seen in Table 4.9. It was found that drivers reduce their speed during rain, and the overall speeds of vehicles are more consistent than in fine weather.

Table 4.9 Speed survey results (Edwards, 1999)

Summary statistics for survey speeds by weather

Parameter	Fine	Rain	Fog
85th percentile (mph)	71.38	68.10	69.00
Mean (mph)	64.29	61.46	62.11
Median (mph)	64	61	62
Mode (mph)	60	57	59
SD	7.09	6.33	6.88
Range (mph)	45	50	40
Count (vehicles)	2600	1400	400
Z statistic		13.04	5.9
Coefficient (%) of variation	11.03	10.30	11.08

A crash site with a posted speed of 70 mph and PAVDRN threshold hydroplaning speed of 65 mph can be represented in Fig. 4.28 using the relevant speed reduction data in Table 4.9. It is realized that any vehicle within the shaded region (having a speed of 65 mph or greater) runs the risk of hydroplaning.
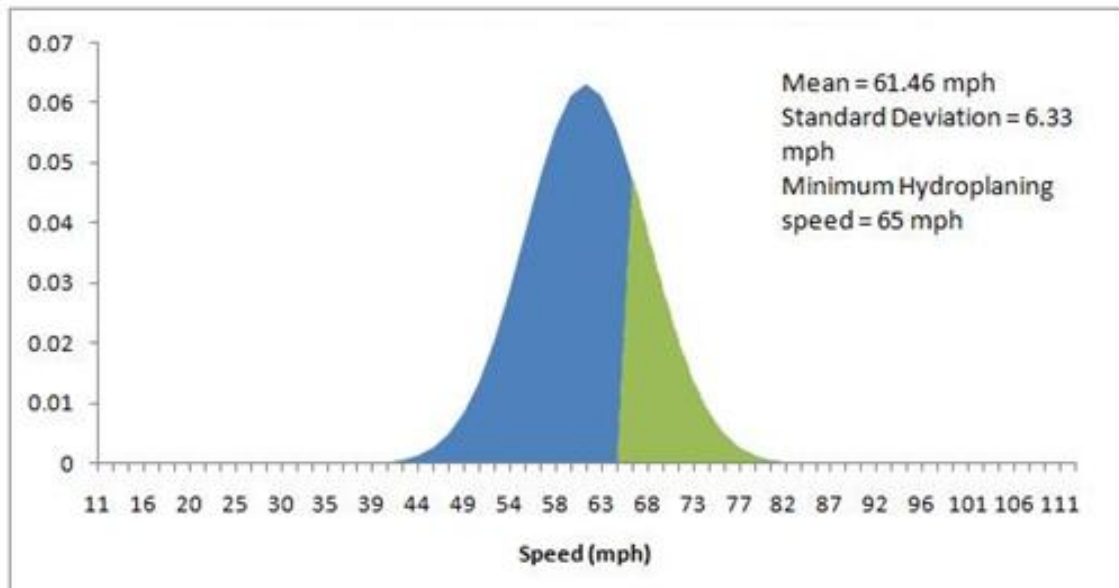
Figure 4.28 Speed distribution at 70 mph and minimum hydroplaning speed of 65 mph

To obtain the mean and standard deviation (SD) at a different speed limit it is assumed that the coefficient of variation (CV%) remains the same and hence the standardized z score of the speed limit is also the same.

At 70 mph the CV% is:

$$CV\% = \left(\frac{SD}{mean}\right) x100 = 10.29938$$

70 mph on the z-scale:

$$z = \frac{(x - mean)}{SD} = \frac{70 - 61.46}{6.33} = 1.349131$$

At 65 mph the CV% is:

$$CV\% = \left(\frac{SD}{mean}\right) x100 = 10.29938$$

65 mph on the z-scale:

$$z = \frac{65 - mean}{SD} = 1.349131$$

As an example, using these two equations the mean of the wet weather speed distribution of a 65 mph posted speed limit roadway is 57.07 mph and the standard deviation is 5.88 mph.Using a program known as R (*R project for Statistical Computing*), the percentage above the threshold hydroplaning speed for each crash was found using the following:

- pnorm(hydroplaning speed, mean, sd, lower.tail=FALSE)

For a 70 mph roadway with a hydroplaning threshold speed of 65 mph
- pnorm(65,61.46,6.33,lower.tail=FALSE)

This would print out the following:
[1] 0.2879

The above value indicates that 28.79% of the distribution is above the threshold speed of 65 mph. This would provide one with a percentage of the traffic volume that is traveling within the hydroplaning zone.

Table 4.10 illustrates a sample of the dataset which was prepared by computing the percentage of vehicles that would have traveled in the hydroplaning speed zone in the crash database considered in this analysis.

Table 4.10 Sample PAVDRN dataset and percentage volume above threshold speed (mph)

CARNUM	CRASHDATE	TIME	RDWYID	I (mm/hr)	I (in/hr)	Incident Lane	Posted Speed	Type	YEAR	Mean in Rain	SD in Rain	pvalue from R (pnorm(speed, mean,sd,lower. tail=FALSE))	Hydroplane Area %
773379370	8/6/2010	5:19	93220000	48	1.8897638	2	65	Open	2010	57.07	5.877857	0.200813	20.0813
773365070	8/5/2010	5:10	93220000	63	2.480315	3	65	Open	2010	57.07	5.877857	0.6992646	69.92646
773375160	8/8/2010	14:53	93220000	95.5	3.7598425	4	65	Open	2010	57.07	5.877857	0.9385897	93.85897
773295700	4/26/2010	8:50	93220000	51	2.007874	4	65	Open	2010	57.07	5.877857	0.7556608	75.56608
773362220	6/4/2010	21:04	93220000	89	3.503937	1	65	Open	2010	57.07	5.877857	0.3713262	37.13262
773372380	7/23/2010	11:46	93220000	108	4.2519685	5	65	Open	2010	57.07	5.877857	0.8058043	80.58043
773398970	8/29/2010	9:00	93220000	76	2.992126	4	65	Open	2010	57.07	5.877857	0.8854712	88.54712
773407520	8/8/2010	15:53	93220000	77.611075	3.0555541	2	65	Open	2010	57.07	5.877857	0.5722223	57.22223
773398560	6/4/2010	20:40	93220000	60.532725	2.3831781	1	65	Open	2010	57.07	5.877857	0.08865269	8.865269
773400250	8/29/2010	19:43	93220000	43.988808	1.7318429	1	65	Open	2010	57.07	5.877857	0.008897563	0.8897563

Based on the method described above, the investigators computed the probability of a vehicle getting into the hydroplaning zone as predicted by PAVDRN. In order to be more meaningful the results are presented in terms of three rainfall categories listed below:

- Low rainfall intensity (30 mm/h – 45 mm/h or 1.2 in/h – 1.8 in/h)
- Moderate rainfall intensity (45. mm/h – 65 mm/h or 1.8 in/h – 2.6 in/h)
- High rainfall intensity (65.01+ mm/h or 2.6+ in/h))

Table 4.11 Percentage of hydroplaning zones

Rainfall Category (Intensity)	Low rainfall intensity (1.2 in/h – 1.8 in/h)	Moderaterainfall intensity (1.8 in/h – 2.6 in/h)	High rainfall intensity (2.6+ in/h)
Probability of entering the Hydroplaning Zone based on PAVDRN	26.60 %	46.55%	67.24%

Table 4.11 shows that with higher rainfall intensities the average percentage of the traffic volume in the hydroplaning zones increases. This can be explained by the fact that as the rainfall intensity increases, the water film thickness increases leading to a lower threshold hydroplaning speed which increases the percentage of vehicles traveling at a speed above the minimum hydroplaning speed.

CHAPTER 5

NUMERICAL PREDICTION OF SKIDDING OF A SMOOTH TIRE SLIDING ON A ROUGH WET PAVEMENT

5.1 Introduction

During rainy weather conditions automobiles and aircrafts could encounter significant reduction of steering and braking abilities due to reduction of tractive forces produced by the development of a water film between the tire and pavement surface. In general, factors affecting wet traction on a tire sliding on a random rough pavement can be categorized based on their sources of origin. Table 5.1 summarizes these factors based on previous researchers' work (Venner and Lubrech, 2005). Due to the complex nature of the factors, the numerical simulation of tractive forces on a tire has always been a challenging task.

Table 5.1 Factors affecting wet friction (Venner and Lubrech, 2005)

Domain	Factor
Tire	Carcass properties Inflation pressure Tread properties (not for smooth tires)
Pavement	Surface Texture (Macrotexture and Microtexture) Wearing characteristics Porosity
Water	Density Viscosity Water film depth
Operating conditions	Load Velocity Percent slip

5.2 Simulation of tractive forces on a smooth locked wheel sliding on a randomly rough pavement

The author made an attempt to numerically simulate the tractive forces on a smooth wheel sliding on a randomly rough pavement. Based on the characteristics of each domain, the simulation model was divided into two domains; fluid and tire domains. Simulation of the fluid domain involves modelling of water by considering principles of mass, momentum and energy conservation. This results in the Reynolds equation which has been simplified later by considering the dimensional factors and the conditions of analysis.

The pavement roughness affects the water flow between the tire and the pavement. Therefore, pavement roughness conditions were also considered in the fluid flow simulation. Due to the flexible nature of the tire, deformations occur as a result of water pressure built against the tire surface. Hence the analysis results of the fluid model must be an input to the analysis of the tire model and vice versa. This situation has been identified as the Fluid-Structure Interaction (FSI). This FSI analysis is repeated in the combined model until the deformation of the fluid and tire become compatible at the interface.

A MATLAB code was developed using the Finite Difference Method (FDM) for the fluid flow and tire models including FSI conditions in order to determine the tractive forces of a sliding tire on a randomly rough pavement. The major objective of developing the numerical model was to predict the wet friction forces. Subsequent efforts were made to determine the validity of the developed model and perform relevant parametric studies. Finally, the authors also attempted to evaluate the feasibility of determining the viscous hydroplaning speeds under certain conditions, using the developed model.

5.3 Development of the Numerical Model

As indicated in Figure 5.1, as the tire slides on the pavement, the entire tire patch loses contact with the pavement since the hydrodynamic pressure developed in front of the tire is adequate to inject enough water to occupy the interface. In a stationary observer frame of reference, the traction force can be simulated by a wheel sliding along a wet pavement surface. In a moving wheel frame of reference on the other hand, the problem can be modeled as a layer of water on the pavement surface moving at a corresponding speed toward the wheel. In either case, a locked wheel is modeled in a sliding maneuver.

The development of the tire traction force model is based on the simultaneous analysis of three aspects: (1) the hydrodynamics of thin film fluids; (2) tire deformation characteristics; and (3) uplift condition. The hydrodynamics of thin film fluid was analyzed in the fluid (water) flow model and the tire deformation characteristics were incorporated in the tire deformation model. Finally the uplift criterion of the tire was satisfied by balancing the tire load and the uplift load induced by the fluid film. As depicted in Figure 5.2, the contact patch was divided into a rectangular grid system and analyzed such that each node was made to satisfy the equilibrium criteria which will be discussed in this chapter.
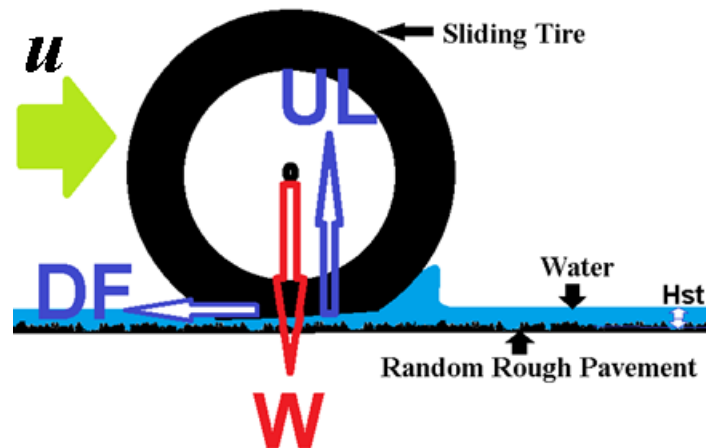
Figure 5.1 Forces acting on a tire sliding on a wet pavement
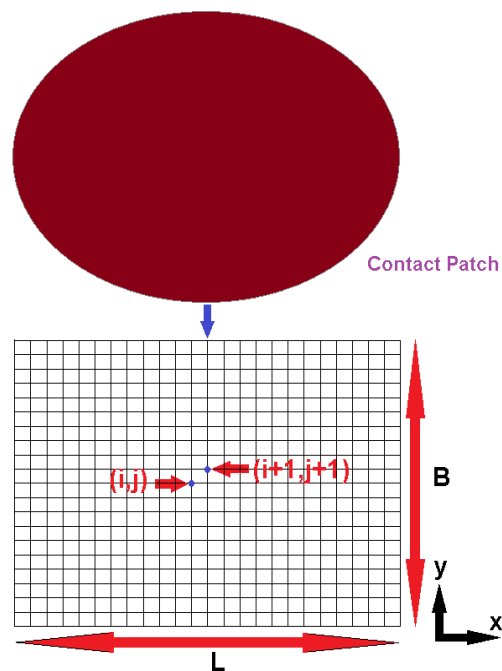
Figure 5.2 The rectangular grid domain in the tire contact patch

5.3.1 Fluid Flow Model

The Reynolds equation (Equation 5.1) has been derived from the universal laws of conservation known as conservation of mass, conservation of momentum and conservation of energy. It enables the prediction of the fluid pressure distribution in the tire contact patch based on the tire

and pavement geometry, boundary conditions and the physical properties of water such as viscosity and density. The following assumptions are used to establish the Reynolds equation;

- Liquid is Newtonian
- Flow is laminar and independent of pressure
- Inertial force and gravity are neglected
- Lubricant is incompressible
- Viscosity is constant $(\eta = c)$

By considering an infinitesimally small moving fluid element as depicted in Figure 5.3, the equation that results from the conservation of mass can be derived as seen in Equation 5.1, which is also known as the continuity equation in Cartesian notation. The symbols ρ, v, u, w and t represent the mean density, velocities in x, y and z directions and time respectively.

$$\frac{\partial \rho}{\partial t} + \frac{\partial \rho u}{\partial x} + \frac{\partial \rho v}{\partial y} + \frac{\partial \rho w}{\partial z} = 0 \qquad (5.1)$$
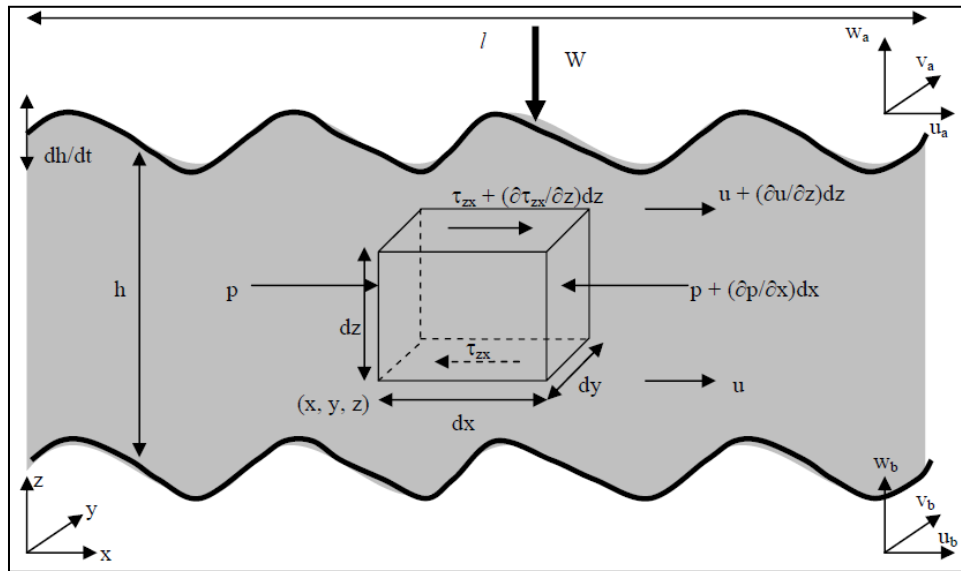
Figure 5.3 Schematic of fluid flow between two surfaces and stresses acting on fluid element and velocities in x-z plane (Ong, 2006)

The momentum equations are expressed in Equations 5.2 to 5.4. The forces considered include body forces f and the surface forces which include pressure p exerted on the surface by surrounding elements and the shear stresses exerted on the surface by fluid friction τ on the same fluid element.

$$\rho \frac{Du}{Dt} = -\frac{\partial p}{\partial x} + \frac{\partial \tau_{xx}}{\partial x} + \frac{\partial \tau_{yx}}{\partial y} + \frac{\partial \tau_{zx}}{\partial z} + \rho f_x \qquad (5.2)$$

$$\frac{Dv}{Dt} = -\frac{\partial p}{\partial y} + \frac{\partial \tau_{xy}}{\partial x} + \frac{\partial \tau_{yy}}{\partial y} + \frac{\partial \tau_{zy}}{\partial z} + \rho f_{xy} \tag{5.3}$$

$$\rho \frac{Dw}{Dt} = -\frac{\partial p}{\partial z} + \frac{\partial \tau_{xz}}{\partial x} + \frac{\partial \tau_{yz}}{\partial y} + \frac{\partial \tau_{zz}}{\partial z} + \rho f_z \tag{5.4}$$

By applying the boundary conditions (i.e., no slip at the surfaces) and assuming the pressure to be independent of z due to the narrow gap between the two surfaces, the equations of conservation of mass and momentum can be combined and simplified to derive the Reynolds equations as shown in Equation 5.5.

$$\frac{\partial}{\partial x}\left(\frac{\rho h^3}{\eta}\frac{\partial p}{\partial x}\right) + \frac{\partial}{\partial y}\left(\frac{\rho h^3}{\eta}\frac{\partial p}{\partial y}\right) = 6u_s \frac{\partial(\rho h)}{\partial x} + 6\rho h \frac{\partial u_s}{\partial x} + 12\frac{\partial(\rho h)}{\partial t} \tag{5.5}$$

Wedge Term   Stretch Term   Squeeze Term

5.3.1.1 Wedge effect

A wedge builds up in front of the tire thus increasing the film thickness in the direction of sliding. When water approaches the wedge, due to decreasing film thickness at the interface, pressure builds up in the wedge area. The tire is subjected to a buildup of hydrodynamic pressure in the front due to the wedge effect thereby contributing to the separation of the tire from the pavement. Since this separation leads to reduced traction forces the wedge term is very important in this study.

5.3.1.2 Squeeze effect

The squeeze term occurs must be included in Equation 5.5 to account for the pressure variation in the analysis domain. In the problem modeled in this study, atmospheric pressure acts on the tire boundary while , the pressure values are relatively higher in the tire contact patch. Therefore, a "squeeze" effect is generated within the wet part of the tire-pavement contact patch under transient loading conditions.

5.3.1.3 Stretch effect

The stretch term in Equation 5.5 considers the rate at which the surface velocity changes in the sliding direction. This effect only occurs if the bodies in contact (tire and/or pavement) in the fluid boundaries are flexible and stretch the boundary surface along the direction of travel. They are neglected in this study since surface stretches are negligible in magnitude when compared to the radial deformations of the tire.

5.3.1.4 Nondimensionalization of the Reynolds Equation

Since the magnitude of the variables "pressure" in 10^6 Pa and "film thickness" in 10^{-6} m vary significantly, nondimensionalization would be beneficial to solve the Reynolds equation fasterby reducing the parameter size. Therefore, nondimensionalization was performed based on the Hertz's theory (Venner and Lubrech, 2005). This theory provides the pressure profile, the geometry of the contact domain, and the elastic deformation of the contacting elements in the case of a loaded contact between two elastic bodies.

The Hertzian pressure profile is given by;

$$p(x,y) = \begin{cases} p_h \sqrt{1 - \left(\frac{x}{a}\right)^2 - \left(\frac{y}{a}\right)^2} & \text{if } |x^2 + y^2| < a^2 \\ 0 \end{cases}$$

(5.6)

where$p_h$refers to the maximum Hertzian pressure in the contact patch:

$$p_h = \frac{2.5F}{2\pi a^2}$$

(5.7)

where$F$ is the external load and a is the radius of the contact patch which is assumed to be circular in the Hertz's derivations;

$$a^2 = \frac{2.5FR_x}{2E'}$$

(5.8)

whereR_x is the reduced radius of curvature of the two bodies in contact in the x direction ($R_x = R_y$ for a circular contact) and E' is the reduced elastic modulus of the contacting bodies. Here the reduced radius of curvature R is given by $\frac{1}{\frac{1}{R_1} + \frac{1}{R_2}}$, where R_1 and R_2 are the radii of curvature of two contacting bodies. The reduced elastic modulus E' is given by$\frac{1}{\frac{1}{E_1} + \frac{1}{E_2}}$, where E_1 and E_2 are moduli of two contacting bodies. Since the pavement modulus value is infinitely large based on the rigid pavement assumption the reduced elastic modulus becomes equal to the tire material elastic modulus. The dimensionless Reynolds equation as given in Equation 5.9 can be obtained by converting all the variables in the Reynolds equation into dimensionless variables given below;

$$\bar{\rho} = \rho/\rho_0,$$
$$\bar{\eta} = \eta/\eta_0,$$
$$X = x/a,$$
$$Y = y/a,$$
$$P = p/p_h,$$
$$H = hR/a^2,$$
$$T = tu_s/(2a),$$

where h is the fluid thickness and, ρ_0 and μ_0 are the density and the viscosity at the ambient pressure.

$$\frac{\partial}{\partial X}\left(\varepsilon\frac{\partial P}{\partial X}\right) + \frac{\partial}{\partial Y}\left(\varepsilon\frac{\partial P}{\partial Y}\right) - \frac{\partial(\bar{\rho}H)}{\partial X} - \frac{\partial(\bar{\rho}H)}{\partial T} = 0$$

(5.9)

Where,

$$\varepsilon = \frac{\bar{\rho}H^3}{\eta\lambda}$$

and λ is the dimensionless parameter given by;

$$\lambda = \frac{6\eta_0 u_s R^2}{b^3 p_h}$$

5.3.1.5 Discretization of the Reynolds Equation

The nonlinear Reynolds equation has been discretized and solved to obtain the pressure distribution in the contact region. The spatial domain $X \in [X_L, X_R]$ is discretized with a uniform grid of $n + 1$ points X_i ($0 \leq i \leq n$) with mesh size h_x. Then the following finite difference approximations have been used in converting the Reynolds equation to the equivalent numerical form.

$$\frac{\partial}{\partial X}(\rho H)_{X_i} \approx \frac{(\rho H)_i - (\rho H)_{i-1}}{h_X} = \frac{\rho_i H_i - \rho_{i-1}H_{i-1}}{h_X}$$

$$\frac{\partial}{\partial X}\left(\varepsilon\frac{\partial P}{\partial X}\right)_{X_i} \approx \frac{\left(\varepsilon\frac{\partial P}{\partial X}\right)_{i+1/2} - \left(\varepsilon\frac{\partial P}{\partial X}\right)_{i-1/2}}{h_X}$$

$$\left(\varepsilon\frac{\partial P}{\partial X}\right)_{i+1/2} \approx \varepsilon_{i+1/2}\left(\frac{P_{i+1} - P_i}{h_X}\right)$$

$$\left(\varepsilon\frac{\partial P}{\partial X}\right)_{i-1/2} \approx \varepsilon_{i-1/2}\left(\frac{P_i - P_{i-1}}{h_X}\right)$$

and,

$$\varepsilon = \frac{\rho H^3}{\eta\lambda}$$

$$\varepsilon_i = \frac{\rho_i H_i^3}{\eta_i\lambda} \longrightarrow \varepsilon_{i+1/2} = \frac{\varepsilon_i + \varepsilon_{i+1}}{2}$$

$$\longrightarrow \varepsilon_{i-1/2} = \frac{\varepsilon_i + \varepsilon_{i-1}}{2}$$

Similarly the spatial domain $Y \in [Y_L, Y_R]$ is discretized with a uniform grid of $n+1$ points Y_i ($0 \le i \le n$) with mesh size h_y and the time domain $T \in [0, T_f]$ is discretized using a time increment of ΔT. Then the discretized Reynolds equation (Equation 3.10) can be written as,

$$\frac{(\epsilon_{i-1,j}^n + \epsilon_{i,j}^n)(P_{i-1,j}^n - P_{i,j}^n) + (\epsilon_{i+1,j}^n + \epsilon_{i,j}^n)(P_{i+1,j}^n - P_{i,j}^n)}{2(\Delta X)^2} \qquad (5.10)$$

$$+ \frac{(\epsilon_{i,j-1}^n + \epsilon_{i,j}^n)(P_{i,j-1}^n - P_{i,j}^n) + (\epsilon_{i,j+1}^n + \epsilon_{i,j}^n)(P_{i,j+1}^n - P_{i,j}^n)}{}$$

$$- \frac{\rho_{i,j}^n H_{i,j}^n - \rho_{i-1,j}^n H_{i-1,j}^n}{\Delta X} - \frac{\rho_{i,j}^n H_{i,j}^n - \rho_{i,j}^{n-1} H_{i,j}^{n-1}}{\Delta T} = 0$$

where $\Delta X = h_x, \Delta Y = h_x$ and the superscript n denotes values at time t_n. Based on the assumption of homogeneous density in the analysis domain, $\rho_{i,j}^n = \rho$.

5.3.2 Tire model

As indicated in Figure 5.4, the smooth tire was modeled using a 3-dimensional spring model. The radial springs (with a spring coefficient k) over the x domain are spanned at distances of dx at the contact patch while the radial springs over the y domain are spanned at distances of dy at the contact patch.

Each radial spring is connected to the four adjoining radial springs by four interconnecting springs (of spring constant q). The spring coefficients of the radial and interconnecting springs are defined as functions of the tire inflation pressure. This model has been used in a previous research as a spring tire model by replacing the intermediate springs by interconnecting radial springs (Chae et al, 2005).
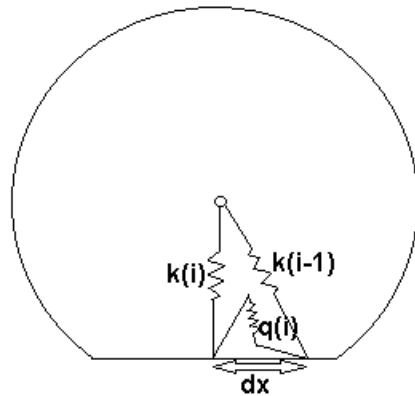
Figure 5.4 Spring diagram of the tire model

5.4 Numerical Solution Procedure

A MATLAB program was developed to solve the discretized nondimensional Reynolds equation and the tire model including the tire-water interaction. In the program, the initial values of length of the contact patch ($L = X_L - X_R$) was determined by performing an approximate preliminary analysis which satisfies the convergence criteria while the width ($B = Y_L - Y_R$) was assigned as 80 mm. This will be discussed later in this section. The boundary conditions are set such that all exterior boundaries have the atmospheric pressure.

5.4.1 Analysis of smooth pavement surfaces

5.4.1.1 The Steady State Solution

A preliminary closed form solution was observed for a rectangular plate with an infinite width and 100 mm long sliding on a flooded smooth surface which was tapered into the direction of sliding on a pavement with a standing water height of 1 mm. Then the results were compared with a similar numerical model developed in MATLAB. The results are depicted in Figure 5.5. Based on the Figure the MATLAB program results are fairly agreed with the closed form results.
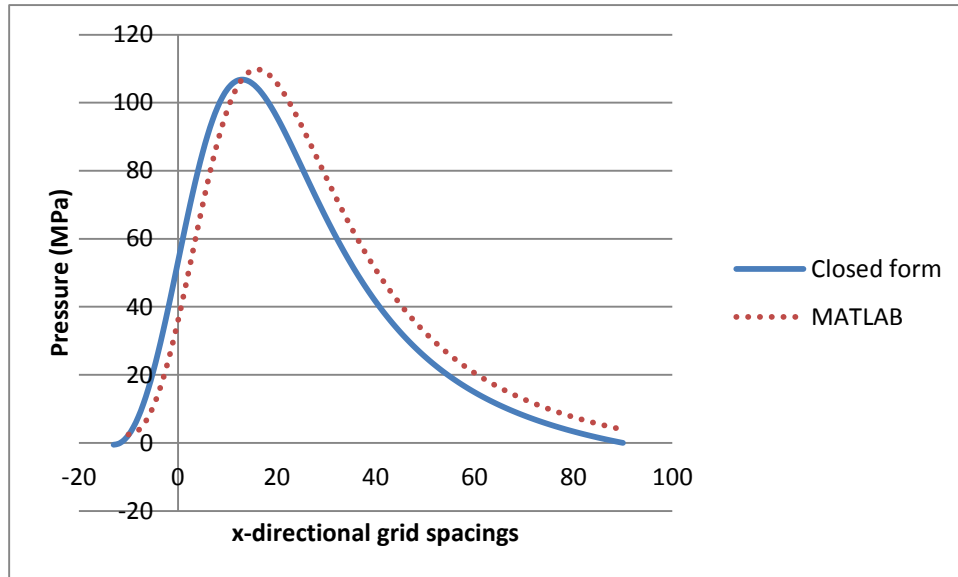
Figure 5.5 Comparison of the closed form solution and the MATLAB program

In the first phase, the analysis was performed only in the space domain by neglecting the time domain variations where the following "squeeze term" was neglected.

$$\frac{\rho_{i,j}^n H_{i,j}^n - \rho_{i,j}^{n-1} H_{i,j}^{n-1}}{\Delta T} = 0 \qquad (5.11)$$

The space domain (contact patch) was divided into 100 x 100 elements with the number of nodes in one direction being 101. The sliding speed (u) was considered as 65 mph (10 m/s). Analysis was performed iteratively until the uplift force induced on the tire surface due to the water pressure is approximately equal to the tire load. Figure 5.6 shows the pressure plot from the analysis of phase 1 which clearly indicates higher pressure values in front of the tire with respect to the sliding direction.

This peak clearly indicates the water approaching to the front of the tire subjects to the wedge effect and starts developing high pressure values as described in section 5.3.1.1.
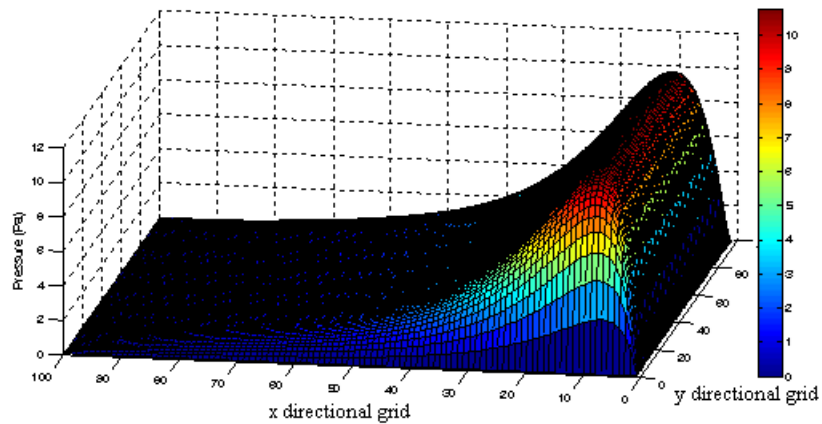
Figure 5.6 Pressure plot for the steady state analysis

5.4.1.2 The Transient Solution

Similarly, the second phase of the analysis was performed in both the space as well as the time domains. This was achieved by increasing the sliding pressure with time in each analysis loop. In order to compare the transient solutions obtained for a given ultimate speed with the steady state solution for that speed, the sliding speed in the transient analysis was increased in steps and maintained constant at the desired steady state analysis performed (65 mph). Figure 5.7 shows the pressure plot of the transient analysis at a speed of 65 mph. Figure 5.8 shows both steady state and transient pressure along the sliding direction (*X*) plotted on the same plot. Since the transient analysis is more time consuming when compared with the steady state analysis, the convergence criteria of the transient analysis were relaxed than that of the steady state analysis.

As it can be seen in Figure 5.8, the difference between the two pressure plots could be explained by the higher tolerance allowed in the transient analysis.
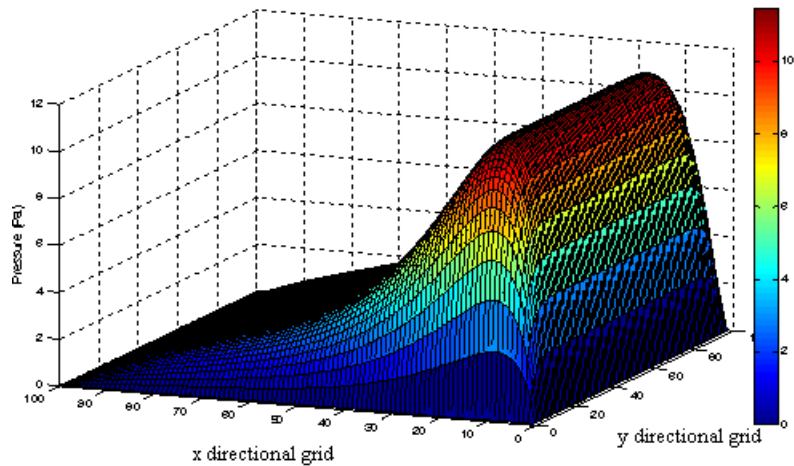
Figure 5.7 Pressure plot for the transient analysis
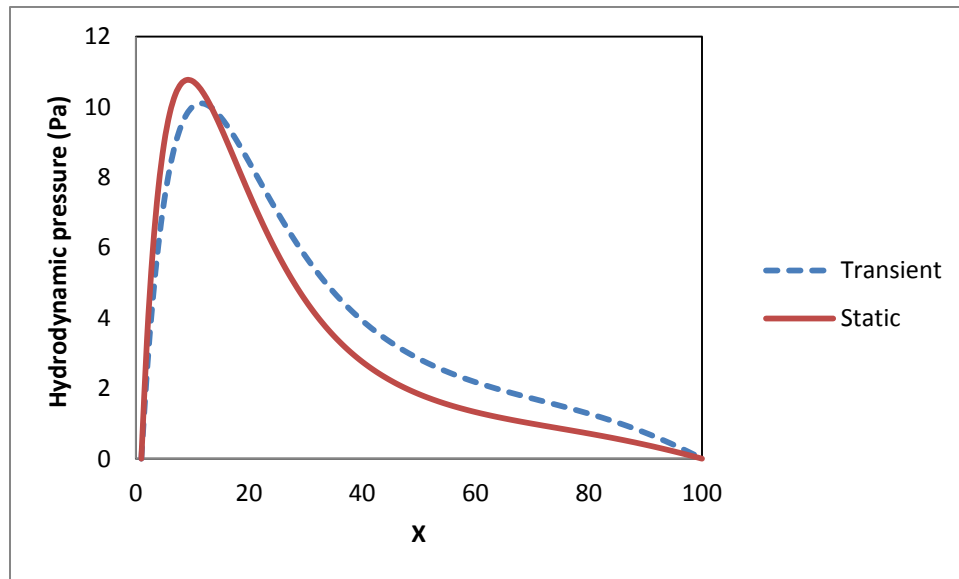
Figure 5.8 Two-dimensional pressure plot comparison for steady state and transient analyses

5.4.2 Analysis of random rough pavement surface condition

Pavement roughness has been incorporated in the model by including a random variation into the water film thickness equation. The results of field texture measurements observed using a circular texture (CT) meter were converted to Mean Texture Depth (MTD). Then the MTD values were used to generate a normally distributed random pavement profile in the MATLAB program. A random pavement profile was generated at each iteration. Figure 5.11 shows the variation of uplift pressure of water acting on the tire surface at a particular instance (time step) in the analysis. Since the pavement surface has a random nature, the pressure plot also shows a random variation over the contact domain. However, the pressure spike built in the domain could be explained by the instability caused by the sudden pressure drop from a very high value

93

to a very low value in the boundary. As depicted in Figure 5.9(a), (b) and (c), the tire patch was dragged to the sliding direction at a rate of one x-directional grid spacing per one time step such that the size of the time step defined as Δt(sec)=(x directional grid spacing (m))/ (sliding speed (u(m/s))). The 3-dimensional pavement profile is shown in Figure 5.10. The analysis was continued for a number of time steps until all the convergence criteria were satisfied. Those convergence criteria were (1) the force equilibrium, where uplift force $(UL)>=$ tire load (W), and (2) the minimum film thickness $(h_{min})>$ threshold value. Then the uplift pressure values were averaged. Since the program averages the results over a number of time steps the pressure spike observed in Figure 5.11 decreases with time. The average pressure distribution is shown in Figure 5.12.
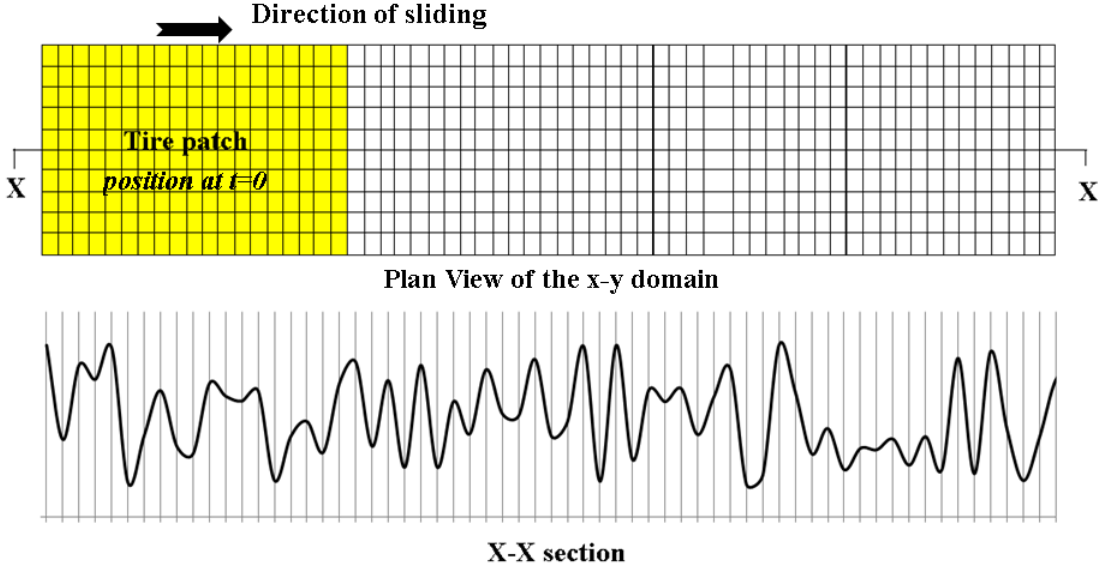
Figure 5.9(a) The tire patch location at t=0
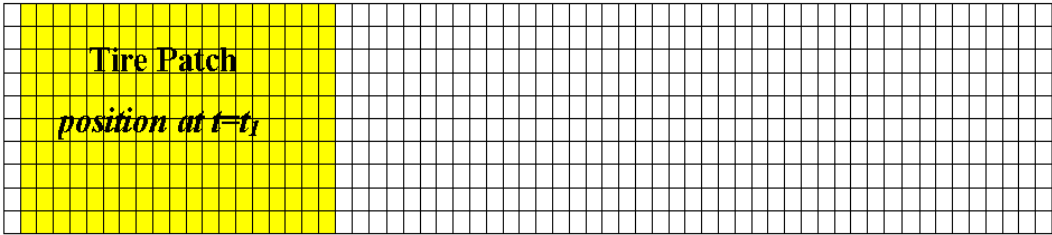
Figure 5.9(b) The tire patch location at t=t₁
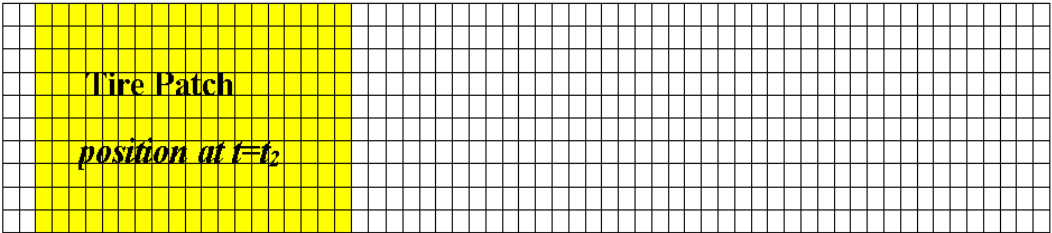
Figure 5.9(c) The tire patch location at t=t₂
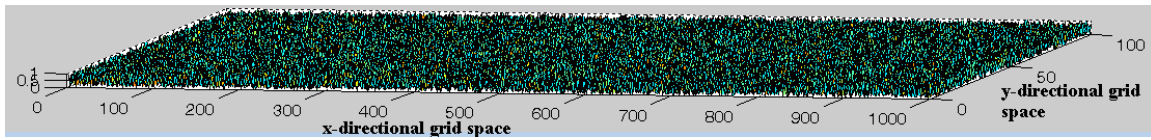
Figure 5.10 Three-dimensional randomly rough pavement
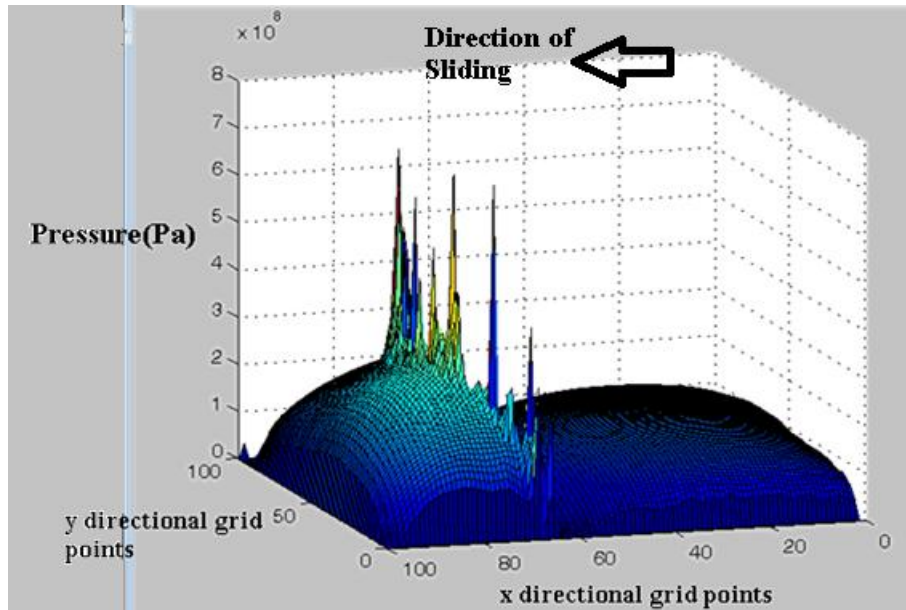
Figure 5.11 Uplift pressure distribution in the contact domain
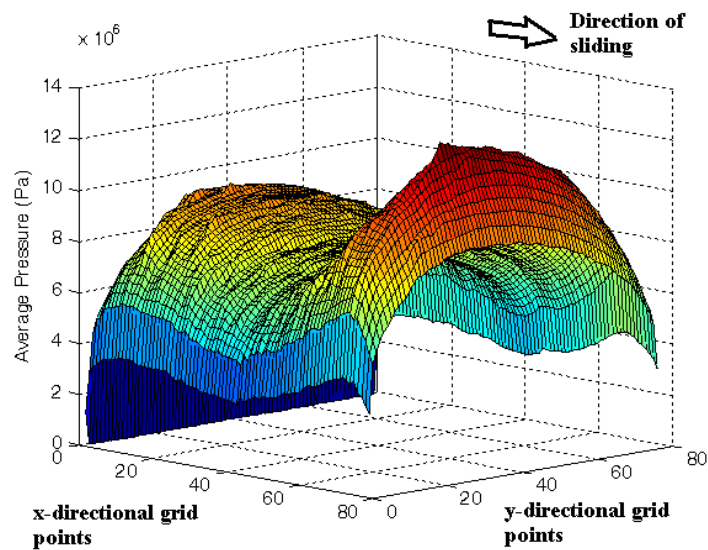
Figure 5.12 Three-dimensional average pressure plot

5.4.2.1 Determination of drag forces

Determination of the drag force is very important to evaluate in this study since when a sliding tire is completely separated from the pavement the drag force is the only force which helps in maneuvering the vehicle by providing the required friction. The study was continued by calculating the drag forces along the sliding direction (x direction) based on Equation 5.12.

$$F_{drag,x} = \frac{\eta u}{h} + \frac{h}{2}\frac{dP}{dx}$$ (5.12)

5.5 Sensitivity analysis of the numerical model

Sensitivity analysis is a technique used to determine how different values of input variables will impact the output under a given set of assumptions. The mesh size and the number of analysis steps were considered as input variables and the drag force is considered as the output variable. Each input variable was changed gradually while calculating the uplift forces and the results were plotted as shown in Figure 5.13(a) and (b) while keeping the following parameters constant at the indicated values;

Tire inflation pressure   = 25 psi
Tire contact width   = 80 mm
Average roughness height   = 0.1 mm
Sliding speed   = 30 mph
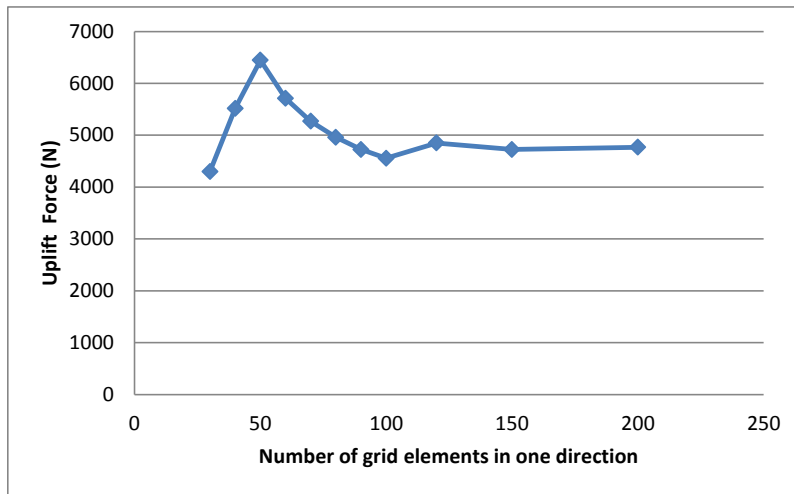
Figure 5.13(a) Sensitivity analysis for the contact grid size
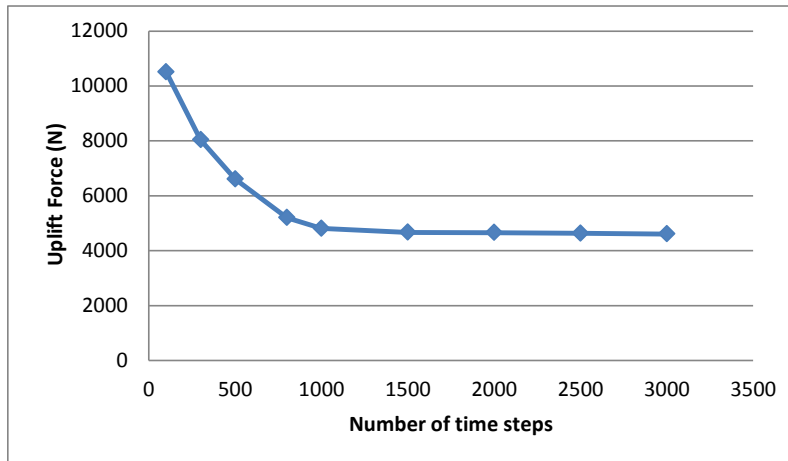
Figure 5.13(b) Sensitivity analysis for the number of time steps

Based on the sensitivity analysis, it is seen that the drag force is not sensitive to the contact grid size for grid sizes greater than 100 and it is also not sensitive to the number of time steps when number of time steps are higher than 1500. Therefore, the ensuring parametric study was conducted with a grid size of 100 and 1500 time steps.

5.6 Parametric study

A parametric study was conducted to evaluate the effect of several significant parameters on the drag force of a smooth tire sliding on a random rough surface. These parameters were standing water film thickness, tire inflation pressure, sliding speed, average roughness height and tire width.

5.6.1 Effect of standing water film thickness on drag force

The standing water film thickness on the pavement was varied from 1 mm to 10.5 mm while keeping the following parameters constant at the indicated values;

Tire inflation pressure	= 25 psi
Tire contact width	= 80 mm
Average roughness height	= 0.1 mm
Sliding speed	= 30 mph
Standing water film thickness	= 1 mm

Figure 5.14 Effect of standing water film thickness to drag force

Based on Figure 5.14, it can be seen that the total drag force (viscous drag + pressure drag) decreases with increasing standing water film thickness until 6mm and then increased. However when considering the viscous drag and pressure drag separately in the plot, it is seen that the viscous drag decreases with increasing standing water film thickness while the pressure drag increases with increasing standing water film thickness. Therefore, the total drag force has the decreasing and increasing trends with a minimum at 6 mm of film thickness.

5.6.2 Effect of tire sliding speed on drag force

The sliding speed of the tire was varied from 30 mph to 60 mph while keeping the following parameters constant at the indicated values;

Tire inflation pressure   = 25 psi
Tire contact width   = 80 mm
Average roughness height   = 0.1 mm
Tire load   = 4850 N
Standing water film thickness   = 1 mm

The results are plotted in Figure 5.15. Based on Figure 5.15, it can be seen that the drag force decreases with increasing tire sliding speed. It is well known that higher sliding speeds reduce viscous drag forces in the contact region. Therefore, higher sliding speeds have lower drag force when the film thickness is low. However, when the film thickness is high and if there is sufficient amount of water in front of the tire, pressure will be built-up in front of the tire causing the increase in pressure drag, i.e., the total drag force.
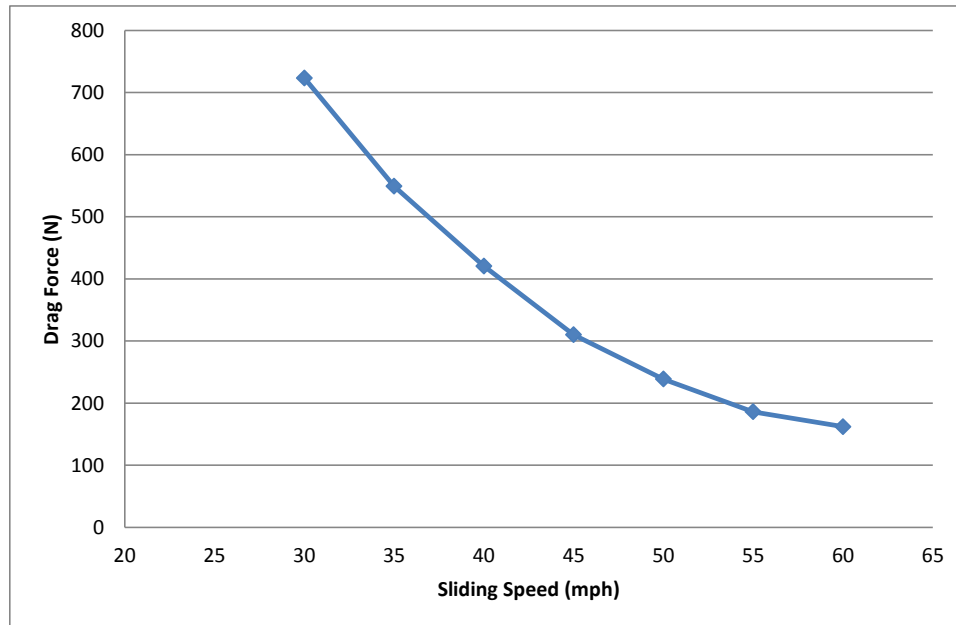
Figure 5.15 Effect of sliding speed to drag force

5.6.3 Effect of inflation pressure to drag force

The tire inflation pressure was varied from 18 psi to 35 psi while keeping the following parameters constant at the indicated values;

Sliding speed   = 45 mph
Tire contact width   = 80 mm
Average roughness height   = 0.1 mm
Tire load   = 4850 N
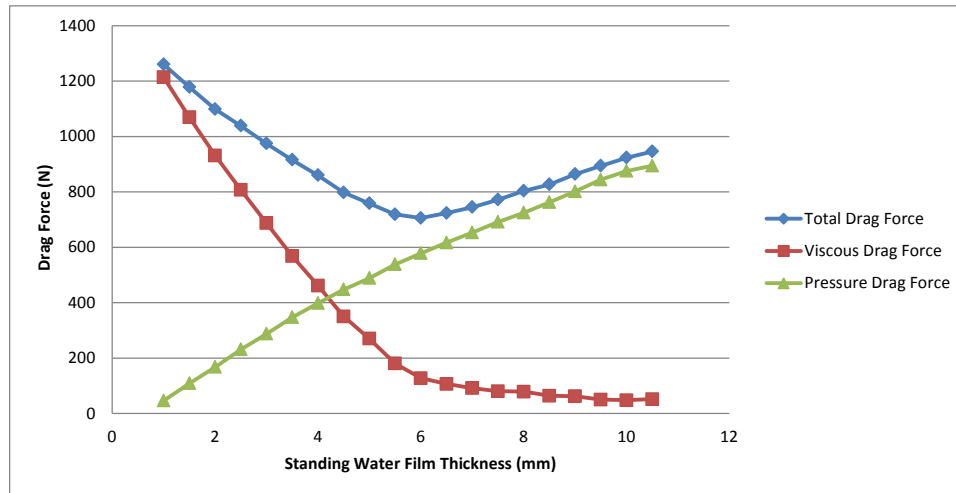Standing water film thickness   = 1 mm

The results are plotted in Figure 5.16. Based on Figure 5.16, drag forced has the highest value when the inflation pressure is 25 psi. When the inflation pressure is lower than its standard value, the tire carcass becomes more flexible and falters under the tire load. Therefore, tire load is mostly transferred to the ground through the side walls of tire. This leads to a low pressure distribution in the middle of the contact patch which could cause the reduction in the drag force buildup. However, when the inflation pressure is higher than its standard value, the tire carcass becomes stiffer and decreases the contact patch area leading to a decrease in drag force. Therefore, it can be concluded that when the tire operates at the inflation pressure closer to its standard value, the drag forces are high as seen in Figure 5.16.
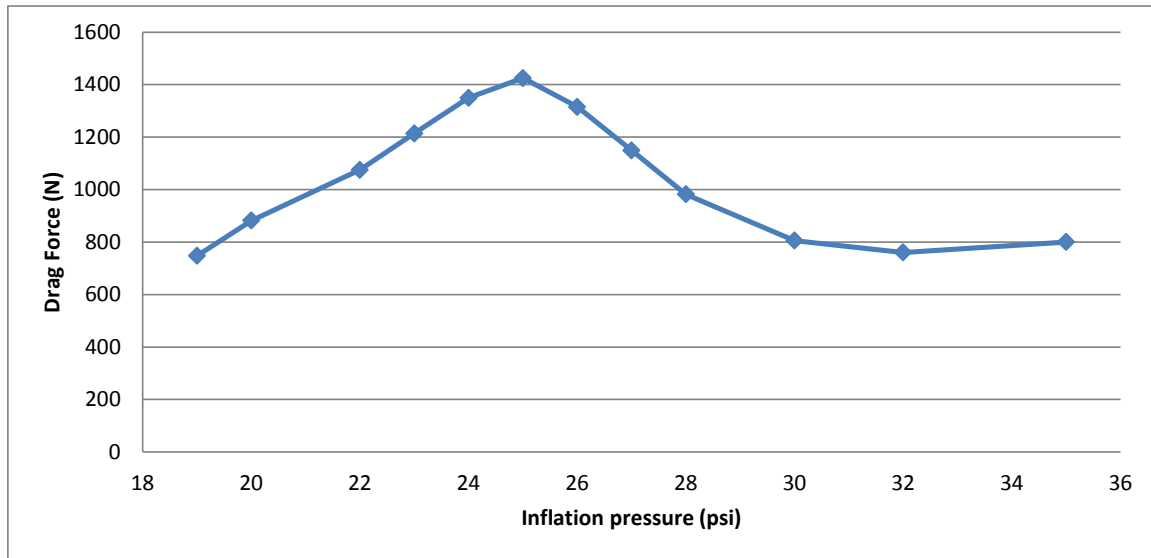
Figure 5.16 Effect of inflation pressure to drag force

5.6.4 Effect of tire contact width on drag force

The tire contact width was varied from 80 mm to 105 mm while keeping the following parameters constant at the indicated values;

Sliding speed = 45 mph
Tire inflation pressure = 25 psi
Average roughness height = 0.1 mm
Tire load = 4850 N
Standing water film thickness = 1 mm

The results are plotted in Figure 5.17. Based on Figure 5.17, the drag force decreasing with increasing tire width until 100 mm and then increases when the tire width is increased further. It must be noted that there are two opposing factors affecting the drag force in this situation. First is the water film thickness which increases with increasing tire width and causes the decrease in the drag force. This is the reason for observing an initial decreasing trend in the drag force. The second other factor is the contact area which increases with increasing tire width and causes the increase in drag force. When combining both increasing and decreasing trends of drag forces with tire width, initially the drag force will decrease up to a certain value and then increases.
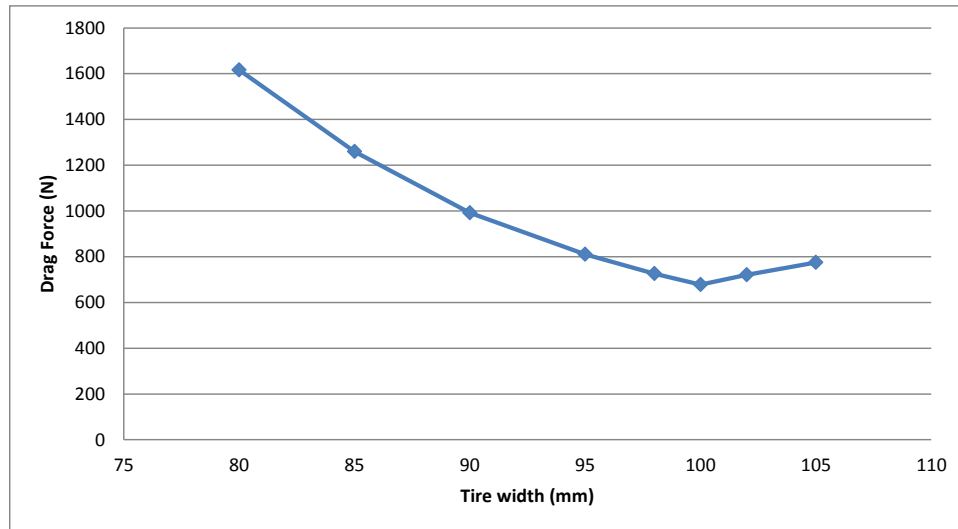
Figure 5.17 Effect of tire contact width to drag force

5.6.5 Effect of average roughness height to drag force

The average roughness height was varied from 0.1 mm to 3 mm while keeping the following parameters constant at the indicated values;

Sliding speed   = 45 mph
Tire inflation pressure   = 25 psi
Tire width   = 80 mm
Tire load   = 4850 N
Standing water film thickness   = 1 mm

The results are plotted in Figure 5.18
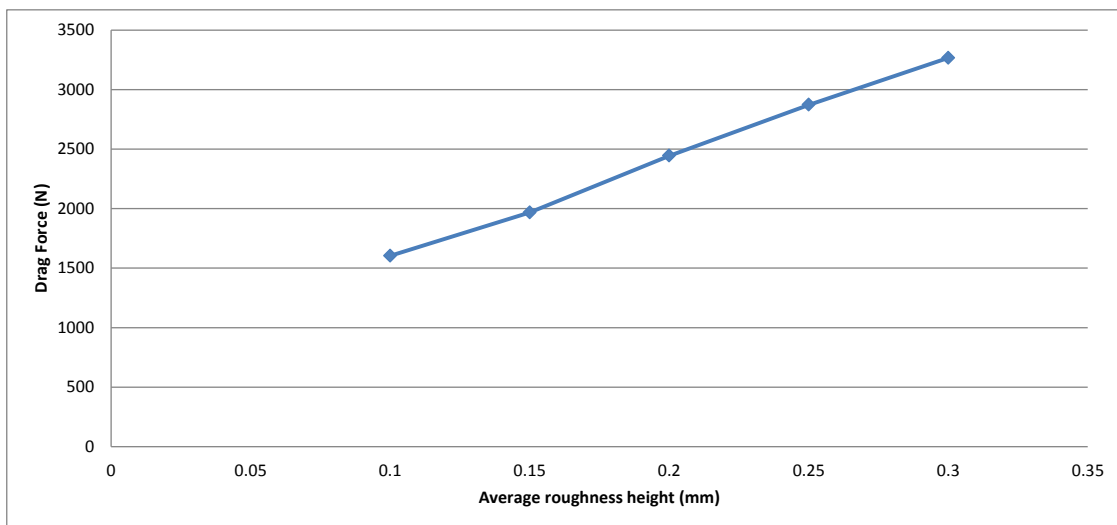
Figure 5.18 Effect of average roughness height to drag force

Based on Figure 5.18, the drag force increases with increasing tire width. This could be due to the fact that increasing roughness height decreases the average film thickness thereby increasing the drag force.

5.7 Comparison with field experiments

Locked wheel skid tests were performed at a selected site on a wet pavement with an average standing water film thickness of 6.5 mm at four different speeds (30 mph, 40 mph, 50 mph, 60 mph). Then the field texture measurements were observed on the test wheel path using a CT meter. The average texture depth (MTD) was calculated and used as an input to the MATLAB program that generates a randomly rough pavement for the above pavement site, the MTD value was 1.12 mm. The program was then assigned the same standing water film thickness and the analysis was performed for different speeds while calculating drag forces. Figure 5.19 shows the two plots of experimental and numerical results. Based on the plot, the numerical model under predicts the results. This could be since the numerical model is only capable of simulating laminar conditions between the tire and the pavement whereas in reality the flow conditions are turbulent on rough pavements. The difference could be explained by the higher drag force created by turbulence flows.
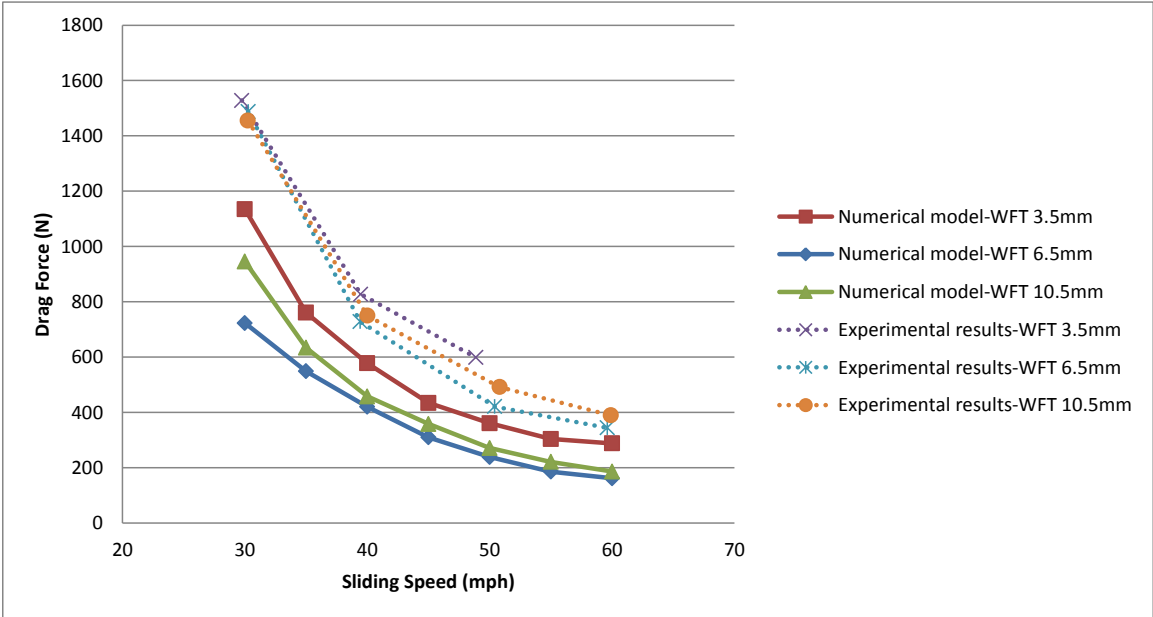
Figure 5.19 Comparison of numerical model and field experiments

CHAPTER 6

FIELD VERIFICATION STUDY

6.1 Experimental evaluation of the water film thickness in sheet flow

In order to quantify the hydroplaning risk potential due to a given rainfall event, the water film thickness must be known. Water film thickness varies with pavement characteristics and rainfall intensity. A custom-built rainfall simulator was constructed to produce a uniform rainfall on an actual roadway segment, the intensity of which can be regulated. This system consists of an irrigation system that delivers uniform water droplets mimicking actual rainfall behavior. The elevation of the simulator allows water to flow on the pavement unhindered. The area of coverage was made large enough such that the simulated rainfall event accurately simulated the characteristics of a real rainfall event.

In this experiment, the physical parameters measured included: longitudinal slope, cross slope for each lane, Mean profile depth (MPD) (measured using Circular Track Meter – ASTM E2157), rainfall intensity (measured using ACURITE Professional Weather Center model #01515), and water film thickness. Once water flow reached the steady state condition, water film thickness measurements were taken at predetermined locations across the pavement drainage basin.

Figure 6.1 Constructed rainfall simulator

The rainfall simulator shown in Figure 6.1 is 28 feet in width and 35 feet in length. It is spaced such that the center to center spacing of the sprinkler heads is always 7 feet. This layout was chosen because it was important that the rainfall coverage was uniform at the locations where

measurements were to be taken. It can be seen that a location closer to the perimeter of the system will receive less rainfall compared to a location in the interior due to the fact that more sprinkler heads contribute to sprinkling in the center compared to a location along an edge or at a corner. The length was expanded to ensure that the hydraulic flow path, determined by the resultant slope of the pavement, received uniform rainfall.

6.2 Experimental evaluation of hydroplaning

For this experiment, a water delivery system has been constructed at the University of South Florida to produce a regulated, but variable, water film thickness at the test location. This system sprays water at the crest of the test section, resulting in sheet flow of water across the lane. Under these conditions, the ultimate water film thickness developed is limited by the flow capacity of the water source. A dam was constructed at the site to develop and maintain higher levels of water film thickness. However, profile variations of the test site lead to areas of non-uniformity of water film thickness. Adjustability in the dam height allows for careful regulation of consistent water film thickness along the entire test section. Figure 6.2 shows the development of water film thickness using the water delivery system and the dam at a high level of water film thickness.

Figure 6.2 Development of water film thickness using water delivery and dam system

The Locked Wheel Skid Tester (LWT) measures the average Skid Number (SN) of a paved surface, in accordance with ASTM E274. The SN can be calculated using Equation 6.1.

$$SN = \frac{Traction}{Load} * 100 \qquad\qquad (6.1)$$

The LWT is comprised of a pickup truck and skid trailer fitted with a standard smooth tire (ASTM E501). The test wheel on the trailer uses a disc brake assembly which is installed in conjunction with a 2-axis force transducer for measurement of vertical load and horizontal traction forces under braking conditions. The pickup truck houses the computer based data acquisition system for data control, monitoring, and collection during the test. For each test, the truck is maintained at a target speed and the operator initiates a test at a pre-determined location. The braking mechanism and data collection are automated based on a predetermined timing schedule for each test speed. The data collected are shown in real time in the truck, and all test data is saved to the hard drive for subsequent analysis.

The standard skid test conducted using the LWT uses water delivered to a nozzle located ahead of the smooth (with no treads) test wheel from a regulated water supply and pump system installed on the truck. This setup allows for a constant equivalent water film thickness of 0.5mm to be developed at all speeds. In this study, various water film thicknesses were created on the roadway to test the effects of its variation on the hydroplaning potential. The tests conducted are thus "Pre-wet" tests since the water is provided by a system other than the standard pumping system described above. Under these conditions, care must be taken not to let the truck tires, followed immediately by the test wheel, pass through the regulated collection (or pool) of water. To ensure that there is minimal interference on the tested water film thickness from the truck tires, the tongue of the trailer has been modified so that the wheel path of the trailer is offset from the wheel path of the truck. With this configuration, shown in Figure 6.3, a well regulated water film on one side of the dam can be skid tested while the truck travels on the opposite side of the dam such that splashing of water due to the truck tires no longer changes the water film tested.

Figure 6.3 Locked skid tester illustrating the offset trailer used for the current experiment

With the dam and water delivery system in place, a uniform water film thickness throughout the length of the test section can be achieved. Adjustments can be made to the placement of the water delivery system and the drainage capacity of the dam, at the operator's discretion. The dam allows the building of water film thickness higher than with the pipe system alone, and drains can be opened at any locations that accumulate excess water. Subsequent measurements of the water film thickness at ten foot intervals along the test section confirmed evenness of the water film thickness along the entire test section.

Two different tests are required for each combination of speed and water film thickness. In one test, the LWT is driven up to the desired speed and the test is started at a pre-determined location. Data is collected over the entire pre-wetted test strip, but the tire is maintained in a free rolling condition. Normal and traction loads are recorded during this time, but the only horizontal force acting on the test tire is a "drag" force resulting from the water being dispersed from under the tire. Since the tire is free rolling, the frictional force developed in the contact patch area is virtually insignificant. In the second of the two tests, the braking mechanism is activated at the start of the test section to bring the tire to a fully locked sliding condition. Normal and traction loads are recorded during sliding.

In this test, in addition to more or less the same drag force experienced under free rolling due to the same water film thickness, friction is also developed in the contact patch. Figure 6.4 shows the free body diagrams of the test tire under three fully locked test conditions. On the other hand, when free rolling tests are conducted, the only difference in the free body diagram is that the friction force becomes negligible for all speeds and water film thickness. A total of 4 test speeds (30, 40, 50, and 60 mph) were tested in triplicate to ensure consistency of results.
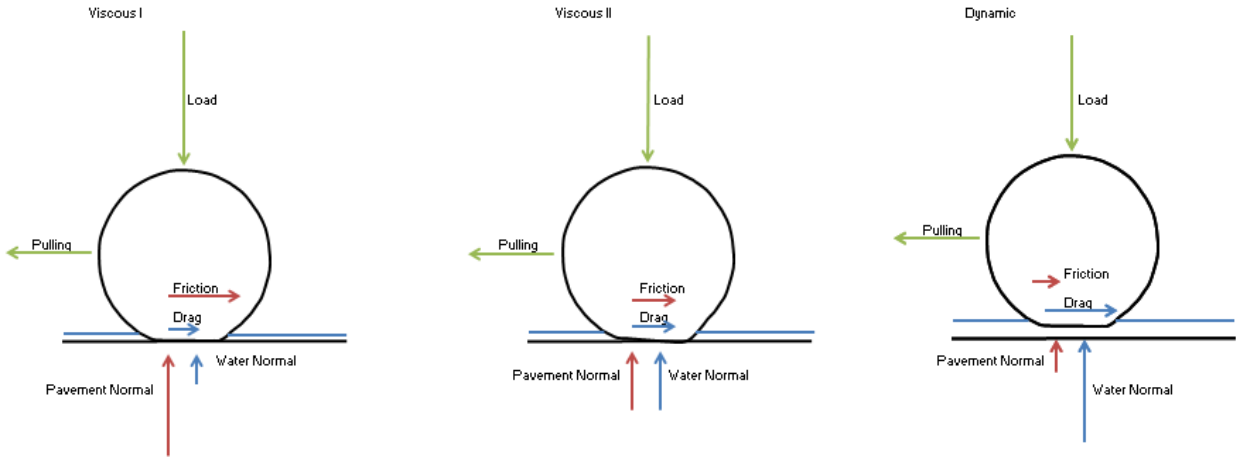
Figure 6.4 Free-body diagrams of tires under locked conditions

For a free rolling test, there is a non-zero level of traction that is recorded throughout the zone where no braking force has been applied. This drag force is converted to an equivalent SN for comparison with the typical skid resistance using Equation 6.1. For the same speed and water film, the SN of the locked phase of the test reflects the sum of the drag and friction components. Repeated trials under similar conditions yield consistent results throughout the tests conducted. There were no free rolling tests which showed a higher SN than the corresponding locked skid tests, supporting the assumption that water produces the same amount of drag whether the tire is free rolling or locked.

6.**3 Results of experimentation**

6.3.1 Water film thickness

In the rainfall simulator experiment, a three lane OGFC road segment with uniform longitudinal slope and minimal signs of wear was tested on SR60 in Brandon, FL. The site exhibited the following characteristics:

Longitudinal Slope   = 1.4%
Cross slopes   = 2.3% (Lane 1), 2.2% (Lane 2), and 2.1% (Lane 3)
MPD   = 0.35mm.

The two rainfall intensities 4.03 and 2.19 in/h were simulated. Water film thicknesses were measured at predetermined locations across the pavement section. The lateral distance and resultant cross slopes determined the drainage length to each point tested.
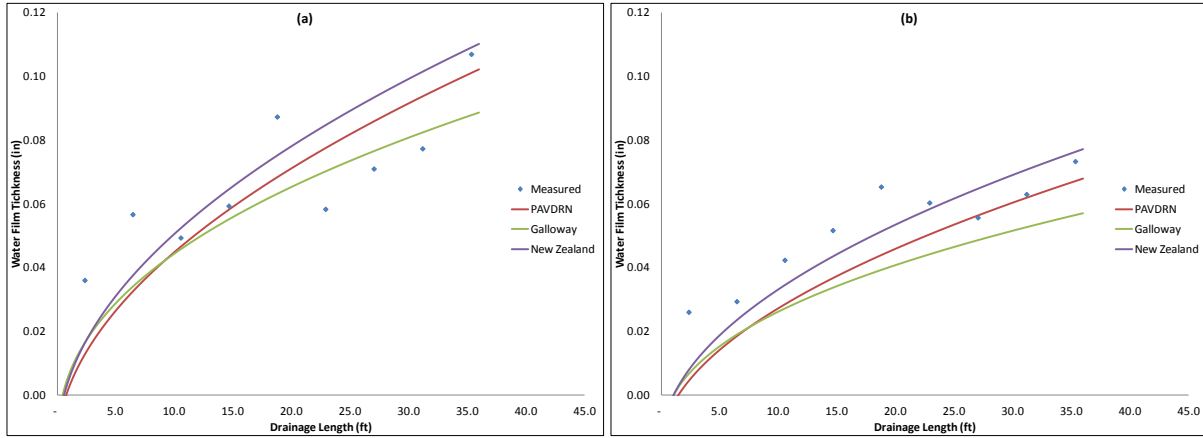
Figure 6.5 Measured and predicted water film thickness values for (a) 4.03 in/h and (b) 2.19 in/h

It can be seen in Figure 6.5 that the three water film predictions dependent on drainage length follow the same trend as the measured water film thickness data. Although the three methods tend to underestimate the water film thickness at a short drainage length, the PAVDRN software and the New Zealand Laboratory equation tend to produce more conservative estimates as the drainage length increases. It should be noted that the measured point at a drainage length of approximately 18' coincided with a wheel rut producing an increased water film thickness at that point.

6.3.2 Hydroplaning Speed

In the hydroplaning experiment, the average value of all thickness readings have been averaged for the entire test section for each water setting. For each speed and test type, the friction values from all tests have also been averaged to a single value. The average drag force has been plotted with the sum of the drag and frictional forces against speed, as shown in Figure 6.6. For the lowest thickness, the drag force increases with speed, with substantial friction values exhibited in addition to the drag at all speeds. The typical trend of reducing friction with speed is evident. For the intermediate thickness, the drag force increases with speed up to about 50 mph, then starts to decrease with speed. At low speeds, the friction values are significant, but they diminish greatly at higher speeds. For the highest thickness, the drag forces exhibit increasing and then decreasing trends as seen before, but at a higher overall magnitude. Friction is substantial at lower speeds, but is negligible at the highest speeds.
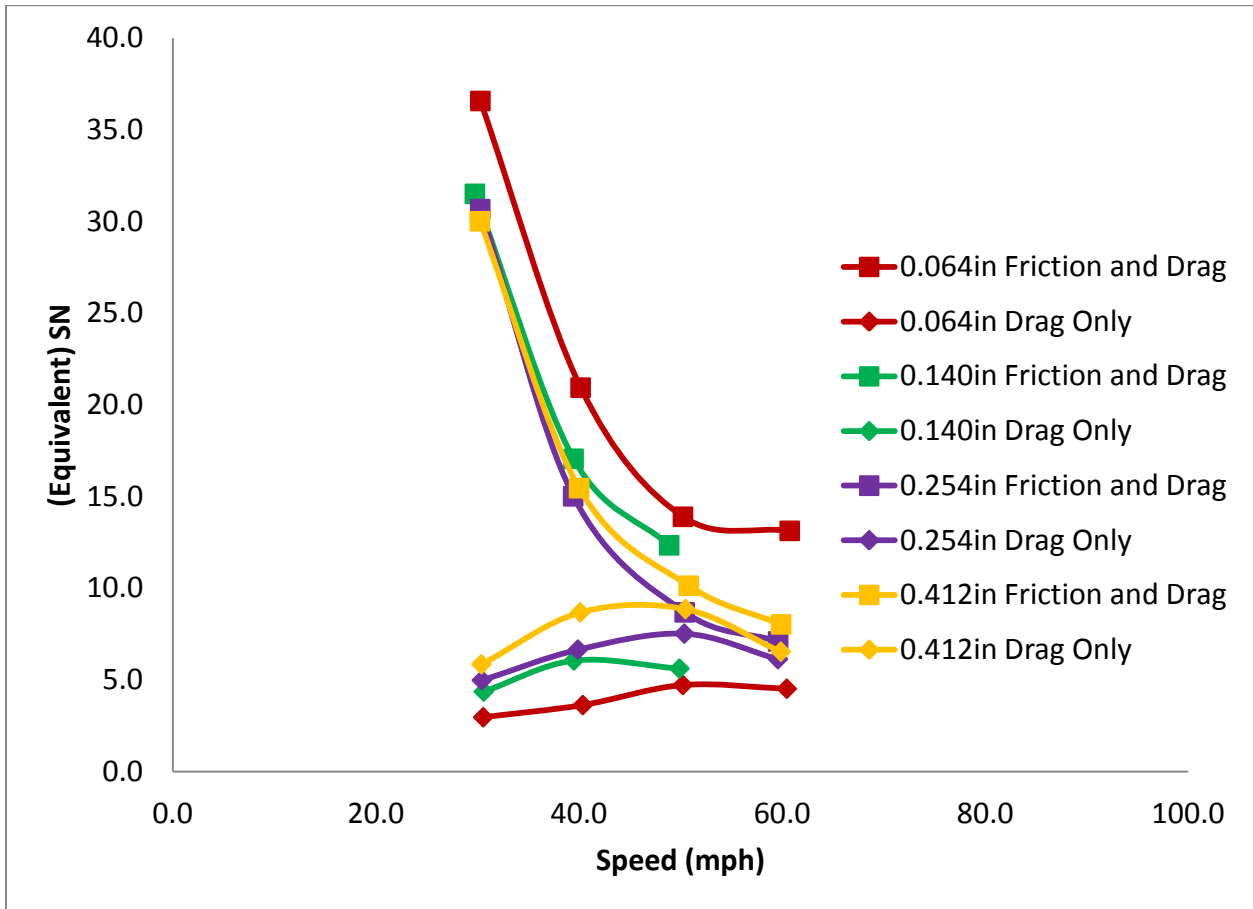
Figure 6.6 Friction and drag variation with speed and water film thickness

Based on the data in Figure 6.6, the pavement friction component, which is the difference between the two curves corresponding to each water film thickness, can be plotted in Figure 6.7. It is seen that the pavement friction component reduces as the water film thickness and speed increase. Dynamic hydroplaning is assumed to occur when the skid resistance becomes insignificant with respect to the drag force from the water. These critical hydroplaning speeds for different water film thicknesses have been shown in Table 6.1. It can also be seen that the drag force decreases with the onset of hydroplaning, due to diminished water squeezing during hydroplaning.
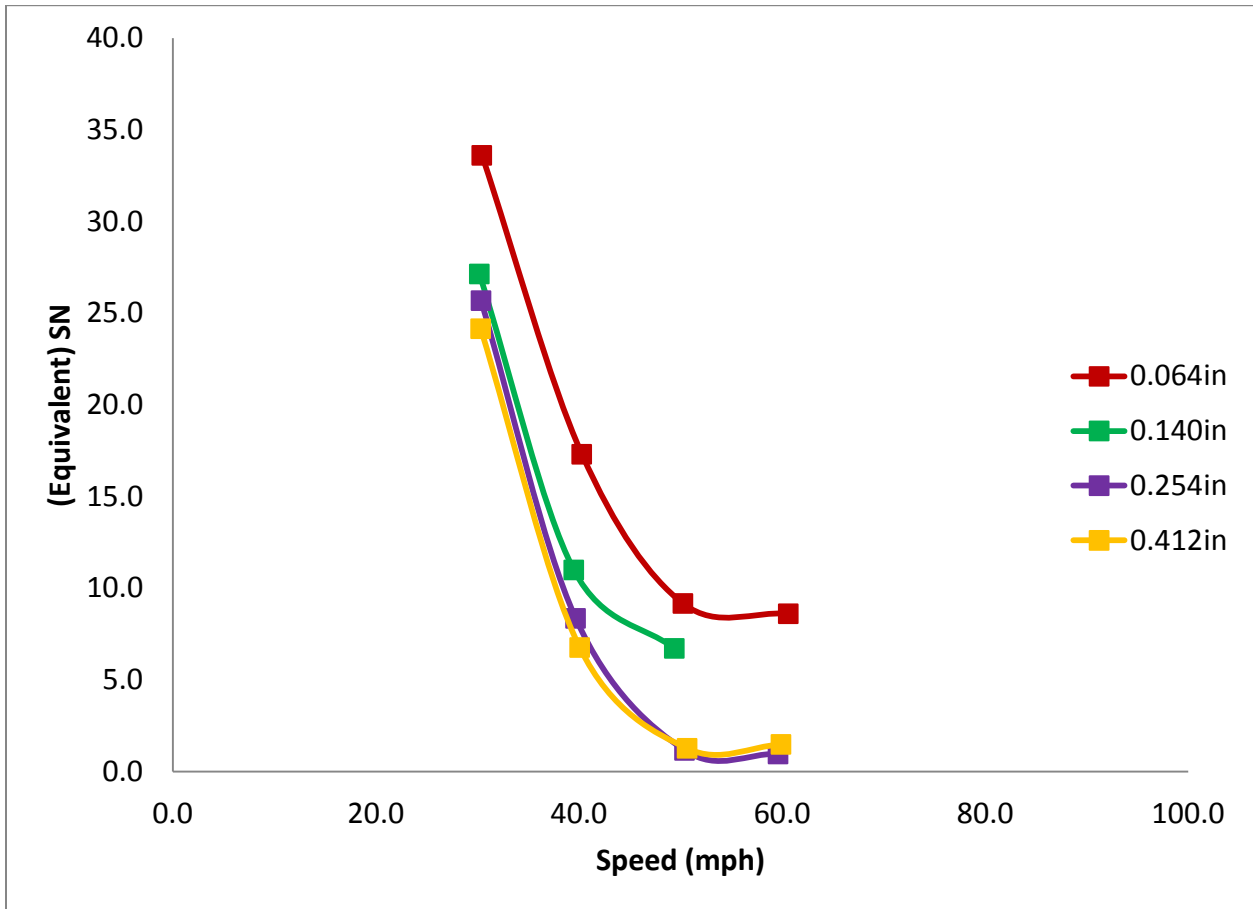
Figure 6.7 Friction component variation with speed and water film thickness

Table 6.1 Hydroplaning threshold speed with water film thickness

Water Film Thickness (in)	Hydroplaning Speed (mph)
0.064	> 60
0.140	> 60
0.254	40 - 50
0.412	40 - 50

CHAPTER 7

CONCLUSIONS AND RECOMMENDATIONS

The primary findings of this research can be highlighted as follows:

1. Models that provide reliable estimates of wet weather speed reduction are available. However, this investigation revealed that different models are applicable under different rainfall intensities. Moreover, wet weather speed reduction is seen to be not only dependent on the rainfall intensity but also on the instantaneous traffic volume. The investigators' field test results are in general agreement with most of the above models.

2. Two most important pavement properties needed to estimate the water film thickness formed during sheet flow are permeability and the Manning's coefficient. The general ranges of values of the above parameters for open-graded and dense-graded pavements were obtained from an exhaustive literature search. The investigators' field test results fall within the above ranges.

3. Analytical and empirical methods available for prediction of hydroplaning speeds of locked-wheel trailers and heavy trucks were gathered. Investigators' subsequent research on the above models yielded more generalized relationships that would be applicable for other vehicles as well. When compared with competing prediction tools, the well established PAVDRN software was observed to be reliable in the prediction of hydroplaning speeds under heavy rain conditions only. Therefore, the investigators have been able provide FDOT with a predictive tool that combines the best of all the available prediction models.

4. All available empirical methods of predicting the water film thickness formed during sheet flow were explored and their reliability was investigated. Based on the above models, the investigators have been able to formulate analytical equations for predicting the critical water film thickness under different road geometric conditions such as straight runs, superelevations and transition sections.

5. Wet weather crash analysis was performed using crash statistics, geometrical data, pavement condition data and other relevant information available in numerous FDOT databases. The results of this extensive effort clearly indicated the following:
   a. Wider sections are more likely to produce hydroplaning crashes
   b. Dense-graded pavements are more likely to induce conditions conducive to hydroplaning than open-graded ones.

c. PAVDRN software would have predicted, to a significant degree of accuracy, most of the documented hydroplaning incidents on two major highways (I-75 and I-95) in Florida.

d. PAVDRN is seen to be more reliable in predicting hydroplaning incidents on outer lanes including those of wider road sections.

6. A numerical model based on the finite difference methods was formulated by the investigators to predict the friction and drag forces induced on a smooth tire sliding on a wet random rough surface. This software is only based on the Reynolds equation for viscous hydroplaning and not on other theories that account for turbulent flow conditions that generally occur during hydroplaning. Nonetheless, this simple model's predictions of the water film thicknesses needed under different tire speeds to create drastically reduced friction and drag forces seem to approach the water film thicknesses needed to realize actual hydroplaning conditions observed during the investigators' field hydroplaning tests. Furthermore, a parametric study based on the model predictions produced results that are physically intuitive.

REFERENCES

Agrawal, S.K., Meyer, W.E., and Henry J. J. (1977).Measurement of Hydroplaning Potential.Pennsylvania Transportation Institute, Pennsylvania State University, PA, USA.

Anderson, D A, Huebner, R S, Reed, J R, Warner, J C, and Henry, J J. (1998)."Improved Surface Drainage of Pavements."NCHRP Web Document, Issue Number 16, National Cooperative Highway Research Program, Washington, D.C.

Bathelt, H. (1973). "Die Berechnung des Aquaplaning-Verhaltens von glatten und profiliertenReifen", AutomobiltechnischeZeitschrift (ATZ), No. 75, 10, pp. 368-374.

Brilon, W. and Ponzlet, M. (1996). "Variability of Speed-Flow Relationships on German Autobahns", *Transportation Research Record 1555*, TRB, National Research Council, Washington, D.C., pp. 91-98.

Chae, S., El-Gindy, M., Johansson, I., Oijer, F., Trivedi, M., (2005)."In-Plane and Out-of-Plane Dynamic Response Predictions of a Truck Tire Using Detailed Finite Element and Rigid Ring Models", ASME International Mechanical Engineering Congress and Exposition, Florida, USA.

Charbeneau, R.J., Jeong, J., Reeder, E., and Chan, W.S. (2007). "Physical modeling of sheet flow on highway pavement surfaces", Presented at the 32nd Congress of IAHR, Venice, Italy, July 1-6, 2007, International Association of Hydraulic Engineering and Research.

Charbeneau, R.J., Jeong, J., and Barrett, M.E. (2008)."Highway drainage at superelevation transitions", Rep. No. FHWA/TX-08/0-4875-1, Center for Transportation Research, The University of Texas at Austin, Austin, Texas.

Charbeneau, R.J., Jeong, J., and Barrett, M.E. (2009). "Physical Modeling of Sheet Flow on Rough Impervious Surfaces", J. Hydraulic Engineering, ASCE, 135(6), 487-494.

Chesterton, J., Nancekivell, N., and Tunnicliffe, N. (2006)."The Use of Gallaway Equation for for Aquaplaning Evaluation in New Zealand", NZIHT & Transit NZ 8th Annual Conference.

Chin, S. M., Franzese, O., Greene, D. L., Hwang, H. L., Gibson, R. C. (2004). *Temporary Loss of Highway Capacity and Impact on Performance: Phase 2*, Oak Ridge National Laboratory, Report no. ORLNL: TM-2004/209, November 2004.

Choubane, B., Page, G.C., and Musselman, J.A. (1998)."Investigation of Water Permeability of Coarse Graded Superpave Pavements", Association of Asphalt Paving Technologists, Volume 67.

Edwards, J. B., (1999). "Speed Adjustment of Motorway Commuter Traffic to Inclement Weather", *Transportation Research*, Part F 2, pp. 1-14.

FDOT (2008).*Flexible Pavement Design Manual*, Florida Department of Transportation, Pavement Management Office, Document No. 625-010-002-G.

FDOT (2009)." Highlands County Performance Data for the Open-Graded Friction Course Test Sections on US-27", www.dot.state.fl.us/statematerialsoffice/pavement/research/reports/stateroad/27.pdf, accessed Oct. 8th.

FDOT (2010)."Standard Specifications for Road and Bridge Construction", Florida Department of Transportation, Tallahassee, Florida.

Federal Highway Administration, (1977).*Economic Impact of Highway Snow and Ice Control*, Final Report.FHWA-RD-77-95, U.S. DOT, Washington D.C.

Fwa, T.F. and Ong, G.P. (2008). "Wet-pavement hydroplaning risk and skid-resistance: Analysis", ASCE Journal of Transportation Engineering, Vol. 12.54, No. 5, May.

Gallaway, B.M., Ivey, D.L., Hayes, G.G., Ledbetter, W.G., Olson, R.M., Woods, D.L. and Schiller, R.E., (1979). "Pavement and Geometric Design Criteria for Minimizing Hydroplaning", FHWA RD-79-31, 278 pp.

Gengenbach, W. (1968). "ExperimentelleUntersuchung von Reifen auf nasserFahrbahn (Experimental Investigation of Tires on Wet Pavements)", AutomobiltechnischeZeitschrift (ATZ) *(Automotive Technology Magazine),* 70, 83-89, 288-293, 310-316.

Hablas, H.(2007). *A Study of Inclement Weather Impacts on Freeway Free-Flow Speed*, Thesis, Virginia Polytechnic Institute and State University, June.

Hawkins, R.K. (1988). "Motorway Traffic Behaviour in Reduced Visibility Conditions", *Proceedings of the 2nd International Conference in Vision in Vehicles*. Elsevier, Amsterdam.

Henry J.J. and Meyer W.D. (1980). "The Simulation of Tire Traction of Wet Pavements", 18th International Automobile Technical Congress, Hamburg, Germany, Proc., No 269, pp. 121-128.

Hogema, J. H. (1996). *Effects of Rain on Daily Traffic Volume and on Driving Behavior,* Report TM-96-B019. TNO Human Factors Research Institute. The Netherlands.

Holdener, D. J. M. (1998). "The Effect of Rainfall on Freeway Speeds", In *Institute of Transportation Engineers Journal,* Volume 68, Issue 11, Washington, D.C., November.

Horne, W.B. and Dreher, R.C. (1963).*Phenomena of Pneumatic Tire Hydroplaning*, NASA TN D-2-56, NASA Langley Research center, NASA, Hampton, Va..

Horne, W. B. and Joyner, U. T. (1965)."Pneumatic tire hydroplaning and some effects on vehicle performance", SAE paper 97.

Horne, W.B., Yager, T.J., and Ivey, D.L. (1986)."Recent Studies to Investigate Effects of Tire Footprint Ratio on Dynamic Hydroplaning Speed", *The Tire Pavement Interface* (M.G. Pottinger and T.J. Yager, eds.), ASTM STP 929, ASTM, West Conshohocken, Pa., pp. 26-46.

Hranac, R., Sterzin, E., Krechmer, D., Rakha, H. and Farzaneh, M. (2006). *Empirical Studies on Traffic Flow in Inclement Weather*, Technical Report, Publication No. FHWA-HOP-07-073, October.

Huang, Y. H. (1993). *Pavement Analysis and Design*, Prentice Hall, Englewood Cliffs, NJ.

Huebner, R.S., Reed, J.R., and Henry, J.J. (1986). "Criteria for Predicting Hydroplaning Potential", *Journal of Transportation Engineering,* 112, 549-553.

Ibrahim, A. T. and Hall, F.L. (1994)."Effect of Adverse Weather Conditions on Speed-Flow-Occupancy Relationships", *Transportation Research Record 1457*, TRB, National Research Council, Washington, D.C. pp. 184-191.

Kockelman, K. M. (1998). "Changes in the Flow-Density Relation due to Environmental, Vehicle, and Driver Characteristics", *Transportation Research Record 1644*, TRB, National Research Council, Washington, D.C., pp. 47-56.

Kyte, M., Khatib, Z., Shanon, P., and Kitchener, F. (2000)."Effect of Environmental Factors on Free-Flow Speed", *Proceedings of the Fourth International Symposium on Highway Capacity, Maui,* June.

Kyte, M., Khatib, Z., Shanon, P., and Kitchener, F. (2001). "Effect of Weather on Free-Flow Speed", In *Transportation Research Record 1776*, TRB, National Research Council, Washington, D.C., pp. 60-68.

Lamm, R., Choueiri, E.M., and Mailaender, T. (1990)."Comparison of Operating Speeds on Dry and Wet Pavements of Two-Lane Rural Highways", *Transportation Research Record 1280*, TRB, National Research Council, Washington, D.C., pp. 199-207.

Leu, M. C. and Henry, J.J. (1982). "Prediction of Skid Resistance as a function of Speed from Pavement Texture", *Transportation Research Record 946,* Transportation Research Board,

National Research Council, Washington D.C., 5.
Lu, Q., Kohler, E., Harvey, J., and Ongel, A. (2009). "Investigation of Noise and Durability Performance Trends for Asphaltic Pavement Surface Types: Three-Year Results", UCPRC-RR-2009-01, University of California Pavement Research Center, California.

Lu, Q., Fu, P.C., and Harvey, J.T. (2010)."Laboratory Evaluation of the Noise and Durability Properties of Asphalt Surface Mixes", UCPRC-RR-2009-07, University of California Pavement Research Center, California.

Mahmassani, H.S., Dong, J., Kim, J., and Chen, R.B. (2009)."Incorporating Weather Impacts in Traffic Estimation and Prediction Systems", Final Report, Publication No.FHWA-JPO-09-065, September.

Mallick, R.B., Cooley Jr., L. S., Teto, M.R., Bradbury, R.L., and Peabody, D. (2003). "An Evaluation of Factors Affecting Permeability of Superpave Designed Pavements", Pub. No: NCAT Report 03-02, Maine Department of Transportation.

Martin, P. T., Perrin, J., Hansen, B., and Quintana, I. (2000). *Inclement Weather Signal Timing*.Research Report MPC01-120,2000, mmwww.ndsu.nodak.edu/ndsu/ugpti/MPC_Pubs/html/MPC01-120.html.accessed in July 2003.

Mehta, P.K. and Monteiro, P. J.M. (1993).*Concrete Microstructure, Properties, and Materials*, Second Edition, McGraw-Hill Inc., New York.

Moore, D. (1975). *The Friction of Pneumatic Tires*, Elsevier Scientific Publishing Co., New York.

National Cooperative Highway Research Program (NHCRP) (1998). *Improved Surface Drainage of Pavements* (Project 1-29 Final Report), Transportation Review Board, Washington, D.C.

OECD Road Research Group (1976). *Adverse Weather, Reduced Visibility and Road Safety – A Road Research Report*, Organisation for Economic Cooperation and Development (OECD), Paris, France.

Ong, G. P. (2006). *Hydroplaning and skid resistance analysis using numerical modeling*, Ph.D. Dissertation, National University of Singapore.

Ong, G.P. and Fwa, T.F. (2006). "Analysis of Effectiveness of Longitudinal Grooving Against Hydroplaning", *Transportation Research Record1949*, Transportation Research Board of the National Academies, Washington, D.C., pp. 113–125.

Ong, G.P. and Fwa, T.F. (2007a). "Effectiveness of Transverse and Longitudinal Pavement Grooving in Wet-Skidding Contro.", *Transportation Research Record 2005*, Transportation Research Board of the National Academies, Washington, D.C., pp. 172–182.

Ong, G.P. and Fwa, T.F. (2007b). "Wet-pavement hydroplaning risk and skid-resistance: Modeling", *ASCE Journal of Transportation Engineering*, Vol. 133, No. 10, October.

OngG.P and Fwa, T.F. (2008). "Modeling and Analysis of Truck Hydroplaning on Highways, Transpo*rtation Research Record, Issue 2068, pp. 99*-108.

Perrin, H. J., Martin, P.T., and Hansen, B.G. (2001)."Modifying Signal Timing During Inclement Weather", *Transportation Research Record 1748, TRB, National Research Counc*il, Washington, D.C., pp. 66-71.

Pisano, P. and Goodwin, L.C. (2003).*Surface Transportation Weather Applications*.http://209.68.41.108/itslib/AB02H261.pdf. Accessed in June 2003.

Rado Z.(1994). *Analysis of Texture Profiles*, PTI Report 9510, Pennsylvania Transportation Institute, State College Park, Pa.

Rakha, H., Krechmer, D., Cordahi, G., Zohdy, I., Sadek, S. and Arafeh, M., (2009).*Microscopic Analysis of Traffic Flow in Inclement Weather*, Publication No.FHWA-JPO-09-066, November.

Ridgeway, H.H. (1976). "Infiltration of water through the pavement surface", *Transportation Research Record 616*. Transportation Research Board: Washington, D.C., pp 98-100.

Russam, K. and Ross, N.P. (1968).*The depth of rain water on road surfaces*, Road Research laboratory, Ministry of Transport, Report No. LR 236, 25 pp.

Texas Department of Transportation Hydraulic Design Manual (2000), http://onlinemanuals.txdot.gov/txdotmanuals/hyd/pavement_drainage.htm.

Transportation Research Board (2010).*Highway Capacity Manual.*5th Edition, Washington, D.C.

Van Es, G. W. H. (2001). *Hydroplaning of Modern Aircraft Tires.*NationaalLucht- en Ruimtevaartlaboratorium.

Venner, C.H. and Lubrech, T. (2005).*Multilevel methods in lubrication*, Tribology Series 37.Elsevier.

Watson, D., Johnson, A. and Jared, D. (1998)."Georgia Department of Transportation's Progress in Open-Graded Friction Course Development", *Transportation Research Record 1616*. Transportation Research Board, Washington, D.C., pp 30-33.

Westerman, J. (1998). "AHTD's Experience with Superpave Pavement Permeability", (presentation), The Arkansas Superpave Symposium, January 21, Little Rock, Arkansas.http://www.utexas.edu/research/superpave/articles/jrw10a.html.